INTERACTIONS OF TETRACYCLINE ANTIBIOTICS WITH DISSOLVED METAL IONS AND METAL OXIDES

A Dissertation
Presented to
The Academic Faculty

by

Wan-Ru Chen

In Partial Fulfillment
of the Requirements for the Degree
Doctor of Philosophy in the
School of Civil and Environmental Engineering

Georgia Institute of Technology
August, 2008

INTERACTIONS OF TETRACYCLINE ANTIBIOTICS WITH DISSOLVED METAL IONS AND METAL OXIDES

Approved by:

Dr. Ching-Hua Huang, Advisor
School of Civil and Environmental Engineering
Georgia Institute of Technology

Dr. Spyros G. Pavlostathis
School of Civil and Environmental Engineering
Georgia Institute of Technology

Dr. Jaehong Kim
School of Civil and Environmental Engineering
Georgia Institute of Technology

Dr. Andrew Stack
School of Earth and Atmospheric Science
Georgia Institute of Technology

Dr. Sotira Yiacoumi
School of Civil and Environmental Engineering
Georgia Institute of Technology

Date Approved: May 7, 2008

[To my parents]

ACKNOWLEDGEMENTS

First of all, I would like to express my deepest sense of gratitude to my advisor Dr. Ching-Hua Huang for her patient guidance, encouragement and excellent advice throughout this study. Her constant support and help made this work successful.

I would also like to thank Dr. Jaehong Kim, Dr. Sotira Yiacoumi, Dr. Spyros G. Pavlostathis and Dr. Andrew Stack for serving as my committer members. Their comments and suggestions are very helpful in improving this thesis.

I am deeply indebted to Dr. Guangxuan Zhu for his guidance and assistance throughout my five year of research in the lab. He showed me a lot invaluable knowledge regarding instrument operation and maintenance which will be very helpful and useful in my future research.

I am thankful to my lab members, Judy Zhang, Amisha Shah, Sanghyuck Park, Lokesh Padhye and Pei Wang for being so helpful in the lab. Those long nights in Daniel lab will not be forgotten. A special thanks goes to Judy for her valuable contributions and discussion to kinetic model development.

I would like to acknowledge my closest friends Rebecca Chang, Nora Chen and Pauline Han for proofreading my thesis and providing valuable feedback. I am grateful to Emily Ko and her family for their generous help and for being with me throughout my stay at Atlanta. I would also like to thank Chien-Chung Huang and Min Cho for saving my data and my thesis while my computer crushed. Throughout the preparation of this thesis and throughout my entire study, I have received help, advice, and encouragement from all of my friends, especially San-Hui Chi, Chia-Hung Hou, KJ Liao, Jane Li, Gayle

Hagler and Dooil Kim from Georgia Tech and Jessica Leung, Wendy Tung, Yudan Gaw, Marcia Rhee and Kate Wang from church.

Lastly, I am deeply and forever indebted to my mother Bao-Lian Yang and my father Tse-Chuan Chen for their unwavering love, support and encouragement throughout my entire life. I am also very grateful to my brothers Yung-Fu Chen and Yung-Chian Chen for being with me all this time. I thank them greatly for being so caring and supportive when I was far away from home. I would never have completed my Ph.D. study without my family.

TABLE OF CONTENTS

LIST OF TABLES

LIST OF FIGURES

LIST OF SYMBOLS AND ABBREVIATIONS

Abs	Absorbance
AES	Atomic Emission Spectrometry
AHTCs	Anhydro-tetracyclines,
ANO	*N*-oxide
CD	Circular dichroism
CDX	Carbadox
CHES	2-(cyclohexylamino)ethanesulfonic acid
CIP	Ciprofloxacin
CTC	Chlorotetracycline
DAD	Diode array detector
DNA	Deoxyribonucleic acid
ECs	Emerging contaminants
EDCs	Endocrine-disruptors
EDTA	Ethylenedinitrilotetraacetic acid
ELISA	Enzyme-linked immunosorbent assay
ENR	Enrofloxacin
epi-TCs	epi-tetracyclines
FQ	Fluoroquinolonic
GC-MS	Gas chromatography-mass spectrometry
h.c.p.	Hexagonal closest packed structure
HPLC	High performance liquid chromatography
ICP	Inductively-Coupled Plasma
iso-TCs	iso-tetracyclines

LC-MS	Liquid chromatograph-mass spectrometer
LOM	Lomefloxacin
MES	2-(N-morpholino)ethanesulfonic acid
MOPS	4-morpholinepropanesulfonic acid
MS/MS	Tandem mass spectrometry
NMR	Nuclear magnetic resonance
NOM	Natural organic matter
NOR	Norfloxacin
OFL	Ofloxacin
OTC	Oxytetracycline
PIP	Pipemidic Acid
PM	N-phenylmorpholine
PP	1-phenylpiperazine
PPCPs	Pharmaceuticals and personal-care products
QDX	Quindoxin
QNO	Quinoline *N*-oxide
QXO	Quinoxaline *N*-oxide
ROS	Reactive oxygen species
SBR	Sequencing batch reactor
SPE	Solid-phase extraction
SOD	Superoxide dismutase
TCs	Tetracyclines
TTC	Tetracycline
UV-Vis	Ultraviolet-visible spectrophotometry

β_{mlh}	Stability constants for the complexation between metal and ligand
δ-MnO_2	Manganese dioxide
γ-Al_2O_3	Aluminum oxide
λ	Wavelength of ultraviolet-visible absorbance
ΔAbs	Absorbance change due to complexation
$Abs^{(X)}$	Absorbance of a solution containing reagent X
ArXH	Precursor complex between the organic reductant and the oxide surface (X = O or N)
ArX•	Organic radical
A_I	Irreversible adsorption
A_T	Total adsorption
C	Concentration of the parent antibacterial at time *t*
C_0	Concentration of the parent antibacterial at time zero
C_e	Concentration of the parent antibacterial at time $t \rightarrow \infty$
e^-	Electron
E_H (pe)	Redox potential
k	Reaction rate constant
k_{obs}	Transformation rate constant
L^{m-}	Ligand with –m charges
m/z	Mass to charge ratio
M^{n+}	Metal ion with +n charges
$>Mn^{III}$, ArX•	Reaction intermediate
$>Mn^{III}$, ArXH	Precursor complex on MnO_2 surface
MnOII	MnO_2 surface reaction kinetic model
$-N(CH_3)_2$	Dimethylamine group

$\bullet OH$	Hydroxyl radical
$O_2^{\bullet-}$	Superoxide radical anion
pK_a	Acid dissociation constant
pH_{zpc}	Zero-point-of-charge of metal oxides
S_{rxn}	Total reactive surface sites
$TC\text{-}M^{n+}$	Tetracycline molecule and metal ion complexation
$TC\bullet$	Tetracycline radical

SUMMARY

Recent studies have demonstrated the omnipresence of antibacterial agents in the aquatic environment due to high usage and widespread applications of these compounds in medicine and agriculture, raising concerns over proliferation of antibiotic-resistant bacteria and other adverse health effects. Tetracyclines (TCs) are among the most widely used antibiotics, and their fate and transformation in the soil-water environment are not yet well understood. Based on TCs' strong tendency to interact with metals, their environmental fate and transport are expected to be greatly influenced by metal species commonly present in waters and soils and thus the focus of this study.

Tetracycline (TTC), chlorotetracycline (CTC), oxytetracycline (OTC) and their related isomers are the focus in this study. The study results show that the TCs are highly susceptible to oxidative transformation mediated by dissolved Mn^{II} and Cu^{II} ions and manganese dioxide under environmentally relevant conditions. Mn^{II} and Cu^{II}, regenerated in a cyclic fashion, play an overall catalytical role in the oxidation of TCs by O_2. The two metal ions, however, operate via different mechanisms. In the TC-Mn^{II}-O_2 system, oxidation of the TC-complexed Mn^{II} to Mn^{III} by oxygen occurs, followed by oxidation of TC by Mn^{III} to regenerate Mn^{II}. In the TC-Cu^{II}-O_2 system, Cu^{II} oxidizes TC within the complex and the yielded Cu^{I} is re-oxidized by the presence of oxygen. Examination of the reactivities of various TC members and transformation products shows that Mn^{II} and Cu^{II} react with TCs at different moieties: the Mn^{II}-mediated reaction occurs at the BCD ring of TC while Cu^{II} induces TC transformation through the A ring.

TCs are rapidly transformed in the presence of MnO_2 (in hours) and experimental evidence indicates that the reaction kinetics are controlled by surface complex formation (*i.e.*, adsorption of TCs to MnO_2 surfaces). Comparisons among TTC, CTC and OTC clearly show that the oxidative transformation by MnO_2 can occur via different structural moieties and reaction pathways depending on the TC molecule structure, leading to complicated product formation patterns. Transformation product analysis indicates that MnO_2 promotes isomerization at the C ring to form iso-TCs, oxidizes the phenolic-diketone and tricarbonylamide groups leading to insertion of up to 2 O to TC molecule, and demethylates the dimethylamine group to yield N-demethylated intermediate and products. To better evaluate the surface reactions of Mn oxide with TCs and other compounds, a new kinetic model (the MnOII model) is successfully developed to describe the complex reaction kinetics based on the experimental results with TCs and three other classes of antibacterial agents. The model characterizes the reaction kinetics by two independent parameters, the reaction rate constant (k) and total reactive surface sites (S_{rxn}). The model fitting indicates that the reaction kinetics of antibacterials with MnO_2 are controlled by either the rate of surface precursor complex formation (for tetracyclines) or by the rate of electron transfer within the precursor complex (for phenols, fluoroquinolones, and aromatic *N*-oxides).

It was also found that TCs adsorbed strongly to aluminum oxide (Al_2O_3), and the surface interaction promoted the acid-catalyzed isomeration and dehydration of TCs. Product evaluation indicates that Al_2O_3 transforms tetracycline (TTC) to its anhydrotetracycline (AHTTC) and two other unidentified products, transforms CTC to

iso-CTC, and transforms OTC to an unidentified isomer product. The formation of AHTTC is of concern because it exhibits considerably higher cytotoxicity than TTC.

Overall, this work significantly advances the fundamental understanding of the reaction mechanisms of TC antibiotics with important metal species in the aquatic environment and provides the knowledge basis for better environmental fate prediction and risk assessment for these biologically active contaminants.

CHAPTER 1

INTRODUCTION

1.1 Research Issue and Objectives

Environmental research is expanding beyond the traditional focus on solid waste management and municipal wastewater pollution control. In recent years, an increasingly growing number of studies have shown that many chemical and microbial constituents that have not historically been considered as contaminants are present in the environment on a global scale. These emerging contaminants (ECs), e.g., pharmaceuticals, household chemicals and pesticides, are commonly derived from municipal, agricultural, and hospital wastewater sources and pathways. The main concern regarding emerging containments is that they are being introduced continuously into water bodies as pollutants, and their biological activity can lead to adverse effects in aquatic ecosystems and potentially impacts drinking water supplies.

In recent years the increasing use of drugs in human health, farming and aquaculture has become a growing concern because of their potential to cause adverse human health and ecological effect. A large percentage of administered drugs are excreted from humans and treated animals and enter the soils and other environmental compartments via wastewater treatment plants, land application of sewage sludge, animal manure and agricultural runoff. Antibacterial agents are a part of such emerging contaminants because of the concern over their potential to foster the development of resistance in microbes in the environment. The frequent detection of agricultural antimicrobial agents in the aquatic environment (Hirsch et al., 1999; Thiele-Bruhn, 2003)

has raised the concern for the serious dangers of antibiotic-resistant bacteria (Barrett, 2005; Chapin et al., 2005). Although the antibiotics given to humans are rarely the same as those given to animals, the structure of the drugs can be similar enough so that the antibiotics used for animals cause resistance to those used for humans (Barrett, 2005; Chapin et al., 2005), or vice versa.

Among antimicrobial agents, tetracyclines (TCs, Figure 1.1) merit special attention. Tetracycline (TTC) and derivatives such as oxytetracycline (OTC) and chlorotetracycline (CTC) are among the most widely used antibiotics in treating diseases for humans and animals as well as in nutrition and feed additives for livestock production (Graslund and Bengtsson, 2001). TCs could come from hospital wastewater, domestic sewage effluent and likely even more significantly the agricultural sources since they are so widely used in agriculture on therapy as well as growth promotion (Ungemach Fritz et al., 2006). If released into the environment, these antimicrobials could lead to problems in the evolution of antimicrobial-resistant bacteria (Khachatourians, 1998; Chee-Sanford et al., 2001). Currently the environmental fate and transport of TCs are still not well understood and more studies are needed in order to properly assess their potential risks. For this purpose, this study focuses on the adsorption and abiotic transformation of TCs in the soil-water environment with a particular emphasis on the influence of common metal species in soils on these processes.

Metal oxides (e.g., Mn, Fe, Al and Si oxides) commonly found in soils and sediments are known to facilitate abiotic reactions of organic pollutants via hydrolysis, oxidation, reduction, isomerization and substitution. Studies with manganese oxides indicate that they are a major contributor in soil redox processes and serve in a catalytic

role in the formation of humic-enzyme complexes in the soil ecosystem (Bartlett, 1988; Shindo et al., 1996). Previous studies have shown that Mn oxides are effective oxidants for various organic compounds including anilines (Laha and Luthy, 1990; Pizzigallo et al., 1998; Li et al., 2003) and phenols (Ulrich and Stone, 1989; Ukrainczyk and McBride, 1993; Pizzigallo et al., 1995). Aluminum oxides have been shown to catalyze oxidation of phenolic compounds in the presence of oxygen (Karthikeyan et al., 1999). Since the structures of TCs contain moieties related to ketone, carboxyl, amino, and hydroxyl groups, it is quite likely that TCs will be also susceptible to transformation reactions mediated by metal oxides as well as dissolved metal species in the soil-water environment. Indeed, our experimental results show that manganese dioxide (δ-MnO_2), aluminum oxide (γ-Al_2O_3) and dissolved Mn^{II} and Cu^{II} ions significantly enhance the abitoic transformation of TCs.

The main objective of this research was to identify the reaction pathways and mechanisms of TCs in the presence of common soil metal oxides and dissolved metal species. A range of studies have been conducted to achieve this research objective. First, the TCs' redox reactions with and adsorption to MnO_2 surface were studied. Additionally, a MnO_2 surface reaction kinetic model was developed to describe the reactions of MnO_2 with TCs, as well as with several other structural classes of antimicrobial agents that had been investigated previously in our lab. Second, adsorptive interactions of TCs and their acid-catalyzed decomposition reactions with Al_2O_3 surfaces were examined. Besides MnO_2, two redox-active metal ions, Mn^{II} and Cu^{II}, were found to induce oxidative transformation of TCs in a cyclic fashioin in the presence of O_2, although the two

reactions followed different reaction pathways. The environmental parameters (e.g., pH, co-solute, etc.) that affect the above reactions were also investigated.

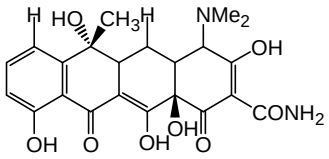

Tetracycline (TTC)
$C_{22}H_{24}N_2O_8$
Mol. Wt.: 444.43

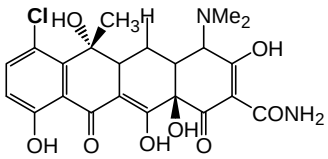

Chlorotetracycline (CTC)
$C_{22}H_{23}ClN_2O_8$
Mol. Wt.: 478.88

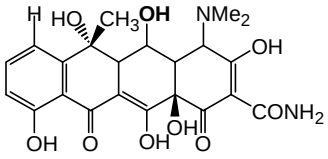

Oxytetracycline (OTC)
$C_{22}H_{24}N_2O_9$
Mol. Wt.: 460.43

Figure 1.1 Structures of tetracycline, chlorotetracycline and oxytetracycline.

1.2 Background

1.2.1 Tetracycline Antibiotics

1.2.1.1 Occurrence of Tetracyclines in the Environment

Tetracycline antibiotics (TCs) have been used extensively to treat humans for several decades. They are also the leading group of antibiotics used in animal feed, accounting for over 60% of veterinary use of medicated feeding stuff (Ungemach Fritz et al., 2006). Residues of TCs and their metabolites were detected in eggs, meat and animals based on different exposure methods (Croubels et al., 1997; Cooper et al., 1998; De Ruyck et al., 1999; Zurhelle et al., 2000); such residues have raised concerns in terms of food safety. Comparing the amount of TCs remaining in eggs and animal bodies, most of these antibiotics tend to be discharged from the dosed livestock animals. Due to large quantities of usage, TCs are continuously introduced to the aquatic environment via treated and untreated sewage and sludge, as well as agricultural waste and runoff.

Researchers have been interested in the occurrence of TCs in the environment since the late 1980s (Jacobsen and Berglind, 1988). Several studies summarized the concentrations of TCs in marine fish farms, sediments, treated wastewater, soils and waters (Smith, 1996; Halling-Sorensen et al., 1998; Halling-Sorensen et al., 2003). As the detection methods keep developing, the detection limit of TCs is now down to trace levels (Lindsey et al., 2001; Aga Diana et al., 2003; Lykkeberg Anne et al., 2004). In several separate studies, the concentrations of TCs ranged from 0.15 μg/L in ground water and surface water samples (Lindsey et al., 2001), 86-199 μg/kg in soil samples, 4.0

mg/kg in liquid manure (Hamscher et al., 2002), and to higher than 3 μg/L in 90% of the farm lagoon samples (Zhu et al., 2001). Evidently, the frequent usage of TCs has rendered them widely distributed in the environment. The potential toxicities and health and ecological threats of TCs in the environment necessitate a better understanding of the fate and transport of these antibiotics in order to properly evaluate their risks.

1.2.1.2 Chemical Properties of Tetracyclines

TCs possess complicated ring systems and are amphoteric molecules with multiple ionizable functional groups. The rings are lettered A through D from right to left, and the numbers begin at the bottom of ring A (Figure 1.2). Substitutions may occur in positions C1 through C12. Three macroscopic pK_a values have been reported for TCs, corresponding to the tricarbonylamide (C1, C2, C3), phenolic diketone (C10, C11, C12), and dimethylamine groups (C4), respectively (Stephens et al., 1956; Qiang and Adams, 2004). Figure 1.3 illustrates complicated speciation of TCs. A TC molecule can behave as a cation, a neutral/zwitterion, an anion or a dianion depending on water pH in aquatic systems. The A ring and the BCD ring are two separate resonance and thus chromophoric systems, contributing to two major absorption bends (250-300 nm and 340-380 nm) of TCs spectra. In general, the A ring chromophore contributes only to the 250-300 nm absorption, whereas the BCD ring chromophore contributes to both absorption bends (McCormick et al., 1957; Wessels et al., 1998b; Schneider et al., 2003).

TCs are generally more stable in acidic than in alkaline conditions (Clive, 1968). TCs can undergo reversible epimerization at position C4 to form the corresponding 4-epi-TCs (Figure 1.2). This epimerization process is more favorable at the pH range of approximately 2-6 (McCormick et al., 1957), and the epimerization rate can be enhanced

by the presence of certain anions such as phosphate and citrate (Walton et al., 1970; Sokoloski et al., 1977; Yuen and Sokoloski, 1977). Note that the only difference between TCs and their epimers is the $-N(CH_3)_2$ group position. When the $-N(CH_3)_2$ group flips from the down position to the up position, epi-TCs are formed. OTC epimerizes less willingly than TTC and CTC because its hydroxyl group at the C5 position may form a hydrogen-bond with the dimethylamine group (Hussar et al., 1968). At alkaline pH, TCs that have a hydroxyl group at C6 can form their respective iso-TCs, via a nucleophilic attack of the C6 hydroxyl group at the C11 carbonyl carbon (McCormick et al., 1957) (Figure 1.2). Among TCs, CTC is especially prone to this irreversible transformation to yield iso-CTC quickly (Waller et al., 1952; Stephens et al., 1954).

Studies have shown that TCs can be susceptible to various transformation via isomerization, dehydration, substitution, and oxygenation (Walton et al., 1970; Liang et al., 1998). Figure 1.2 summarizes the common transformation products of TCs. TCs can form epi-tetracyclines (epi-TCs) (an isomerization reaction) and degrade to anhydro-tetracyclines (AHTCs) by losing a water from the C6 position (a dehydration reaction) by phosphoric acid- or citric acid-catalyzed reactions (Walton et al., 1970; Pena et al., 1998). The AHTCs have been suggested to exhibit higher toxicity than their parent compounds (Klimova and Ermolova, 1976). Due to the additional hydroxyl group at the C5 position, OTC can transform irreversibly to α-apo-OTC and β-apo-OTC in acidic conditions via a nucleophillic attack of this –OH group at C12 (Arikan et al., 2006).

TCs have a strong tendency to complex with metal ions (Jezowska-Bojczuk et al., 1993; Tongaree et al., 1999). Previous studies have reported that the A ring and the BCD ring are probable metal complexation sites of TCs. Mitscher *et al.* analyzed the extensive

circular dichroism (CD) spectral measurements for a series of TCs with a variety of metal ions, and concluded that complex formation occurs through oxygen coordination to the BCD chromophore (Mitscher et al., 1972). On the other hand, the oxygen at C3 is reported as the most probable binding site for the complexes among the C-O oxygens of TCs (Baker and Brown, 1966; Lee and Everett, 1981; Mikulski et al., 1988) because a six-membered chelat ring was formed in combination with the amide group oxygen. Chelation involving both the A ring and the BCD ring chromophores were also commonly suggested (Colaizzi et al., 1965; Caswell and Hutchison, 1971; Jogun and Stezowski, 1976; Wessels et al., 1998a). Because of their strong metal complexation, the *in vivo* antibiotic activity of TCs is dictated by Mg^{II} and Ca^{II} complexes (Lambs et al., 1984). The strong tendency of TCs to interact with metal species will likely play an important role in affecting their fate and transport in the aquatic environment.

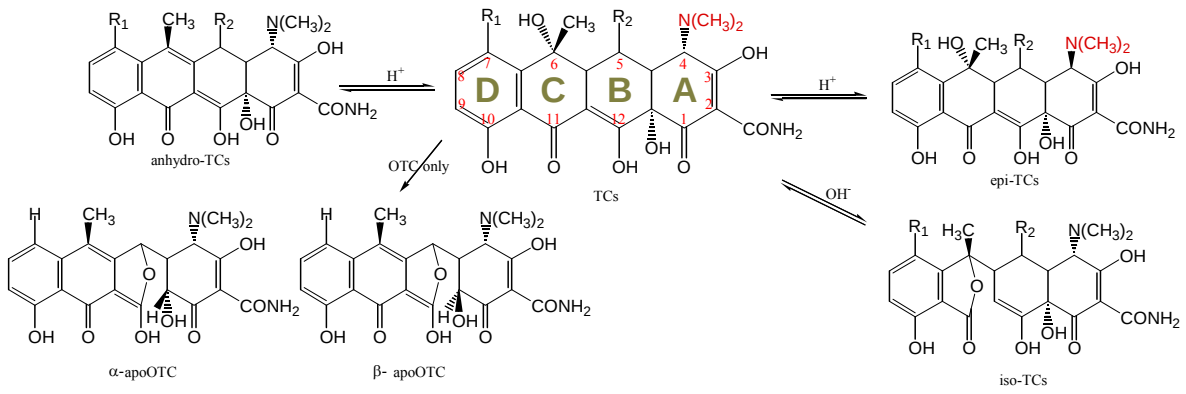

Figure 1.2 Reported transformation products of TCs.

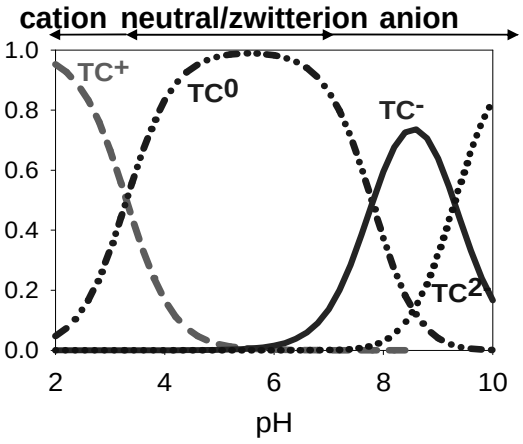

Compound	pK_{a1}	pK_{a2}	pK_{a3}
Tetracycline (TTC)	3.32	7.78	9.58
Oxytetracycline (OTC)	3.22	7.46	8.94
Chlorotetracycline (CTC)	3.33	7.55	9.33

Figure 1.3 Speciation of TC molecule at pH 2-10.

1.2.1.3 Possible Environmental Fate of Tetracycline Antibiotics

Environmental processes of TCs including photolytic degradation, biotransformation, and strong interactions with mineral surfaces and organic matter have been wildly studied. TCs are highly sensitive to light, and the photodecomposition of TCs is extensively studied (Sanniez and Pilpel, 1980; Oka et al., 1989; Olack and Morrison, 1991; Miskoski et al., 1998). The existence of TC radical in the photoreaction was confirmed and a quinine product was observed (Moore et al., 1983). The structure alteration of TC photoproducts was suggested at A ring (Moore et al., 1983; Olack and Morrison, 1991). The pH and water hardness values were reported to affect the photochemical kinetics of TTC degradation (Werner et al., 2006). Biotic elimination of TCs in wastewater treatment plants has been shown as an effective way of TCs' removal (Kim et al., 2005; Gartiser et al., 2007). TTC showed a dissolved organic carbon (DOC) elimination curve typical for biodegradation processes, starting with 18% and reaching the plateau phase at 80% after 21 days (Gartiser et al., 2007). Kim *et al.* operated two lab-scale sequencing batch reactors (SBR) to simulate the activated sludge process on TTC removal in wastewater treatment and concluded that sorption was the principal TTC removal mechanism in activated sludge (Kim et al., 2005).

TCs, with ketone, carboxyl, amino, and hydroxyl groups, exhibit strong adsorption to the soil environments (Kulshrestha et al., 2004; Figueroa and MacKay, 2005; Sassman and Lee, 2005; Pils and Laird, 2007) and several metabolic products commonly found in manure-containing matrices, such as isomerization products (epi-TCs) and dehydration products (AHTCs, α-apoOTC and β-apoOTC) (Loke Marie et al., 2003; Aga et al., 2005; Arikan et al., 2006). In particular, several studies have demonstrated the strong

adsorption of TCs with Al oxide surfaces and clays (Gu and Karthikeyan, 2005; Pils and Laird, 2007). Rapid sorption of TTC on Al and Fe hydrous oxides (in 8 hours) was suggested and TTC was an effective ligand to promote surface dissolution of mineral surfaces (Gu and Karthikeyan, 2005). The sorption process has been shown to highly depend on the pH (Figueroa et al., 2004; Gu and Karthikeyan, 2005) and the presence of dissolved organic matter (Kulshrestha et al., 2004). Rubert and Pedersen (2006) studied the reaction kinetics of OTC with MnO_2 extensively and complicated reaction kinetics were reported, in which the reactions eventually reached a plateau. They concluded that manganese oxides in soils and sediments are likely to promote appreciable degradation of TCs. The metal oxides possibly control the mobility and stability of trace contaminants due to their high surface area, surface charges, and redox potential at various pH conditions (Figueroa and MacKay, 2005; Gu and Karthikeyan, 2005; Rubert and Pedersen, 2006; Pils and Laird, 2007).

In summary, TCs may undergo abiotic degradation depending on pH, redox and light conditions (Clive, 1968; Halling-Sorensen et al., 2003), and are prone to adsorption to soils (Tolls, 2001). The strong metal-binding tendency of TCs contributes to strong and specific interactions with mineral surfaces (Figueroa and MacKay, 2005; Gu and Karthikeyan, 2005; Pils and Laird, 2007) and organic matter (MacKay and Canterbury, 2005), and affects their photoreactivity in natural waters (Werner et al., 2006). Thus, this strong interaction between TCs and metals may induce their abiotic degradation in soil-water system.

1.2.2 Metal Species That Facilitate Transformation of Organic Contaminants in the Aquatic Environment

Many researchers have studied the behavior and properties of metal species in aqueous systems because they are abundant in the environment. Among various forms of metals, metal oxides merit particular attention because of their abundance in the aquatic environment and the capability of mineral surfaces in mediating or catalyzing various reactions of organic compounds including hydrolysis, substitution, redox, and polymerization. Manganese, iron and aluminum oxides, in particular, are commonly found in soils and sediments and play a critical role in controlling the mobility and stability of containments in the environment because they have strong adsorption capacity for organic chemicals and are known to promote oxidative transformation of various organic compounds (Ukrainczyk and McBride, 1992, 1993; Pizzigallo et al., 1995; Karthikeyan et al., 1999; Pecher et al., 2002). As a result, metal oxides serve as an important factor in retarding and transforming organic pollutants in subsoils and aquifers that are classified as porous media with low organic carbon contents (Karthikeyan et al., 1999).

In addition to metal oxides, dissolved metal ions are present in complexes with ligands in many aquatic environments. Much research work has shown that metal ions may mediate or catalyze various reactions of organic contaminants including hydrolysis (Stone and Torrents, 1995), oxidation (Walling and Kato, 1971), reduction (Strathmann and Stone, 2001), isomerization (Pines and Haag, 1960), adsorption (Pils and Laird, 2007), photodegradation (Werner et al., 2006), and biodegradation (Schnappinger and Hillen, 1996) by coordinating the contaminant parent compound molecule, the attacking

nucleophile, and/or the reaction intermediate or product. The role of dissolved metal ions and metal oxides in affecting the environmental fate and transport of organic contaminants is expected to be particularly significant for contaminants that exhibit strong metal-complexing or metal-chelating ability such as TCs. The metal-mediated transformation of contaminants will also be affected by environmental factors such as pH, temperature, and the presence of other competing ions.

1.2.2.1 Metal-ligand Complex Formation

Metal species usually participate in organic compound transformation by complexing the parent compound molecule. The tendency towards complex formation varies with different metals and ligands. Free metal ions in solution are actually aquo complexes; the water itself is a ligand that binds the metal ion, and every complexation reaction in water is a ligand-exchange reaction by replacing water. Ligands that can replace water molecules around the central metal ion are chemical species that have a non-bonding pair of electrons to share with the metal. These include simple anions such as the halides Cl^-, F^-, Br^-, I^-, more complex inorganic ions such as NO_3^-, CO_3^{2-}, SO_4^{2-}, NH_3, S^{2-}, PO_4^{3-}, SO_3^{2-}, CN^-, and a great variety of organic molecules with suitable functional groups, usually containing oxygen, nitrogen, or sulfur atoms as purveyors of electron pairs (*e.g.*, R-COO^-, R-OH, R-NH_2, R-SH) (Morel and Hering, 1993).

The reaction of a metal with a ligand can be of an electrostatic or covalent nature, or both. When it is mainly electrostatic and the reactants retain some water of hydration between them, the product is called an ion pair or an outer sphere complex. This type of interaction is particularly important among the major ions in high ionic strength media

such as sea water. For the reaction of a metal with a ligand that involves coordination at several positions, it is called chelation. Such a reaction requires the combination of a metal with a coordination number greater than 1 (*i.e.*, more than one site for coordination), and a multi-dentate ligand, an organic compound with several reactive functional groups. These organic compounds are called chelators, chelating agents, or complexing agents. TCs have been reported as effective chelators of Ca^{2+}, Mg^{2+}, Mn^{2+}, Zn^{2+} and Cu^{2+} (Lambs et al., 1988; Jezowska-Bojczuk et al., 1993; Ohyama and Cowan, 1995). In this study, we use the word complex to loosely cover all species resulting from the metal-ligand combinations.

The effects of specific ligands on the metal can be illustrated by spectroscopic evidence, such as the absorbance of ultraviolet (Sokoloski et al., 1977) or visible (Davis and Gloor, 1981) light by metal complexes. Difference in the spectra of metal complexes suggests a consistent pattern in the extent to which metal orbitals are perturbed by ligands. Consequently, the ligands in a metal complex sway the electron distribution in the orbitals, which influences both the chemical reactivity and magnetic and spectroscopic properties of the complexes. Some metal-ligand complexes, on the other hand, present interaction of the ligand *p* or *d* orbitals and the metal *d* orbitals, resulting in formation of π bonds. In metal complexes with π donor ligands, there is increased electron density at the metal center; with π acceptor ligands, electron density at the metal center is decreased. These variations in electron density affect the relative stability of metal reduction potential in the complex. For example, halide ions (Cl^-, Br^-) markedly increased conversion rates of Cu^{II}-facilitated breakdown reaction (Huang and Stone Alan, 2003).

Fe^{II} ion is stabilized by π acceptor ligands such as phenanthroline (phen) and Fe^{III} is stabilized by π donor ligands such as oxinate (Figure 1.4).

Metal-ligand interactions are particularly important for the reactions in natural waters, including acid-base reactions, compelxation and solid formation. Equilibrium constants and the stoichiometric coefficients for reactions among 4 metal ions, Cl^- ion, and 2 ligands (TTC and EDTA) that are used in this study are presented in Table 1.1. The logs of equilibrium constants given in Table 1.1 correspond to a general complexation or precipitation reaction shown below:

$$m\mathrm{M} + l\mathrm{L} + h\mathrm{H}^+ \rightleftharpoons \mathrm{M}_m\mathrm{L}_l\mathrm{H}_h$$

$$\beta_{mlh} = \frac{[\mathrm{M}_m\mathrm{L}_l\mathrm{H}_h]}{[\mathrm{M}]^m[\mathrm{L}]^l[\mathrm{H}^+]^h} \qquad \text{M:metal ion,} \quad \text{L:ligand}$$

For any given complex or solid, several different reactions of formation or dissociation can be written, making it necessary to specify the reaction considered when giving an equilibrium constant. All reactions that are considered to take place in the system are also considered to have reached equilibrium. In many cases, complexation of metals by ligands is certainly rapid relative to other processes of interest. The tendency of the organic ligands to form surface complexes with metal oxides is considered similar to that of organic ligands forming complexes with metal ions in solution.

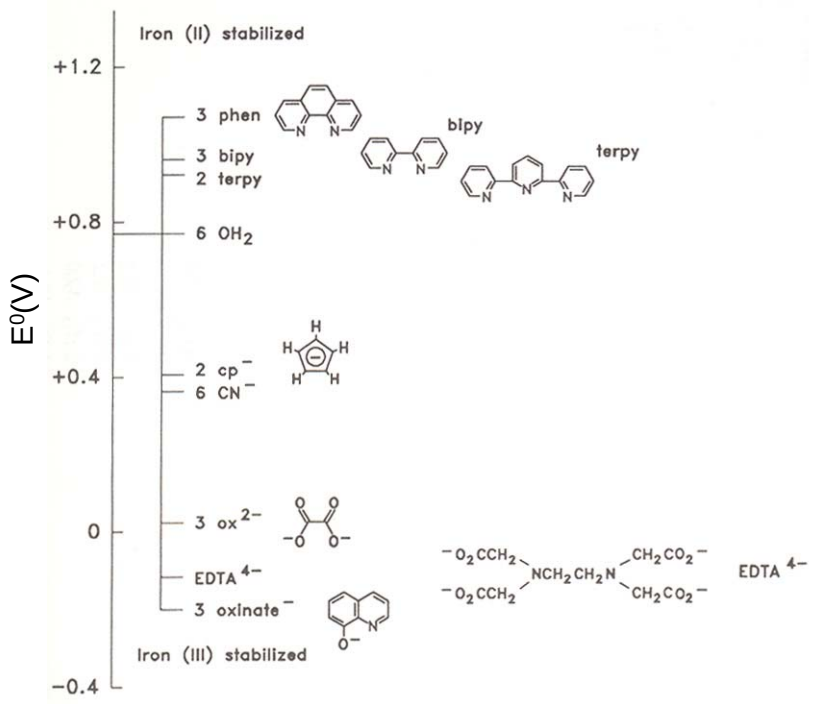

Figure 1.4 Standard reduction potentials for iron complexes. Adapted from Morel and Hering (1993).

Table 1.1 Stability constants for formation of complexes and solids from metals and ligands used in this study.

	TC^{2-}		OH^-		EDTA		Cl^-	
H^+	H_3L^+	20.68						
	H_2L^0	17.36						
	HL^-	9.58						
Mn^{2+}	$MnHL^+$	14.40[b]	MnL^+	3.4	MnL^{2+}	15.6		
			MnL_2^0	5.8	$MnHL^{3+}$	19.1		
			MnL_3^-	7.2				
			MnL_4^{2-}	7.7				
			$MnL_{2.(s)}$	12.8				
Cu^{2+}	$CuHL^+$	17.98[a]	CuL^+	6.5	CuL^{2+}	20.5	CuL^+	0.20
	CuH_2L^{2+}	20.98[a]	CuL_3^-	15.1	$CuHL^{3+}$	23.9	CuL_2^0	-0.26
	$CuH_2L_2^0$	31.28[a]	CuL_4^{2-}	16.0	$CuOHL^+$	22.6	CuL_3^-	-2.29
	$CuH_4L_2^{2+}$	40.67[a]	$Cu_2L_2^{2+}$	17.4			CuL_4^{2-}	-4.59
			$CuL_{2.(s)}$	11.8				
Mg^{2+}	$MgHL^+$	14.57*[b]	MgL^+	2.6	MgL^{2+}	10.6		
			$MgHL^{2+}$	14.3	$MgHL^{3+}$	15.1		
			$MgH_2L_2^{2+}$	30.8				
Ca^{2+}	$CaHL^+$	14.64*[b]	CaL^+	1.3	CaL^{2+}	12.4		
			$CaHL^{2+}$	14.1	$CaHL^{3+}$	16		
			$CaH_2L_2^{2+}$	30.8				

[a] from Jezowska-Bojczuk et al. (1993)

[b] from Ohyama and Cowan (1995)

*The reported stability constants are performed at pH 9.5.

**Besides specified citations, all constants are obtained from MINEQL+ thermochemical data base (Schecher and McAvoy, 2001). Constants are given as logarithms of the overall formation constants, β, for complexes and as logarithms of the overall precipitation constants for solid.

1.2.2.2 Effects of Adsorption on the Kinetics of Surface Reactions

Adsorptive properties are responsible for the formation of surface complexes that are the prerequisite of all reactions at (hydr)oxide surfaces (Stumm, 1992). The surface of aquatic particles contain functional groups with acid-base and other coordinative properties that are similar to (or can be correlated with) those of their counterparts in dissolved complexes. The obligatory proximity of the functional groups on a surface makes them accessible to long-range coulombic (*i.e.*, electrostatic) interactions from other neighboring groups. The complexing properties of ligands can lead to the detachment of surface-bound M^{n+} (M^{n+}: metal ion) and the formation of M^{n+}-organic complexes in solution, a process named ligand-assisted dissolution (Kostka et al., 1995; Klewicki and Morgan, 1999). For example, reductant properties have been shown to possibly cause the conversion of $Mn^{III/IV}$ oxides to much a more soluble Mn^{II} (Stone, 1987b). Stone (1987a), employing a phase consisting of $Mn^{III/IV}$ oxides, observed that decreasing the pH from 6.0 to 5.0 yielded a 23-fold increase in the rate of dissolved Mn production by oxalic acid, and a threefold increase in the rate of dissolved Mn production by pyruvic acid. In this study, the metal oxide is in excess amount of the ligand so the surface must exhibit metal-like coordination properties (Morel and Hering, 1993).

In many cases, reactions occurring at mineral surfaces present saturation kinetics, *i.e.*, a plateau in the reaction rate are observed at high (dissolved) reactant concentrations. This effect has been known for both dissolution reactions and surface-catalyzed redox reactions (Morel and Hering, 1993). If the rate-limiting step of a reaction involves a surface species, the reaction rate depends on the surface concentration of that species. A similarity between the dependence of surface concentration and of reaction rate on the

dissolved product concentration of the reacting species can be expected. A simple Langmuir model has been applied to describe observed dissolution kinetics for proton-promoted, ligand-promoted, and reductive dissolution of metal oxides (Furrer and Stumm, 1986; Sulzberger et al., 1989). In addition, pseudo-first-order kinetics was commonly used to characterize the initial reaction rate for organic contaminant degradation when reacting with excess amount of metal oxides (Zhang and Huang, 2003, 2005b, a).

Although dissolution or redox reactions are considered to proceed in parallel at surface sites with varying reactivity, a constant distribution of sites is usually assumed. Consequently, the contribution of different sites to the overall reaction rate cannot be distinguished and electrostatic effects are not explicitly considered. Detachment of a surface metal atom (destabilized by formation of a surface complex, protonation of neighboring hydroxyl groups, or reduction or oxidation to a more labile oxidation state) from the lattice is mainly adopted to be the rate-limiting step in oxide dissolution. Rapid and reversible adsorption is commonly assumed, as is rapid regeneration of the mineral surface.

1.2.2.3 Redox Reactions at the Mineral-water Interface

Oxidation is one of the most important reactions for organic pollutants to degrade in the aquatic environment. Besides carbon, oxygen, nitrogen and sulfur, the elements most involved in redox cycles are the most abundant redox reactive metal species, such as iron, manganese and copper. For example, manganese oxides and iron (oxyhydr)oxides are widely distributed in sediments, soils and water, and are among the most important natural oxidants in facilitating pollutant degradation (Nowack and Stone, 2003).

Redox reactions involve the transfer of one or more electrons between a reductant and an oxidant. For redox couples such as Fe^{II}/Fe^{III} or Cu^{I}/Cu^{II}, only one-equivalent reactions are possible. When the stable oxidation states of the redox couple differ by two electrons, for example, Mn^{II}/Mn^{IV}, the reactants are formally two-equivalent redox agents. Redox reactions are referred to as complementary reactions when both oxidant and reductant are either one-electron or two-electron equivalent redox agents and as non-complementary when a one-electron redox agent reacts with a two-electron redox agent. Redox reactions may also be characterized as either inner- or outer-sphere reactions. The distinction between inner- and outer-sphere redox reactions depends on whether the electronic interactions are promoted by chemical bonds between reductant and oxidant. In the reaction of metal complexes, this corresponds to inner-sphere mechanism. In the outer-sphere reaction, the coordination spheres of the metals are essentially intact. Rate laws for inner- and outer-sphere redox reactions have the same form and the reaction mechanisms cannot be differentiated on the basis of kinetics.

Both inner- and outer-sphere electron transfer reactions can occur at the mineral-water interface as well as in solution. In heterogeneous reactions, the solid may be either a reactant or catalyst in the redox reaction. In the first case, reduced minerals (such as pyrite, $iron^{II}$-containing silicates, or uraninite) may be oxidized or oxidized minerals (such as Fe^{III} or $Mn^{III/IV}$ oxides) reduced. In the second case, redox reactions may be facilitated by associating with the reactants with the mineral surface. In either case, the kinetics of redox reactions is constrained by a particular characteristic of surface reactions. That is, once the surface becomes saturated with some chemical species and its maximum surface concentration is attained, further increase in the dissolved

concentration of that species cannot increase its rate of reaction at the surface.

Minerals as redox reactants. Redox reactions at the mineral-water interface in which the solid itself is oxidized or reduced often result in the dissolution of the solid because of the variation of metal solubilities with oxidation state. For a given mineral, the rates of redox-enhanced dissolution can be significantly greater than the rates of proton- or ligand-promoted dissolution (Wang and Stone, 2006). As for non-reductive dissolution, the rate of redox-enhanced mineral dissolution is generally considered to be surface-controlled. As with other surface-controlled dissolution reactions, we may expect a direct dependence of the redox-enhanced dissolution rate on the surface area of the reacting mineral; such dependence has been proposed for the dissolution of magnetite (Fe_3O_4) in anoxic marine sediments. The dependence of the rate on the dissolved concentration of the reductant (or oxidant) may be expected to vary from first-order at low surface coverage of the mineral to zero-order when the surface is saturated. The extent of surface coverage is likely to vary greatly among different types of environments.

Minerals as catalysts. Redox reactions can also occur at the mineral-water interface in which the mineral itself is not oxidized or reduced but, rather, catalyzes the electron transfer reaction. As illustrated by previous studies, the oxygenation of Mn^{2+} is accelerated by both hydrolysis and by complex formation at oxide surfaces (Morgan, 2004). Surface catalysis can also be important in isomerization processes.

Overall, redox kinetics in natural waters are often complex and difficult to describe systematically owing to the presence of various speices. The reactions may occur either

in solution or at solid-water interfaces. In heterogeneous redox reactions, the solid may be either a reactant or a catalyst. Therefore, a priori prediction of reaction rates is often difficult.

1.2.3 Metal Species Used in This Study

1.2.3.1 Manganese Oxides

Manganese oxides/hydroxides commonly exist in soils and sediments as colloidal particles or coatings of other minerals. They are reported as major contributors in soil redox processes and serve a catalytic role in the formation of humic-enzyme complexes in the soil ecosystem (Bartlett, 1988; Shindo et al., 1996). In aquatic chemistry, the oxidation states of manganese which have received the greatest attention are Mn^{II}, Mn^{III} and Mn^{IV}. Mn^{II} is usually present in the soluble phase while $Mn^{III/IV}$ are sparingly soluble oxides and hydroxides. Manganese(IV) oxide is the chemical compound MnO_2; this blackish or brown solid occurs naturally as the mineral pyrolusite, which is the main ore of manganese. It is also present in manganese nodules. A variety of recipes are commonly used for MnO_2 synthesis. Generally, the reagent is generated by treatment of an aqueous solution of $KMnO_4$ with a Mn^{II} salt (typically Mn^{II} sulfate). In this study, a hydrous manganese dioxide suspension was prepared according to Murray (Murray, 1974) by reacting $NaMnO_4$ very slowly with $MnCl_2$ under alkaline conditions (Zhang and Huang, 2003). The generated MnO_2 is structurally similar to the naturally occurring mineral birnessite, δ-MnO_2(s).

In spite of the existence of pure Mn^{IV} phases (Murray et al., 1984), soils and sediments usually contain (hydr)oxides that are combinations of Mn^{III} and Mn^{IV} (Guest et

al., 2002; Wang and Stone, 2006). In soil/sediment environments, manganese oxide is believed to be among the strongest oxidizing agents that may be encountered in the absence of molecular oxygen. Solid phases of the composition of MnO_2 have often been assumed to be common oxidation products of Mn^{2+}, which decreases the mobility of manganese and its availability to organisms (Stone and Morgan, 1984b, a). Organic compounds have been reported to promote reductive dissolution of manganese oxides (e.g., Stone, 1987b; Ukrainczyk and McBride, 1993). Although most of the dissolved Mn product is in the +II oxidation state, the formation of the +III oxidation state are also detectable (in 1–5 μM concentration range) when capillary electrophoresis method was applied (Wang and Stone, 2006). These oxidative processes involving manganese oxides may constitute an important abiotic degradative pathway for organic contaminants in subsurface environments.

Manganese oxides can act as strong oxidizing agents, even in the absence of oxygen, that are effective in organic pollutant transformation with reduction potentials of 1.50 V and 1.23 V for MnOOH and MnO_2, respectively (Stone, 1987b) (Table 1.2). Manganese oxides have been shown to be effective oxidants for a wide range of organic pollutants including phenols (Stone, 1987b; Ukrainczyk and McBride, 1993), anilines (Laha and Luthy, 1990; Klausen et al., 1997), aliphatic amines (McArdell et al., 1998), and triazines (Wang et al., 1999). Many antibacterial agents are also susceptible to oxidative transformation by Mn oxides (e.g., Zhang and Huang, 2003, 2005b, a). The oxidation kinetics of Mn oxides have been found to be affected by various factors including properties of oxides, organic compound structures, and environmental factors such as pH, Mn^{II} ion and other competing ion concentration as well as the presence of humic acid

(HA) (Stone, 1987b; Ukrainczyk and McBride, 1992, 1993). Often times, adsorption occurs along with oxidative transformation of organic contaminants toward Mn oxide adsorptive sites (*i.e.*, valence-unsatisfied OH^- or water ligands coordinated to the surface-bound $>Mn^{III,IV}$ (McBride, 1994b)) on the oxide surfaces.

Earlier studies by Stone and Morgan (1984b) illustrated some features of the reductive dissolution reaction between manganese oxide and organic solutes and some of the factors that influence the rate of the reaction. Stone (1987b) considered the reductive dissolution of manganese(III/IV) oxides by substituted phenols. Those investigations were performed with various manganese oxide suspensions. Hydrous oxides of Mn are widely distributed in soil and sediments as discrete particles and as coating on surfaces of other minerals. One aspect of considerable interest and practical importance is the sorption of other metal ions at Mn oxide surfaces. As a result, Mn oxides deposited in aqueous systems commonly contain substantial amounts of certain other metal oxides. Viewed in another way, the concentrations of certain metal ions in natural waters may be controlled by sorption processes on Mn oxides surface.

1.2.3.2 Aluminum Oxides

Aluminum is the most abundant metal in the earth crust and an important constituent of many soils. Aluminum oxide is an amphoteric oxide of aluminum with the chemical formula Al_2O_3. It is also commonly referred to as alumina or aloxite in the mining, ceramic and materials science communities. Aluminum (hydr)oxide, $Al_2O_3 \cdot x\ H_2O$, can exist in a variety of modifications depending on a number of factors such as temperature, moisture content, particle size and impurity content. The most

thermodynamically stable phase of aluminum oxide is α-aluminum oxide, where all Al atoms are equivalent in octahedral coordination in a h.c.p. (hexagonal closest packed structure) oxide array. Besides α-Al_2O_3 (the only one thermodynamically stable anhydrous phase), several metastable transition aluminum oxides, such as γ-, θ-, and δ-Al_2O_3, also exist. Moreover, there are several important hydrated forms of alumina corresponding to the composition AlOOH and $Al(OH)_3$. γ-Al_2O_3, the most used form of alumina and one of the most used materials in any field of technologies, is mainly obtained by decomposition of the boehmite oxyhydroxide γ-AlOOH (giving medium surface area lamellar powers, ~ 100 m^2/g) or of a poorly crystallized hydrous oxyhydroxide at 600 to 800 °K, giving high surface area materials (~ 500 m^2/g) (Fierro, 2006).

Most of the solid phase in soil and natural water contain aluminum oxides. The aluminum oxides electrolyte interface plays an important role in regulating the composition of soil-water, sediment-water, and other natural water systems. Aluminum oxide is widely studied for its surface complex formation (Davis and Gloor, 1981; Stone et al., 1993; Kraemer et al., 1998; Avena and Koopal, 1999). Owing to its high surface area and positive surface charge at neutral pH conditions, Al oxide surfaces can retard the process of heavy metals and organic contaminant spreading out. Numerous experiments dealing with the adsorption of heavy metals (Kosmulski, 1997; Wootton et al., 1998) and organic compounds (Davis and Gloor, 1981; Kraemer et al., 1998; Gu and Karthikeyan, 2005) on hydrous oxides and hydroxide of Al have been reported. It has been commonly demonstrated that the mechanism with metal ions is essentially an ion exchange process in which cations replace bound protons upon adsorption. For the reaction with organic

compounds, their specific adsorption on aluminum oxide surface is interpreted in terms of a ligand exchange process in which anions of the organic compounds replace the surface hydroxo groups of the Al oxide surface (Kummert and Stumm, 1980). Surface complex formation equilibrium constants and the type of surface species formed are usually evaluated from measurements on the extent of adsorption and alkalimetric/acidimetric titration curves of the Al_2O_3 particles dispersed in the presence and absence of the chemical contaminant. Thus, the specific adsorption depends on the acid-base properties of the surface hydroxo groups of aluminum oxides, of the specifically adsorbable chemicals, and of the affinity of the surface metal ions for the chemicals.

In addition to providing a surface for adsorption as adsorptive materials, high-surface-area aluminas are widely used as catalysts and catalyst supports. α-Al_2O_3 is known as corundum which are widely applied in catalysis as supports because they have low Lewis acidity, low catalytic activity (Yamamoto et al., 2001) and they are mechanically and thermally strong. The Al^{III} atom of Al oxides has been reported as an acid center and can catalyze the dimerization (Sohn et al., 2006) and isomerization (Skotak et al., 2004) of organic compounds. Al (hydr)oxides surface may catalyze the oxidative transformation of organic compounds if oxygen is present (Karthikeyan et al., 1999). It is reasonable to expect that TCs have a strong tendency to form surface complexes with aluminum oxides (Gu and Karthikeyan, 2005). This strong interaction between aluminum oxides and TC molecules may affect the way TCs spread within the surrounding environment and induce TCs' transformation. The reaction may depend on pH and other solution variables.

1.2.3.3 Transition Metal Ions

Catalytic systems for oxidation principally depend on the efficient reversible redox processes of a catalyst, and transition metal complex catalysts are of potential importance in this respect. Various metal ions such as Mn^{II}, Fe^{II} and Cu^{I} are invoked as redox mediators in oxidation reactions when oxygen is present. The catalysis appears to depend on the reversible redox cycle of metal ion under oxygen. For example, Mn^{2+} has been shown to catalyze phosphonic acid degradation in the presence of oxygen (Nowack and Stone, 2003). The $M^{(n-1)+}$–M^{n+} system often acts as an electron carrier. A possible schematic example is given by Figure 1.5.

The oxidation of Mn^{II}, Cu^{I}, Fu^{II} and VO^{II} by oxygen is favored thermodynamically and kinetically by hydrolysis and by specific adsorption to hydrous oxide surfaces. Mn^{II} and other transition elements Fe^{II}, VO^{II} and Cu^{I} may more readily associate with O_2 if they are present as complexes with OH^- (*i.e.*, hydrolysis species) or as complexes with hydroxo surface groups of hydrous oxides (e.g., Tamura et al., 1976; Wehrli and Stumm, 1989; Wehrli et al., 1990). Figure 1.6 illustrates that hydrolysis and adsorption enhance the oxygenation of transition-metal ions.

TCs can participate with transition metal ions in chemical reactions leading to the formation of reactive oxygen species (Quinlan and Gutteridge, 1991). It has been shown that TCs caused degradation of carbohydrate in the presence of a ferric salt at pH 7.4, and this degradation involved hydroxyl radicals (Quinlan and Gutteridge, 1988). The effect of Fe^{II} is usually attributed to hydroxyl radical (•OH) formation and induced chemical transformation (Beckett and Hua, 2003). The reaction between H_2O_2 and ferrous iron

(Fe^{II}) is known to produce •OH and is commonly referred to as the Fenton process ($Fe^{2+} + H_2O_2 + H^+ \rightarrow Fe^{3+} + H_2O + \bullet OH$, Walling (1975)). The presence of Cu^{II} in advanced oxidation process may facilitate oxidation via a similar mechanism as the Fenton reaction (Walling and Kato, 1971; Kosaka et al., 1998). Besides the transition metal ion mentioned above, Al^{III} has been shown to catalyze the slow oxidation of catechol by oxygen in the pH range 4.5-7.0 (McBride and Sikora, 1990). Based on the strong tendency of TCs with interact with metal ions, it is possible that transition metal ions can induce similar reactions and lead to transformation of TCs. Equations 1-7 summarize some of the possible reactions which may occur when TCs associate with transition metal ions in the presence of oxygen (Quinlan and Gutteridge, 1988).

(1) $TC + M^{n+} \rightleftharpoons TC\text{-}M^{n+}$

(2) $TC\text{-}M^{n+} + O_2 \rightarrow TC\bullet + M^{n+} + O_2^- + H^+$

(3) $TC\bullet + O_2 \rightarrow \text{product} + O_2^- + H^+$

(4) $2O_2^- + 2H^+ \rightarrow H_2O_2 + O_2$

(5) $O_2^- + M^{n+} \rightleftharpoons M^{(n-1)+} + O_2$

(6) $TC\bullet + M^{n+} \rightleftharpoons \text{product} + M^{(n-1)+} + H^+$

(7) $M^{(n-1)+} + H_2O_2 \rightarrow M^{n+} + OH^- + \bullet OH$

Table 1.2 Half redox reactions for manganese and copper.

Reductive Half Reaction	$pe^0 = \log K$
Mn	
$\frac{1}{5}MnO_4^- + \frac{8}{5}H^+ + e^- \rightleftharpoons \frac{1}{5}Mn^{2+} + \frac{4}{5}H_2O$	+25.5[a]
$\frac{1}{2}MnO_{2(s)} + 2H^+ + e^- \rightleftharpoons \frac{1}{2}Mn^{2+} + H_2O$	+20.8[a]
$Mn^{III}OOH_{(s)} + 3H^+ + e^- \rightleftharpoons Mn^{2+}_{(aq)} + 2H_2O$	+24.51[b]
$Mn^{3+} + e^- \rightleftharpoons Mn^{2+}$	+25.52[b]
Cu	
$Cu^{2+} + e^- \rightleftharpoons Cu^+$	+2.6[a]
$\frac{1}{2}Cu^{2+} + e^- \rightleftharpoons \frac{1}{2}Cu_{(s)}$	+5.7[a]

[a] from Morel and Hering (1993); [b] from McBride (1994)

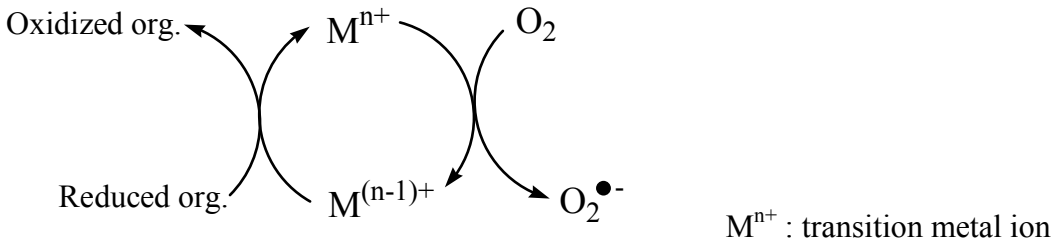

Figure 1.5 Reversible redox cycle of metal ion in the presence of oxygen

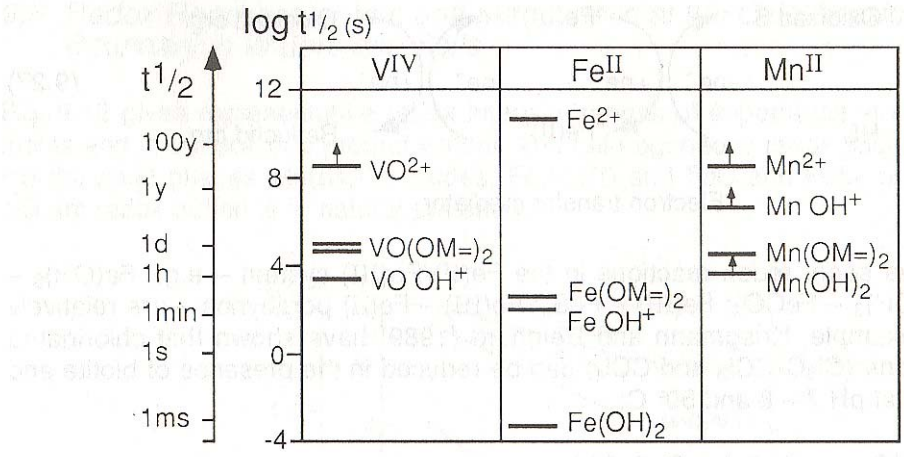

Figure 1.6 Effect of hydrolysis and adsorption on the oxygenation of transition-metal ions. Adopted from Morel and Hering (1993).

1.3 Research Tasks and Methodology

As described in the Background section, tetracycline antibiotics (TCs) have strong tendency to interact with metal species, common constituents in natural waters, soils and sediments. Such metal-TC interactions not only significantly affect the mobility of TCs in the environment and may enhance transformation of TCs. The objective of this study was to investigate the abiotic transformation of TCs in the presence of metal oxides and dissolved metal ions that are common soil constituents, and elucidate the involved reaction kinetics and mechanism. A better understanding of the interactions of TCs with environmental metal species is critical to accurately evaluate their fate in the soil-water environment and properly evaluate the risks associated with TCs.

To achieve the research objective, experiments were designed and conducted to examine the reaction kinetics and mechanism between TCs and metal species including δ-MnO_2 and γ-Al_2O_3 metal oxides and dissolved Mn^{II} and Cu^{II} ions. δ-MnO_2 and γ-Al_2O_3 were selected because of their high surface areas and the strong affinity of TCs to these oxides. Preliminary examination of a range of metal ions including Mn^{II}, Cu^{II}, Fe^{II}, Zn^{II}, Mg^{II}, and Ca^{II} found that Mn^{II} and Cu^{II} significantly enhance the oxidative transformation of TCs when oxygen is present.

Two principle methodologies were employed to achieve the goal to elucidate reaction pathways: (1) structurally related TC derivatives and isomers were selected and examined in order to distinguish the reactive site(s) of the parent compound, and (2) reaction intermediates and end-products were identified by LC/MS and UV-Vis spectroscopic techniques. Solution pH is an important variable that affects the speciation and reduction potential of reactants. Thus, the influence of pH on adsorption and transformation reaction kinetics was investigated extensively. The effect of other environmental factors such as reactant loading, the presence of co-solutes

(*e.g.*, other metal ions and natural organic matter) on the reaction kinetics and product distribution was also evaluated in order to extrapolate the experimental results to various environmentally relevant conditions. To gain more insight into the surface reaction kinetics involving tetracyclines and Mn oxides, a kinetic model that can describe the entire reaction course was developed.

1.4 Thesis Organization

As shown above, Chapter 1 states the research problem and objective of this study and provides a summary on the background information of tetracycline antibiotics (TCs) and the relevance of metal species in the aquatic environment in modulating the fate and transformation of organic contaminants such as TCs. Chapter 2 illustrates oxidative transformation mechanism of TCs by two redox-reactive metal ions (Mn^{II} and Cu^{II}) with two different catalytic cycles involved. Chapter 3 reports the successful development of a new MnO_2 suface reaction kinetic model (MnOII model) to describe the entire reaction time course of TCs with MnO_2, as well as those of three other different structural classes of antibacterial agents reported in previouse studies The reaction of TCs with MnO_2 was fast and complicated, generally rapid reaction initially followed by gradual slow down, and couldn't fit any particular order of rate equation. The validation of this model was evaluated by the influence of reactant concentration, solution pH, and the presence of co-solutes.

Chapter 4 describes the reaction kinetics of TCs with MnO_2 using the model developed in Chapter 3 and characterizes the yielded transformation products and involved reaction pathways in detail. Chapter 5 examines the non-redox transformation of TCs by Al_2O_3 and the anhyro-derivative product formation. Chapter 6 summarizes the research results and lists possible

extension studies that link to this work. Analytical methods and experimental protocols for the studies of each metal species on TC transformation are discussed in detail in each individual chapter.

CHAPTER 2

TRANSFORMATION OF TETRACYCLINES MEDIATED BY MANGANESE(II) AND COPPER(II) IONS IN THE PRESENCE OF OXYGEN

2.1 Introduction

A wide range of antibiotics are used in large quantities in human and veterinary medicine. In addition, many antibiotics are used at sub-therapeutic levels to prevent epidemics and increase the growth rate and weight gain in livestock for food production. A large percentage of the administered antibiotics are excreted from the treated hosts, and subsequently contaminate the environment via various routes. Recently, concerns have been raised regarding the occurrence of antibiotics and other pharmaceuticals in water (Graslund and Bengtsson, 2001; Thiele-Bruhn, 2003) and soil (Thiele-Bruhn, 2003). Among the antibiotics, tetracyclines (TCs) have been used extensively to treat humans for several decades, and are also the leading group of antibiotics used in animal feed. Tetracycline (TTC) and its derivatives such as oxytetracycline (OTC) and chlorotetracycline (CTC) (Figure 1.1) are widely used in nutrition and feed additives and in aquaculture (Graslund and Bengtsson, 2001). TCs can be released into the environment via municipal wastewater effluent, biosolids, animal waste and agricultural runoff. Recent studies have reported detection of TCs at about 0.15 μg/L in groundwater and surface waters (Lindsey et al., 2001), at 86-199 μg/kg in soils, at 4.0 mg/kg in liquid manure (Hamscher et al., 2002), and at 3 μg/L in farm lagoons (Qiang and Adams, 2004). The widespread use and frequent detection of TCs in the environment has raised concerns

over proliferation of antibiotic-resistant bacteria, decrease in the effectiveness of medical antibiotics, and other potential adverse human health and ecological effects (Kolpin et al., 2002). To more accurately assess the risk of TCs, a more thorough understanding of their fate in the environment is critical.

TCs possess complicated ring systems and are amphoteric molecules with multiple ionizable functional groups. The rings are lettered A through D from right to left, and the numbers begin at the bottom of ring A (Figure 1.2). Substitutions may occur at positions C1 through C12. Three macroscopic pK_a values have been reported for TCs, corresponding to the tricarbonylamide (C1, C2, C3), phenolic-diketone (C10, C11, C12) and dimethylamine groups (C4), respectively (Stephens et al., 1956; Qiang and Adams, 2004). The tricarbonylamide (A ring) and the phenolic-diketone (BCD ring) are two separate resonance groups, contributing to two major absorption bends (250-300 nm and 340-380 nm) of TCs' spectra. In general, the A ring chromophore contributes only to the 250-300 nm absorption, whereas the BCD ring chromophore contributes to both absorption bends (McCormick et al., 1957; Wessels et al., 1998; Schneider et al., 2003).

TCs are generally more stable in acidic than in alkaline conditions (Clive, 1968). TCs can undergo reversible epimerization at position C4 to form the corresponding 4-epi-TCs. The only difference between TCs and their epimers is the $-N(CH_3)_2$ group's position: when the $-N(CH_3)_2$ group flips from down to up position with respect to the ring plane, epi-TCs are formed. The epimerization process gradually occurs at pH 2-6 (McCormick et al., 1957); however, its rate can be enhanced by the presence of certain anions such as phosphate and citrate (Sokoloski et al., 1977; Yuen and Sokoloski, 1977). OTC epimerizes less willingly than TTC and CTC because its hydroxyl group at the C5

position may form a hydrogen-bond with the dimethylamine group (Hussar et al., 1968). At alkaline pH, TCs that have a hydroxyl group at C6 cleave readily to from their respective iso-TCs (McCormick et al., 1957). Among TCs, CTC is especially prone to this irreversible transformation to yield iso-CTC quickly (Figure 1.2) (Waller et al., 1952; Stephens et al., 1954).

TCs have a strong tendency to complex with metal ions (Jezowska-Bojczuk et al., 1993; Tongaree et al., 1999). Previous studies have reported that both the A and BCD rings are probable metal complexation sites. Mitscher *et al.* analyzed the extensive circular dichroism (CD) spectra for a series of TCs and a variety of metal ions and concluded that complex formation occurs through oxygen coordination at the BCD ring (Mitscher et al., 1972). Other studies, however, suggest the oxygen at C3 was the most probable binding site for metal complexes (Baker and Brown, 1966; Lee and Everett, 1981; Mikulski et al., 1988) because a six-membered chelate ring was formed in combination with the amide group oxygen. Chelation involving both the A and BCD rings were also commonly suggested (Colaizzi et al., 1965; Caswell and Hutchison, 1971; Jogun and Stezowski, 1976; Wessels et al., 1998). Owing to their strong metal complexation, the *in vivo* antibiotic activity of TCs is dictated by their Mg^{II} and Ca^{II} complexes (Lambs et al., 1984).

TCs may undergo abiotic degradation depending on pH, redox, and light conditions (Clive, 1968; Halling-Sorensen et al., 2003), and are prone to adsorption to soils (Tolls, 2001; Figueroa and MacKay, 2005; Pils and Laird, 2007). The strong metal-binding tendency of TCs contributes to strong and specific interactions with mineral surfaces (Figueroa and MacKay, 2005; Gu and Karthikeyan, 2005; Pils and Laird, 2007) and

organic matter (MacKay and Canterbury, 2005), and affects their photoreactivity in natural waters (Werner et al., 2006). The present study examined a range of metal ions including Mn^{II}, Cu^{II}, Fe^{II}, Zn^{II}, Mg^{II}, and Ca^{II} for their potential effect on the transformation of TCs and related isomers. Among the metal ions, Mn^{II} and Cu^{II} can significantly enhance the transformation of TCs with the presence of oxygen required by the Mn^{II}-mediated reaction. These two metal ions apparently operate via different mechanisms to facilitate the transformation of TCs. A range of TCs, their isomers, and reaction conditions were examined to probe the reactive sites of TCs and the involved mechanisms.

2.2 Materials and Methods

2.2.1 Chemicals

TTC, OTC and CTC were obtained from Sigma at 90-98% purity. Epi-TCs, iso-CTC, bathocuproinedisulfonic acid disodium hydrate, sodium pyrophosphate decahydrate and ethylenediamine were obtained from Acros at higher than 98% purity. Copper(I) bromide was obtained from Stern. All other reagents used (*e.g.*, buffers, NaCl, acids, etc.) were obtained from Fisher Scientific, Acros or Aldrich at analytical grade. Superoxide dismutase (MP Biomedicals, from bovine erythrocytes) solution were prepared by dissolving 15 KU of the lyophilized powder in 2 mL water and adding it to 20 mL of reaction mixture to give *ca.* 100,000 units L^{-1}. All reagent solutions were prepared using water from a Millipore Milli-Q Ultrapure Gradient A10 purification system. Stocks of

TCs were prepared in methanol at 1.6 mM, protected from light, stored at -15ºC, and used within a month of preparation.

2.2.2 Reaction Setup

All glassware was soaked in 5 N HNO_3 and thoroughly rinsed with reagent water prior to use. Batch experiments were conducted in 30 mL screw-cap amber glass bottles with Teflon septa at room temperature (22-25ºC). All the reactions were homogeneous and thus no additional mixing was needed. Reactions with Mn^{II} ions and oxygen were maintained at pH 8-9.5 with 10 mM 2-(cyclohexylamino)ethanesulfonic acid (CHES) buffer. Reactions were initiated by adding certain amounts of the antibiotic stock to solutions containing Mn^{II} ions, buffer, and constant ionic medium. Oxygen was purged to the reactors for 2 minutes every time after taking sample aliquots for analysis. Similar experiments were conducted but with nitrogen purging to evaluate the role of O_2. Reaction aliquots were collected periodically and quenched by adding HCl to a pH around 2 because little TC-metal ion complex formation occurred at this low pH and thus the metal-facilitated transformation of TCs stopped (Ohyama and Cowan, 1995). The acidification also improved the stability and analytical results of the parent TC compounds. The samples were then stored in 2 mL amber vials at <5 ºC and analyzed within a couple days. The experimental setup for the reactions of TCs with Cu^{II} ions were similar to that with Mn^{II} ions except that the pH was maintained at 4-5.5 with 10 mM acetic acid/sodium acetate buffer and active O_2 purging was not used (the reactors were still exposed to the ambient air). Preliminary results showed that the reaction rate of

TCs within hours to days of reaction periods were nearly the same with and without active O_2 purging. All experiments were performed in duplicate. Control experiments without metal ions were also conducted under the same conditions.

2.2.3 Analysis of TCs, Mn^{II} ions, Cu^{I} Ions and Metal-TC Complexes

The concentration of TCs was measured by an Agilent 1100 high performance liquid chromatography (HPLC) system with a DAD UV detector and an Agilent Zorbax RX-C_{18} column (250×4.6 mm, 5 μm) coupled with a guard column. The mobile phase A was 0.01 M oxalic acid and 10 μM ethylenedinitrilotetraacetic acid (EDTA), while the mobile phase B was pure acetonitrile. Both mobile phases were degassed by ultra-sonication for 3 minutes. The gradient was as follows: 0-3 min 96% A and 4% B; 3-10 min a linear gradient to 73.7% A and 26.3% B; 10.0-19.0 min 73.7% A and 26.3% B; and 19.0-25.0 min linear gradient to 96% A, and 4% B. This final mixture was maintained for the remainder of the 30 minute run time. The injection volume was 100 μl and the flow rate was 1 mL/min. The UV detector was set at 275 nm and 365 nm.

Mn^{II} concentration was measured by Inductively-Coupled Plasma (ICP)-Atomic Emission Spectrometry (AES) (Thermo Jarrell Ash Corporation, ICAP 61E Trace Analyzer). All samples were filtered by pre-wetted 0.22 μm Millipore GVWP membranes and acidified with 1% nitric acid prior to analysis. Formation of Cu^{I} was detected photometrically as an orange bathocuproine (2,9-dimethyl-4,7-diphenyl-1,10-phenanthroline) complex measured by a Beckman DU520 UV/Vis spectrophotometer at λ_{max}=484 nm according to Moffett *et al.* (1985). Samples were taken after 20 hours of reaction time and 0.02 M ethylenediamine was added before the bathocuproine addition

to ensure complete complexation of Cu^{II} by ethylenediamine in order to mask the interference from Cu^{II} ions (Moffett et al., 1985). In these experiments, N_2 was purged throughout the entire time to prevent oxidation of Cu^{I} by O_2.

Complexation of TCs with Cu^{II} or Mn^{II} ions was examined photometrically at varying metal-to-ligand ratios. For complexation with Cu^{II}, the TC solution was kept at pH 5 with 10 mM acetate buffer and titrated by $CuCl_2$. The sample was allowed to equilibrate for 1 min and then transferred to a 4-mL quartz cuvette (1 cm optical path length) and analyzed by a UV/Vis spectrophotometer. $Abs^{(X)}$ represents the absorbance of a solution containing electrolyte, buffer and reagent X. At a fixed wavelength, the increase in absorbance due to complexation (called ΔAbs) was calculated from the following equation:

$$\Delta Abs = Abs^{(\text{metal ion + TCs})} - Abs^{(\text{metal ion only})} - Abs^{(\text{TCs only})} \qquad \text{(eq. 1)}$$

The $Abs^{Cu(II)}$, Abs^{TCs} and $Abs^{Cu(II)+TCs}$ were measured at 276-286 and 374-386 nm, where the maximum ΔAbs from Cu^{II} complexation was observed. For complexation with Mn^{II}, the TC solution was maintained at pH 9 with 10 mM CHES buffer and titrated by $MnCl_2$. The $Abs^{Mn(II)}$, Abs^{TCs} and $Abs^{Mn(II)+TCs}$ were measured at 290 and 350 nm, where the maximum ΔAbs from Mn^{II} complexation was observed.

2.2.4 Product Analysis

To identify reaction intermediates and products, reaction mixtures (~70% TC conversion) were concentrated 100 times by a blowdown device with N_2 gas, and analyzed by an Agilent 1100 HPLC/DAD/MSD system. The separation was performed by a Zorbax SB-C18 column (2.1×150mm, 5 μm) at a flow rate of 0.2 mL/min with two

mobile phases as described above. Mass spectrometric analysis was conducted by positive electrospray ionization at both low and high fragmentation voltages (110 and 250 eV) with a mass scan range of *m/z* 50-1000. The drying gas was at 10 L/min at 350°C, the nebulizer pressure 25 psig, and the capillary voltage 4000 V.

2.2.5 Complexation Calculation

The computer program MINEQL+ (Version 4.5) (Schecher and McAvoy, 2001) was used to calculate the complex formation between metal ion (Mn^{II} and Cu^{II}) and tetracycline (TTC) in this study. The equilibrium calculations were based on the stability constants listed in Table 1.1. Only the $MnHTC^{+}$ complex had a reported stability constant and thus was included in the calculations. Under the experimental conditions of $[TTC]_0 = [Mn^{2+}]_0 = 40$ μM and pH = 9, calculations showed that around 50% of TTC complexes with Mn^{II} ions forming $MnHTTC^{+}$. Reported stability constants were available for four Cu^{II}-TC complexes ($CuHL^{+}$, CuH_2L^{2+}, $CuH_2L_2^{0}$, $CuH_4L_2^{2+}$) and all four were included in the calculations. Under the experimental conditions of $[TTC]_0 = 40$ μM, $[Cu^{2+}]_0 = 1$ mM and pH = 5, 99% of TTC complexes with Cu^{II}, predominantly in the form of $CuHTC^{+}$. The stability constants of EDTA-Mn^{II} and EDTA-Cu^{II} complexes suggest that EDTA is an effective ligand to prevent the complexation of Mn^{II} and Cu^{II} with TTC. When 40 μM of EDTA was added in the Mn^{II}-mediated reaction and 0.05 M of EDTA was added in the Cu^{II}-mediated reaction, the Mn^{II}-TTC and Cu^{II}-TTC complex formation were completely inhibited.

To investigate the impact of competing metal ions on the reaction rate of TTC with Mn^{II} in the presence of oxygen, a high concentration of Mg^{II} or Ca^{II} (0.8, 4 and 8 mM)

was premixed with a high concentration of TTC (0.8 mM) and then the mixture was introduced into the reactor containing Mn^{II}. The pre-mixing ensured formation of Mg^{II}-TTC or Ca^{II}-TTC complexes at the beginning of the reaction with Mn^{II} and O_2. The percentages of TTC complexed with Mg^{II} versus with Mn^{II}, or complexed with Cu^{II} versus Mn^{II} were calculated by MINIQL+ using the stability constants listed in Table 1.1. As shown in Table 2.1, with the higher Mg^{II} or Ca^{II} co-solute concentration, TTC tended to complex with the co-solute metal ion, resulting in low Mn^{II}-TTC complexation. The complexation efficiency for Mg^{II}-TTC and Ca^{II}-TTC complexes is similar.

2.3 Results

2.3.1 Mn^{II}-Mediated Transformation of TCs

2.3.1.1 pH Effect

While TTC was stable in the absence of metal ions, significant loss of TTC occurred in the presence of Mn^{II} ions and oxygen at pH 8-9.5 (Figure 2.1a). The rate of TTC disappearance followed pseudo-first-order kinetics with active oxygen purging, otherwise deviated from first-order decay. If oxygen was excluded from the solution, degradation of TTC ceased to occur (Figure 2.1a). Equilibrium calculations indicated that about 50% of TTC was complexed with Mn^{II} ions under the employed experimental conditions ($[TTC]_0 = [Mn^{II}]_0 = 40$ μM, pH 9).

The TTC transformation rate constant (k in h^{-1}) increased linearly with log $[Mn^{II}]_0$ (Figure 2.2). Adding 40 μM of the strong chelating ligand EDTA to the solution inhibited the degradation of TTC by Mn^{II} and oxygen (Figure 2.1a), indicating that

complexation of TTC with Mn^{II} is crucial for the reaction to occur. The Mn^{II} ion concentration was found to maintain at a constant level close to $[Mn^{II}]_0$ throughout the reaction, and no precipitation of Mn(III/IV) oxide was observed. Complete degradation of TTC could be achieved when the added Mn^{II} ion concentration was only one-eighth of the initial TTC concentration, suggesting a catalytic role of Mn^{II}. Attempts were made to measure Mn^{III} as Mn^{III}-pyrophosphate complex with absorbance at 484 nm (Klewicki and Morgan, 1998); however, Mn^{III} was not detectable. Adding radical species scavengers, *i.e.*, superoxide dismutase (SOD) for superoxide radical (Megan et al., 2005) or *t*-butyl alcohol for hydroxyl radical (Canle L et al., 2005), to the reaction exerted little effect on the rate of TTC loss with Mn^{II} and oxygen, indicating that $O_2^{\bullet-}$ and •OH was not responsible for the disappearance of TTC. Within pH 8.0-9.5, the rate constant of TTC transformation increased with increasing pH (Figure 2.3).

2.3.1.2 Competing Ion Effect and Reactivity Trend

To evaluate the impact of competing metal ions on the reaction of TTC with Mn^{II} in the presence of oxygen, TTC was pre-mixed with Mg^{II} or Ca^{II} ions before being added to the reactor containing Mn^{II} ions, with the overall conditions of $[TTC]_0 = [Mn^{II}]_0 = 40$ μM, [Mg^{II} or Ca^{II}]$_0$ = 0-400 μM and pH 9. Equilibrium calculations showed that the TTC-Mn^{II} complex decreased from being 50% of the total TTC to 6.4% and 5.2% of the total TTC as Mg^{II} and Ca^{II} concentrations were increased, respectively, leading to a greater proportion of Mg^{II}- or Ca^{II}-complexed TTC. The presence of Mg^{II} or Ca^{II} both decreased the degradation rate of TTC with Mn^{II}; the inhibitory effect of Mg^{II} was

proportionally greater with higher Mg^{II} concentration, but the inhibitory effect of Ca^{II} did not correlate to Ca^{II} concentration (Figure 2.4).

Similar experiments with Mn^{II} ions and oxygen at pH 9.0 were also conducted for epi-TTC, OTC, epi-OTC and iso-CTC. Iso-CTC, instead of CTC, was examined because CTC transformed to iso-CTC quickly (in hours) at pH 9.0. Results showed degradation of all compounds except for iso-CTC; the degradation rate followed the order of OTC > epi-OTC ~ TTC > epi-TTC >> iso-CTC (Figure 2.1b).

2.3.2 Cu^{II}-Mediated Transformation of TCs

2.3.2.1 pH Effect

The degradation of TTC in the presence of Cu^{II} was studied at pH 4-6 because of precipitation of $Cu(OH)_2(s)$ at higher pH. In the experiments, 1 mM of Cu^{II} was used to ensure sufficient TTC-Cu^{II} complex formation. Equilibrium calculations showed that approximately 99% of TTC was complexed with Cu^{II} under the employed experimental conditions ($[TTCs]_0$ =40 μM, $[Cu^{2+}]_0$ =1 mM, pH 5). Compared to negligible degradation in the absence of metal ions, the presence of Cu^{II} significantly promoted TTC degradation (Figure 2.5a). The TTC degradation followed pseudo-first-order kinetics, and the rate constant (k in h^{-1}) increased with increasing pH (except for the last data point) (Figure 2.6) and with increasing Cu^{II} concentration (Figure 2.7). Addition of SOD had little impact on the reaction. Adding excess amounts of EDTA (0.05M) significantly decreased the reaction rate (Figure 2.5a). In contrast to the Mn^{II}-mediated transformation, oxygen was not absolutely needed in the reaction with Cu^{II}; transformation of TTC, although slower, still occurred when oxygen was excluded (Figure 2.5a). It was suspected that TTC was

oxidized by Cu^{II}, yielding Cu^{I}. The accumulation of Cu^{I} in the reaction solution when oxygen was excluded was confirmed by the method by Moffett *et al*. (1985) (Figure 2.8).

2.3.2.2 Competing Ion Effect and Reactivity Trend

Addition of competing metal ions including Mg^{II}, Ca^{II} and Zn^{II} at up to 2 mM did not affect the reaction of TTC with Cu^{II} at pH 5; equilibrium calculations indicate that the complexation of TTC with these metal ions was negligible at this acidic condition. Different than the reactivity trend observed with Mn^{II}, the degradation rate with Cu^{II} were in a reverse order of CTC > TTC > OTC ~ epi-CTC > epi-OTC and epi-TTC (Figure 2.5b).

2.3.3 Complexation of TCs with Mn^{II} and Cu^{II} Ions

A slight, but discernable peak shift of TTC's UV spectrum at 290 and 350 nm occurred when Mn^{II} was added at pH 9 (Figure 2.9a). Complexation with Cu^{II} at pH 5 caused a greater peak shift (Figure 2.9b), with severe peak broadening at 275 nm and strong peak shift at 365 to 380 nm. UV absorbance values were obtained within 10 minutes after adding Mn^{II} or Cu^{II} into the TC solution. Within this time period, TC degradation was negligible (< 0.3%) and the absorbance change was due only to complexation. The change in UV absorbance with increasing Mn^{II}-to-TC ratio was measured at 290 and 350 nm (ΔAbs_{290} and ΔAbs_{350}) for TTC, OTC and iso-CTC (Figure 2.10). The change in UV absorbance with increasing Cu^{II}-to-TC ratio was measured at selected wavelengths within 276-286 nm and 374-386 nm ($\Delta Abs_{276\text{-}286}$ and $\Delta Abs_{373\text{-}386}$) for TTC, OTC, CTC and their epimers (Figure 2.11). The observable ΔAbs indicated

metal-TC complex formation but could not distinguish specific complexes (*i.e.*, 1:1, 1:2 and/or 2:1 metal-to-TC complexes). It is possible that 2:1 complex was formed at higher metal-to-ligand ratio (Jezowska-Bojczuk et al., 1993; Wessels et al., 1998). In order to compare the complexation of Cu^{II} with various TCs in the same plot, the measured ΔAbs values for each TC compound at varying $[Cu^{II}]/[TC]$ ratios were normalized by the ΔAbs value of its $[Cu^{II}]:[TC] = 1:1$ complex (Figure 2.11).

As mentioned earlier, both the A ring and BCD ring chromophores contribute to the 250-300 nm absorption, while only the BCD ring chromophore contributes to the 340-380 nm absorption (McCormick et al., 1957; Wessels et al., 1998; Schneider et al., 2003). TTC and OTC showed absorbance change at 290 nm and 350 nm with increasing Mn^{II} concentration (Figure 2.10), suggesting that complexation with Mn^{II} could occur at either the A ring and/or the BCD ring. However, iso-CTC showed absorbance change only at 290 nm and had little absorbance at 350 nm despite increasing Mn^{II} concentration (Figure 2.10b). Iso-CTC's lack of absorbance at 350 nm coincides with its inactivity to Mn^{II} in the presence of oxygen, raising the possibility that the BCD ring may be the crucial site to be susceptible to the Mn^{II}-mediated reaction once complexed with Mn^{II}.

As shown in Figure 2.11, $\Delta Abs_{276\text{-}286}$ and $\Delta Abs_{374\text{-}386}$ both increased with increasing Cu^{II} for all TCs, suggesting that complexation with Cu^{II} could occur at either the A ring and/or the BCD ring. However, there is no obvious order for the normalized $\Delta Abs_{374\text{-}386}$. In contrast, the normalized $\Delta Abs_{276\text{-}286}$ values were in good agreement with the degradation kinetic trend: CTC, with the highest $\Delta Abs_{276\text{-}286}$, has the fastest reaction rate, followed by TTC and OTC. In addition, all epi-TCs showed negligible $\Delta Abs_{276\text{-}286}$, coinciding with their inactivity to reaction with Cu^{II} and oxygen. The above results

suggest that the A ring is likely the crucial reactive site for the reaction mediated by Cu^{II} once it is complexed with Cu^{II}

2.3.4 Transformation Product Evaluation.

Reactions of TCs with Mn^{II} and Cu^{II} also appeared to yield different products. When analyzed by HPLC-UV, the degradation products from the Cu^{II}-mediated reaction showed absorbance at 365 nm, while the degradation products from the Mn^{II}-mediated reaction did not (Figures 2.12 and 2.13). This result indicates that the reaction with Mn^{II}, not the reaction with Cu^{II}, disrupted the BCD ring's phenolic-diketone resonace, and supports the hypothesis that the BCD ring is the key reactive site with Mn^{II}. When analyzed by LC/MS, the Mn^{II}-mediated reaction of TTC yielded a (M + 14) and a (M + 16) products (M = the molecular weight of TTC), suggesting insertion of oxygen. The Cu^{II}-mediated reaction yielded two (M – 18) and a dimer (*m/z* 849) products, suggesting water loss and radical coupling.

2.4 Discussion

2.4.1 Proposed Mechanism for Mn^{II}-Mediated Reaction.

The experimental results show that Mn^{II} ions can promote the oxidation of TCs in a catalytic fashion with oxygen as the ultimate oxidant at pH 8.0-9.5. The oxidation rate of Mn^{II} by oxygen to yield Mn^{III} and superoxide radical anion ($O_2^{\bullet -}$) in simple aqueous media is proportional to $[OH^-]^2$, and only becomes appreciable at approximately above pH 9.0 (Morgan, 2004). The half-life of Mn^{II} oxidation by oxygen is estimated at 60 to

611 hours using the reported rate constants in different laboratory buffer solutions (Morgan, 2004) and the conditions employed in this study (*i.e.*, pH = 9.0, P_{02} = 0.21 atm, T = 25°C), considerably longer than the measured half-life of 44 hours for TTC degradation in the presence of Mn^{II} and O_2 (Figure 2.1a). Furthermore, while the rate constant of TTC degradation increased from pH 8.05 to 9.43, the trend does not correlate well to the increased oxidation rate constant of Mn^{II} by oxygen (Morgan, 2004) (Figure 2.2). Similar results were also observed with OTC. Therefore, the degradation of TC in the TC-Mn^{II}-O_2 system cannot be explained by the oxidation of free Mn^{II} by oxygen to generate Mn^{III}, $O_2^{\bullet-}$ and other reactive oxygen species (ROS) which then oxidize TC.

Nowack and Stone (2000, 2003) reported a Mn^{II}-mediated oxidation of phosphonates in the presence of oxygen: the reaction began with complexation of Mn^{II} with phosphonate followed by oxidation of the phosphonate-complexed Mn^{II} to Mn^{III} by oxygen and subsequent oxidation of phosphonate by Mn^{III} to return to Mn^{II}. Overall, Mn^{II} participated in the redox reaction in a catalytic cycle. For the TTC-Mn^{II}-O_2 system, the importance of Mn^{II}-TTC complexation for the degradation of TTC to occur was confirmed by (i) the inhibitory effect of competitor metal ions (Mg^{II} and Ca^{II}) and ligand (EDTA) on the reaction rate, and (ii) the increasing reaction rate with higher [Mn^{II}], which corresponds to a greater proportion of Mn^{II}-complexed TTC. The above observations are similar to those by Nowack and Stone, suggesting that a similar mechanism is likely operative for TTC. As proposed in Figure 2.12a, the TC molecule first forms a strong complex with Mn^{II}. Complexation with TC facilitates the oxidation of Mn^{II} by O_2 because TC helps stabilize Mn^{III}. The generated Mn^{III} then oxidizes TC within the complex to produce a TC radical and converts back to Mn^{II}. The TC radical

may further react with oxygen, $O_2^{\bullet-}$ or another TC radical to yield the products. Other possible sinks for $O_2^{\bullet-}$ in this reaction scheme may include reaction with Mn^{II} (Pick-Kaplan and Rabani, 1976), reaction with TC (Suzuki et al., 1998), and self-disproportionation (Bielski and Allen, 1977). Overall, Mn^{II} plays a catalytic role in the oxidation of TCs by O_2 and the cycle can continue in the presence of sufficient oxygen. Note that the inability to detect Mn^{III} in the system is not too surprising since it is possible that the Mn^{III} concentration was quite low at any given time due to its high reactivity and/or the strong pyrophosphate complex of Mn^{II} might prevent its interactions with TTC and thus quenched the reaction.

The above reaction scheme involves superoxide radical and its disproportionation (Reaction 1) and thus potential Fenton reaction needs to be considered, *i.e.*, Mn^{II} reacts with hydrogen peroxide to yield hydroxyl radical (Reaction 2):

$$2\ O_2^{\bullet-} + 2\ H^+ \rightarrow H_2O_2 + O_2 \qquad \text{(Reaction 1)}$$

$$M^{n+} + H_2O_2 \rightarrow M^{(n+1)+} + OH^- + \bullet OH \qquad \text{(Reaction 2)}$$

Superoxide radicals, however, were shown to be unimportant for the loss of TCs in the reaction based on the SOD expereimntal results. Hydroxyl radical, if formed by the Fenton reaction, would be a powerful oxidant to oxidize TC and Mn^{2+}. Hydroxyl radical did not appear to be important in the degradation of TTC with Mn^{II} and O_2 either because of (i) the little effect of •OH scavenger *t*-BuOH on the reaction, and (ii) the apparently different oxidation products produced from the Mn^{II}- versus Cu^{II}-mediated reactions; since the Fenton reaction is also possible with reduced copper (see more discussion later), reaction of TTC with the non-selective •OH oxidant should yield similar products from both systems.

The rate of TTC degradation increased with increasing pH (Figure 2.3); this may be caused by the increased rate of Mn^{II} oxygenation as discussed above, by the decreased rate of $O_2^{\bullet-}$ disproportionation (Bielski and Allen, 1977), and by the change of TTC speciation. Figure 2.3 shows that the rate of TTC degradation correlated quite well to the mole fraction of the fully deprotonated species (*i.e.*, L^{2-}) as pH was increased. The significance of the L^{2-} species may be related to (i) its higher negative charge and thus stronger affinity to complex with Mn^{II} cation compared to the other TTC species (H_3L^+, H_2L^0 and HL^-); unfortunately the abundance of the MnL^0(aq) complex in the reaction could not be calculated (in section 2.2.5) because the stability constant was not available, (ii) its high electron density that should better stabilize the generated Mn^{III}, and (iii) possibly its conformation (see below).

Stezowski and co-workers reported that TCs display two conformations at different pH or for different metal ion coordination (Stezowski, 1976; Prewo and Stezowski, 1977; Hughes et al., 1979). A conformation change from twisted to extended is caused by a rotation of the C4a-C12a bond (Hughes et al., 1979). In aqueous solutions, TCs adopt the twisted conformation at low pHs while adopting the extended conformation at high pHs. In other words, the H_3L^+, H_2L^0 and HL^- species are in the twisted conformation whereas the L^{2-} species in the extended conformation (Stezowski, 1976; Wessels et al., 1998). Lee reported that Mn^{II} coordinates to TTC in the extended conformation by forming chelate rings with two oxygen sites of the ring A tricarbonylmethane and also the oxygens attached at C12 and C12a (Lee and Everett, 1981). The same conformation may render L^{2-} and Mn^{II} complexation more favorable and therefore facilitate the reaction.

Furthermore, in the study of the effect of competing Mg^{II} and Ca^{II} ions, TTC was pre-mixed with Mg^{II} or Ca^{II} co-solute before being added to the reactor containing Mn^{II}.

Complexation with either Mg^{II} or Ca^{II} both decreased the degradation rate of TTC with Mn^{II} and oxygen, but with different trends. The rate constant decreased steadily as the Mg^{II} co-solute concentration was increased; in contrast, increasing the Ca^{II} co-solute concentration did not proportionally decrease the reaction rate (Figure 2.2). In general, Mg^{II} appeared to inhibit the reaction more effectively than Ca^{II}, particularly at lower co-solute concentration, despite that Mg^{II} and Ca^{II} have similarly strong affinity to complex with TTC. Wessels *et al.* suggested that in aqueous solutions at pH 8.0, Ca^{II} forms a 1:2 ligand:metal complex with TTC and induces the extended conformation of TTC, which is stabilized through hydrogen bonding between the deprotonated dimethylamino nitrogen, N4, and OH12a. In contrast, Mg^{II} binds to N4-O3 and thereby stabilizes the twisted conformation of TTC (Lambs et al., 1988; Wessels et al., 1998). Pre-complexation with Ca^{II} may still allow the TTC to coordinate with Mn^{II} because of the similar conformation as long as the Ca^{II} concentration was not high enough to occupy all of the available functional groups of TTC for metal coordination. On the contrary, complexation with Mg^{II} adopts the twisted conformation that is unfavorable for Mn^{II} coordination and thus effectively lowers the reaction rate.

2.4.2 Proposed Mechanisms for Cu^{II}-Mediated Reaction.

Similar to the reaction with Mn^{II}, TC-Cu^{II} complexation is a critical step in the degradation of TC with Cu^{II}, as highlighted by (i) the inhibitory effect of competing ligand EDTA on the reaction rate (Figure 2.5a), and (ii) the increasing rate constant with

increasing Cu^{II} concentration (Figure 2.7), which corresponds to a greater proportion of Cu^{II}-complexed TTC. However, the different requirement for oxygen, reactivity trend among TCs and product formation in the presence of Cu^{II} than those with Mn^{II} and O_2 clearly suggest a different reaction mechanism. As proposed in Figure 2.14b, the TC molecule first forms a strong complex with Cu^{II}. Cu^{II} is the oxidant within the complex to oxidize TC, forming Cu^{I} and a TC radical. Without oxygen, the TC radical can be further oxidized by Cu^{II} or couples with another TC radical to yield products and Cu^{I} accumulates in the system as confirmed by its detection in the oxygen-free experiments. With the presence of oxygen, the TC radical can be intercepted by oxygen to yield TC oxidation products, and Cu^{I} can be oxidized back to Cu^{II} by oxygen. In the latter, the superoxide generated may react with Cu^{II} (Quinlan and Gutteridge, 1991), TC and/or TC radical, and disproportionate (Reaction 1). In the presence of oxygen, Cu^{II} plays a catalytic role in the overall reaction with oxygen as the ultimate oxidant.

As mentioned earlier, superoxide radical did not appear to important to affect eh rate of TC loss in the presenence of Cu^{II} and oxygen. Whether the Fenton reaction of Cu^{+} to produce •OH radical contributes to the degradation of TCs in the TC-Cu^{II}-O_2 system is evaluated here. Quinlan and Gutteridge (1988, 1991) reported that TTC, in the presence of Cu^{II}, brings about oxidative damage to DNA bases, and hypothesized that TTC can react with Cu^{II} and oxygen to generate ROS including $O_2^{\bullet-}$ and •OH to oxidize DNA molecules. The •OH radicals are powerful, but non-selective oxidants. The Fenton reaction does not appear to be important for the degradation of TCs in the TC-Cu^{II}-O_2 system because that different TCs with almost identical structures (e.g., TCs and their

epimers) showed drastically different degradation rates, and similar products were formed in the presence and absence of oxygen.

The rate constant of TTC degradation increased when pH was increased from 4 to 5.5 (Figure 2.4). No $Cu(OH)_2(s)$ precipitation occurred at pH 6.0 and the drop-off in *k* may be related to the different pH buffer at pH 6.0 (MES) than that of pH 4-5.5 (acetate) (Figure 2.4). At pH 4-6, the dominant TTC species have the same twisted conformation (Jezowska-Bojczuk et al., 1993). The increase of rate constant with increasing pH is likely related to (i) an increasingly deprotonated TTC molecule should be more susceptible to oxidation, and (ii) an increasing proportion of Cu^{II}-copmlexed TTC as pH increases).

2.4.3 Reactive Moieties of TCs

For the TC-Mn^{II}-O_2 system, the degradation rate followed the order of OTC > epi-OTC ~ TTC > epi-TTC >> iso-CTC (Figure 2.1b). The most significant structural difference of iso-CTC than the other TCs was the disruption of the phenolic-diketone resonance in the BCD ring resulted from a cleaved bond at C6 (Figure 1.2). This disrupted resonance appeared to lead to poor complexation of iso-CTC's BCD ring with Mn^{II} and thus inactivity to the Mn^{II}-mediated reaction. Analysis of the transformation products of TTC and OTC confirmed that their BCD ring was altered by reaction with Mn^{II} and oxygen. Together, these results strongly suggest that the BCD ring of TC is the primary reactive site for the Mn^{II}-mediated transformation in the presence of oxygen. There are no clear explanations for the higher reactivity of OTC than TTC based on the current experimental data. However, OTC and TTC differ at the BCD ring, where OTC

has one additional –OH substituent at the C5 position than TTC, consistent with the proposed reactive site.

For the TC-Cu^{II}-O_2 system, the reactivity followed a reverse order of CTC > TTC > OTC >> epimers (Figure 2.5b). The epimers have only the change in the position of the A ring's dimethylamine group (-$N(CH_3)_2$) compared to their original counterparts. The inactivity of the epimers in the Cu^{II}-mediated reactions indicates that the A ring plays an important role in the reaction. The complexation study yielded spectrophtometric evidence that complexation with Cu^{II} can occur at either the A, BCD or both ring systems. The possible complexation sites on the BCD ring and A ring are C10-C12 and C1-C3 respectively (Jezowska-Bojczuk et al., 1993; Wessels et al., 1998). However, only the complexation to the A ring exhibits a consistent trend similarly to the trend of reactivity among the TC compounds. The preference of Cu^{II} for ligands with N-donor atoms is well established in the literature (Housecroft and Sharpe, 2001). Figure 2.11 shows a sharp rise followed by a languid increase of both normalized ΔAbs at 276-286 nm and 374-386 nm. Because metal ions tend to complex with TCs through the BCD ring when the pH is lower than 7.5 (Mitscher et al., 1972), it is likely that the sharp increase was mostly caused by the BCD ring chromophore when the Cu^{II} to TC ratio was below 1. The following ΔAbs increase (Cu^{II}:TC > 1) may be due to the complexation of TC with the A ring. The above results together strongly suggest that the A ring of TCs is the critical site for the Cu^{II}-facilitated transformation. The lower reactivity of OTC (than TTC and CTC) may be due to the hydroxyl group at the C5 position of OTC interfering with the -$N(CH_3)_2$ group to complex with Cu^{II} (Hussar et al., 1968).

Overall, both Mn^{II} and Cu^{II} ions are found to be able to mediate the oxidative transformation of TCs in the presence of oxygen via a catalytic fashion. However, the two redox reactive metal ions catalyze the transformation of TCs via different mechanisms and at different structural moieties. The strong metal complexation tendency of TCs will plays a significant role in their environmental fate. The results of this study show that the transformation of TCs can initiate via different moieties with different metal ions. Therefore, the reactivity of TC members may differ significantly when different metal species are involved.

Table 2.1 Effect of competing Mg^{II} or Ca^{II} ions on the complexation of TTC with Mn^{II} ($[TTC]_0 = [Mn^{2+}]_0 = 40$ μM, pH 9).

Co-solute / TTC to M^{2+} ratio	Metal-TTC complex (%Total TTC)			
	Mg^{2+} as co-solute		Ca^{2+} as co-solute	
	Mg^{II}-TTC	Mn^{II}-TTC	Ca^{II}-TTC	Mn^{II}-TTC
no M^{2+}	N.A.	49.6	N.A.	49.6
TTC:M^{2+}= 1:1	42.3	32.7	45.0	31.5
TTC:M^{2+}= 1:5	81.9	11.5	84.0	10.2
TTC:M^{2+}= 1:10	90.4	6.2	91.7	5.4

(M^{2+} = Mg^{2+} or Ca^{2+})
(N.A. = not applicable)

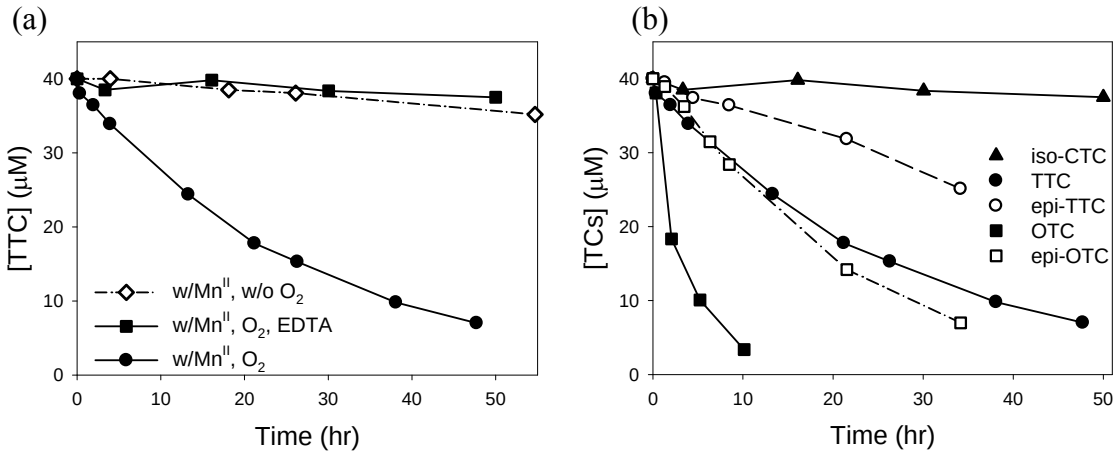

Figure 2.1 (a) Reaction of TTC with Mn^{II} in the presence and absence of O_2 and EDTA. ($[TTC]_0 = [Mn^{II}] = [EDTA] = 40$ μM, pH 9); (b) Reaction of varies TCs in the presence of Mn^{II} and O_2.

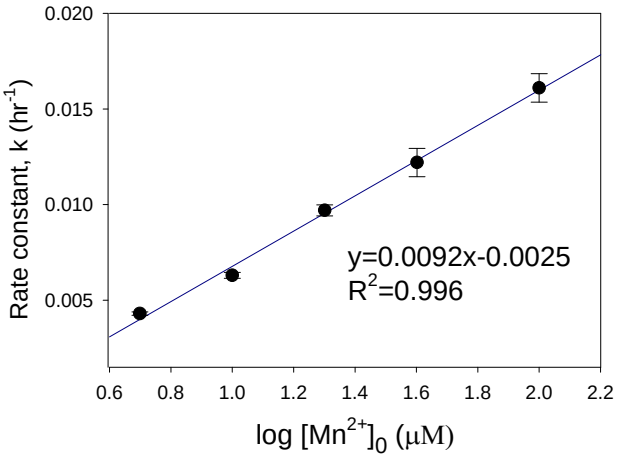

Figure 2.2 TTC degradation rate constant (k in h^{-1}) increased linearly with log $[Mn^{II}]_0$. ($[TTC]_0 = 40$ μM, pH 9).

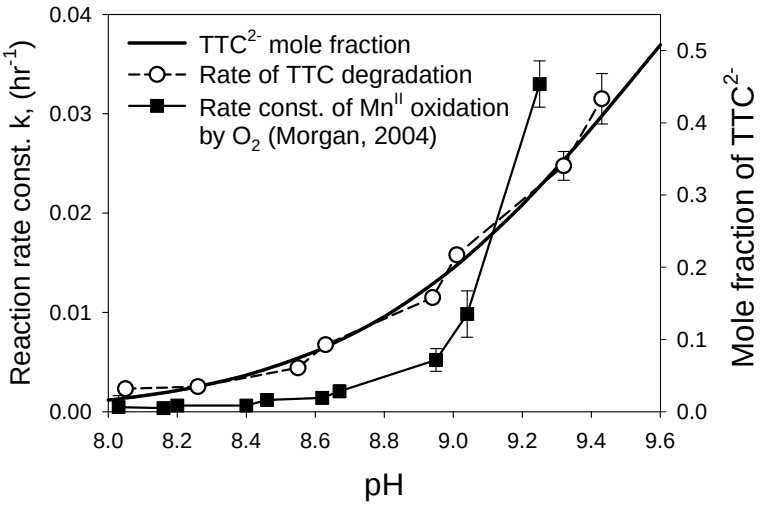

Figure 2.3 Effect of pH on the reaction rate constant of Mn^{II}-mediated transformation of TTC in the presence of O_2 ($[TTC]_0$ = 40 μM, $[Mn^{II}]$ = 40 μM, pH 8.0 - 9.4).

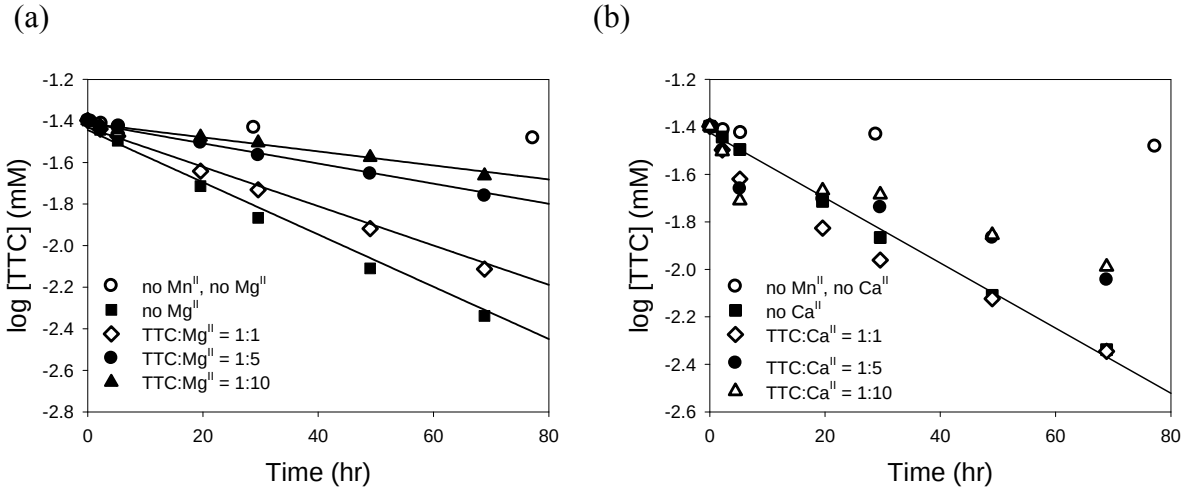

Figure 2.4 Effect of Mg^{II} and Ca^{II} co-solutes on the reaction of TTC with Mn^{II} and oxygen. (a) Mg^{II}, (b) Ca^{II} ($[TTC]_0 = [Mn^{2+}]_0$ = 40 μM, pH 9).

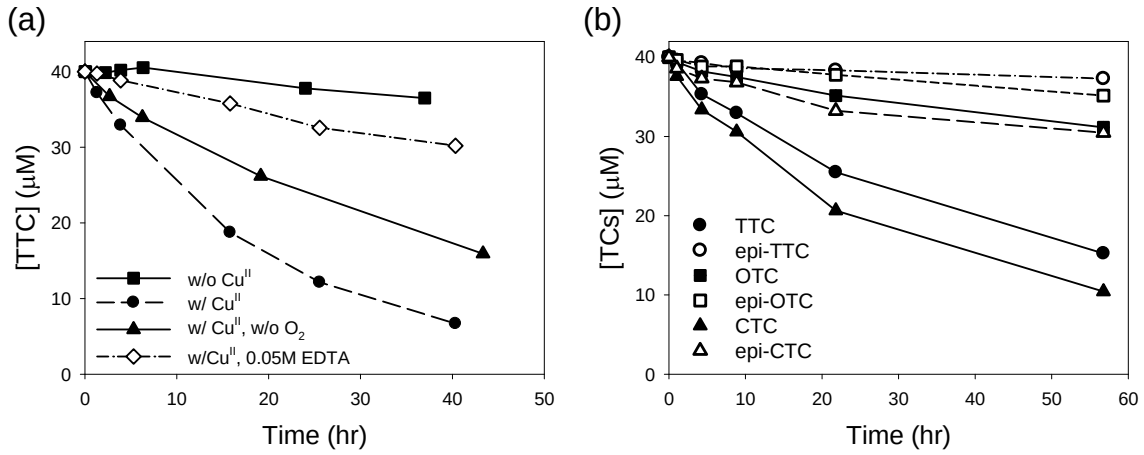

Figure 2.5 (a) Reaction of TTC with Cu(II)/O_2 and EDTA. ($[TTC]_0 = 40$ μM, $[Cu^{II}] = 1$ mM, [EDTA] = 0.05 M, pH 5); (b) Reaction of varies TCs in the presence of Cu^{II} and O_2.

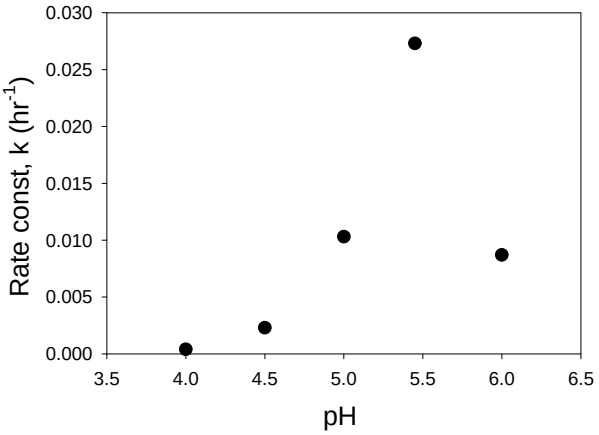

Figure 2.6 Effect of pH on the reaction rate constant of Cu^{II}-mediated reaction of TTC. (Experimental condition: pH 4.0 – 5.5 (acetate buffer), pH 6.0 (MOPS buffer); $[TTC]_0 = 40$ μM, $[Cu^{II}] = 1$ mM.)

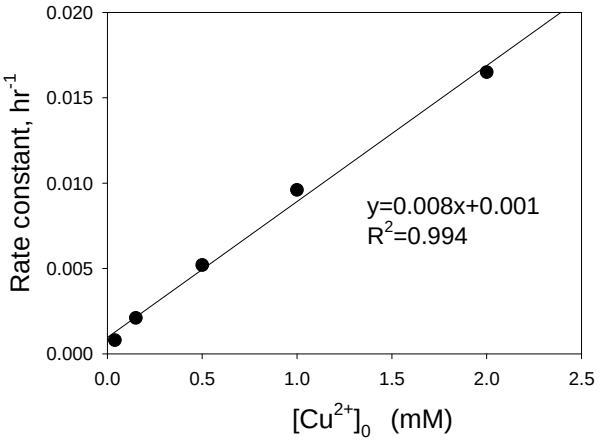

Figure 2.7 The TTC degradation rate constant (k in h^{-1}) increased linearly with $[Cu^{II}]_0$. ($[TTC]_0 = 40$ μM, pH 5).

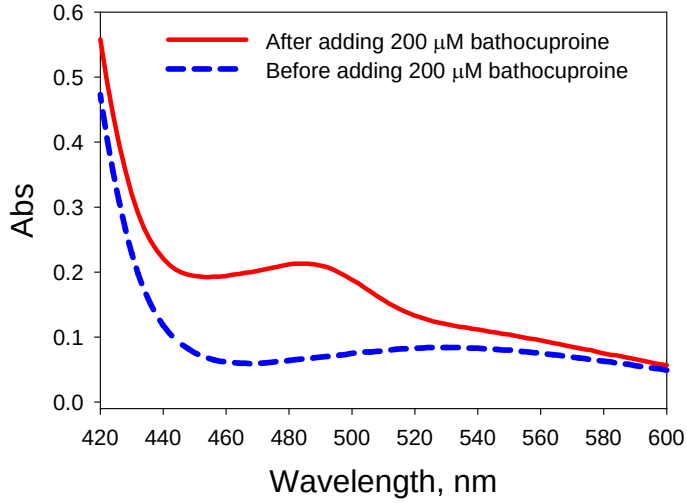

Figure 2.8 Detection of Cu^{I}-bathocuproine at 484 nm. (Experimental condition: absence of oxygen, $[TTC]_0 = 40$ μM, $[Cu^{II}] = 1$ mM, pH 5. Samples were taken after 20 hours reaction time.)

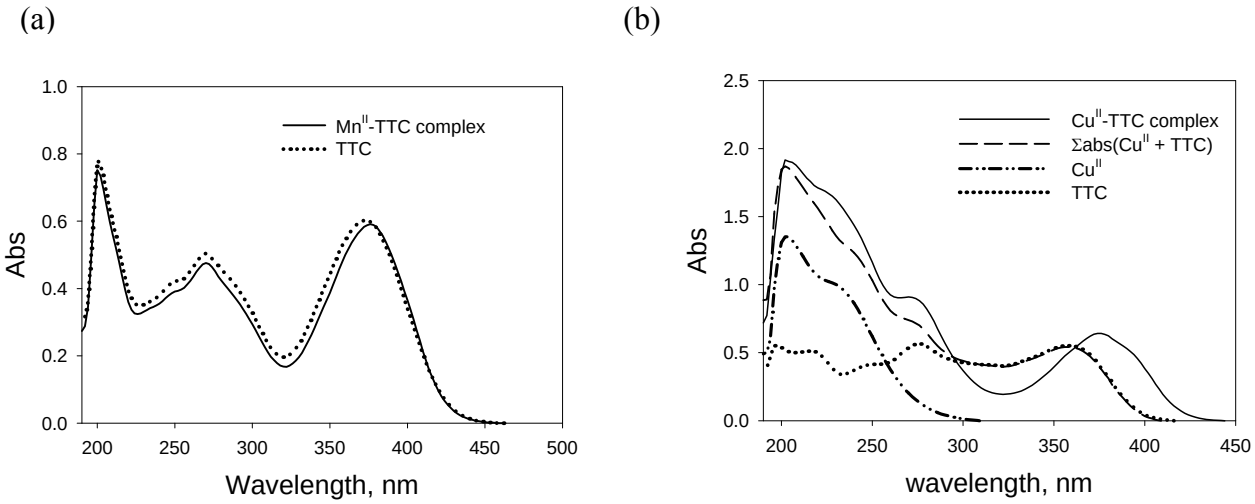

Figure 2.9 Ultraviolet absorption spectra. (a) free TTC and Mn^{II}-TTC complex in pH 9 (CHES) buffer ([TTC] = [Mn^{II}] = 40 μM) (b) free TTC, Cu^{II}, and Cu^{II}-TTC complex in pH 5 (acetic acid) buffer. ([TTC] = 40 μM, [Cu^{II}] = 1 mM)

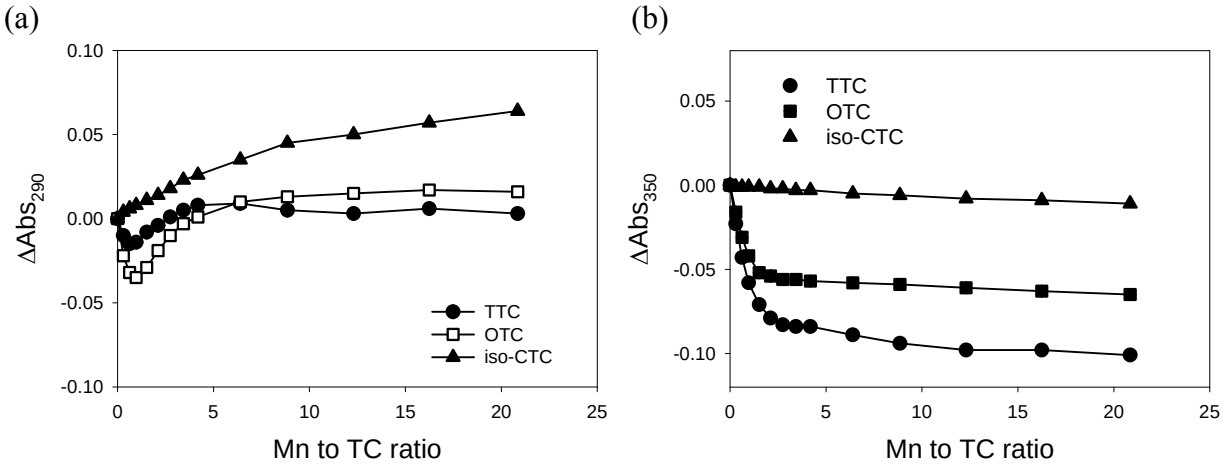

Figure 2.10 Titration curves of TC complexes with Mn^{II} (a) 290 nm (b) 350 nm. Forty μM TC with 10 mM NaCl and 10 mM CHES buffer at pH 9 was titrated by 0-880 μM of $MnCl_2$.

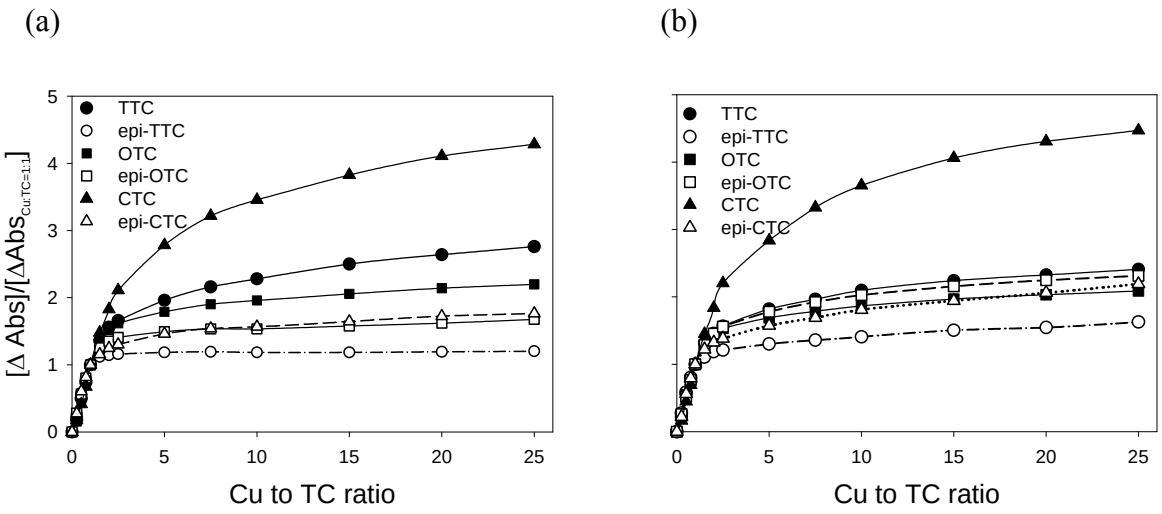

Figure 2.11 Titration curves of TC complexes with Cu^{II} (a) 276-286 nm (b)374-386 nm. Forty μM TC with 10 mM NaCl and 10 mM acetate buffer at pH 5 was titrated by 0-1000 μM of $CuCl_2$.

(a)

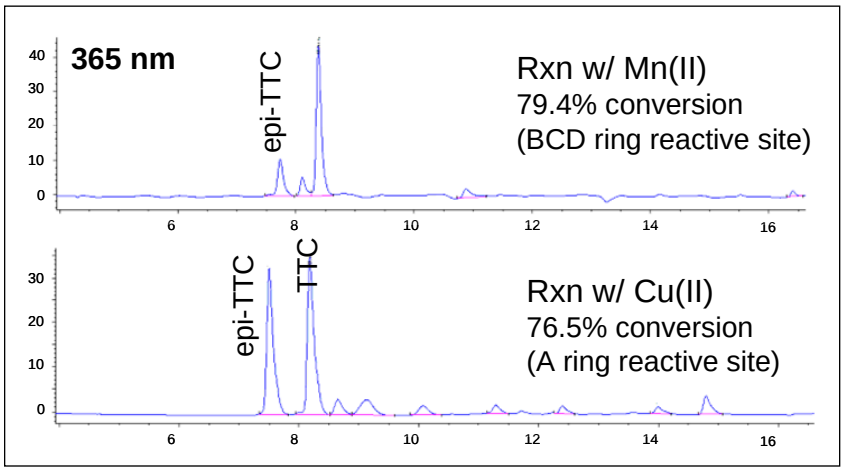

(b)

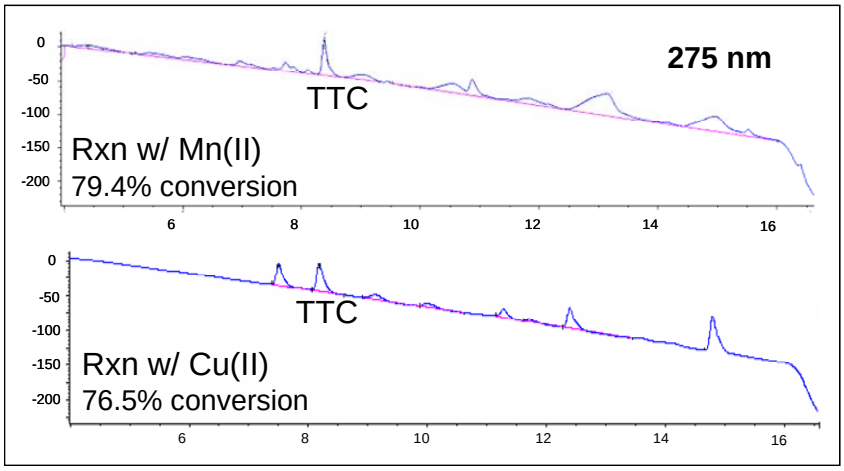

Figure 2.12 Product analyses by HPLC-UV for the Mn^{II}- and Cu^{II}-mediated reactions of TTC in the presence of oxygen: (a) measurement at 365 nm, (b) measurement at 275 nm.

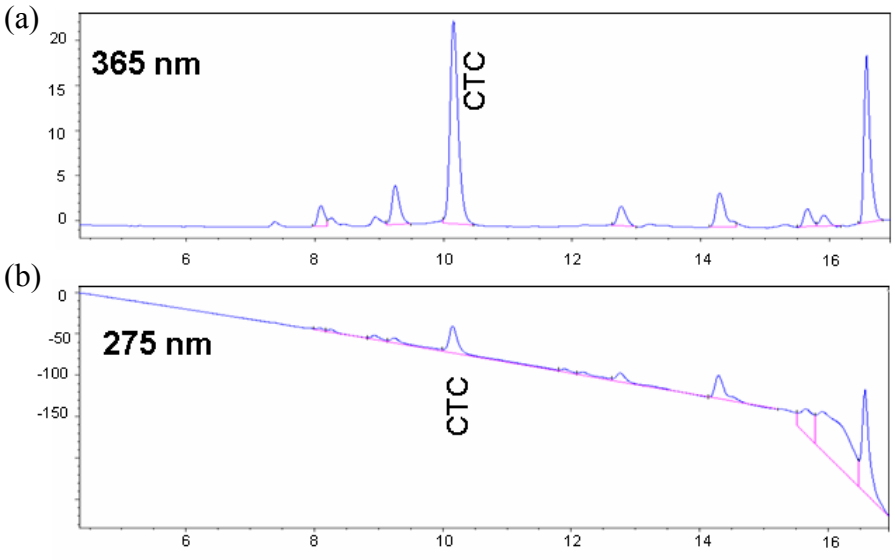

Figure 2.13 Product analyses (92% conversion) by HPLC-UV for the Cu^{II}-mediated reaction of CTC in the presence of oxygen: (a) measurement at 365 nm, (b) measurement at 275 nm.

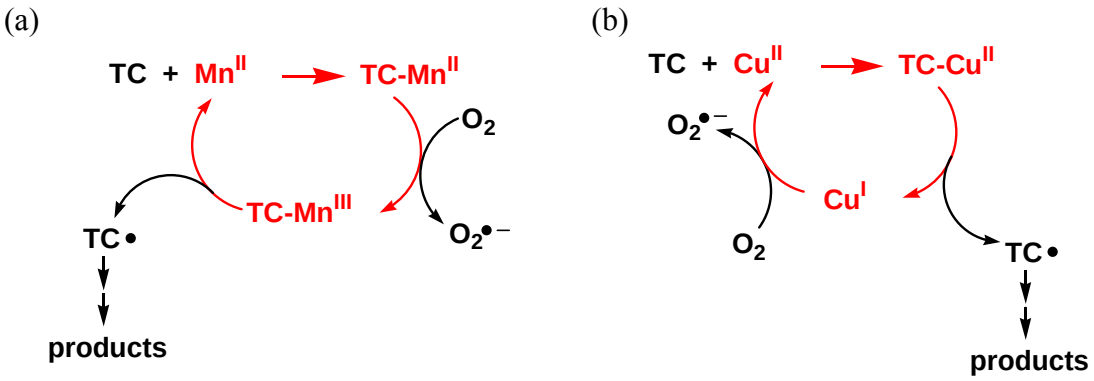

Figure 2.14 Proposed scheme for the (a) Mn^{II} -mediated transformation of TC; (b) Cu^{II} -mediated transformation of TC.

CHAPTER 3

KINETIC MODELING OF OXIDATION OF ANTIBACTERIAL AGENTS BY MANGANESE OXIDE

3.1 Introduction

Recent studies have reported the ubiquity of many antibacterial agents in the aquatic environment (Kolpin et al., 2002; Miao et al., 2004; Lindberg et al., 2005). The presence of antibacterial residues in the environment merits concern due to their potential to promote growth of resistant bacteria and pose adverse health effects to humans (Walsh, 2003; Levy and Marshall, 2004). Understanding the fate and transport of antibacterials in the soil-water environment is critical to properly assess the risk associated with these emerging contaminants. Metal oxides such as Mn and Fe oxides in soils are reactive surfaces that play an important role in affecting the fate and transport of organic contaminants via adsorption, hydrolysis, and/or redox reactions. Manganese oxides, in particular, are among the most important natural oxidants (with reduction potentials of 1.50 V and 1.23 V for MnOOH and MnO_2, respectively (Stone, 1987b) that are capable of oxidizing organic contaminants with a wide range of functionalities including phenol (Stone, 1987b; Ukrainczyk and McBride, 1993), aniline (Laha and Luthy, 1990; Klausen et al., 1997), aliphatic amine (McArdell et al., 1998), and triazine (Wang et al., 1999).

The authors recently demonstrated that phenolic, fluoroquinolonic (FQ) and aromatic *N*-oxide (ANO) antibacterials are highly susceptible to oxidative transformation by Mn oxides under environmentally relevant conditions (Zhang and Huang, 2003, 2005b, a). New results in this and other (Rubert and Pedersen, 2006) studies show that tetracycline (TC) antibiotics are also highly susceptible to oxidation by MnO_2. These four groups of compounds are among the leading antibacterials widely used to treat humans and animals and in nutrition and feed additives

for livestock (Katritzky, 1971; Albini, 1991; Graslund and Bengtsson, 2001; Walsh, 2003) or as active ingredients in many personal care products. In total, our study examined twelve antibacterials and nine structurally related model compounds (structures shown in Table 3.1). The antibacterials included two phenols (triclosan and chlorophene), six FQs (ciprofloxacin, enrofloxacin, norfloxacin, ofloxacin, lomefloxacin and pipemidic acid), one ANO (carbadox), and three TCs (tetracycline, chlorotetracycline, and oxytetracycline). The model compounds included four phenols (phenol, 3-chlorophenol, 2,4-dichlorophenol and 2-methyl-4-chlorophenol), two amines (1-phenylpiperazine and *N*-phenylmorpholine) and three ANOs (quinoline *N*-oxide, quinoxaline *N*-oxide and quindoxin).

Our previous studies (Zhang and Huang, 2003, 2005b, a) show that the interfacial reactions between antibacterials and Mn oxide involve complicated kinetics, *i.e.*, typically rapid initial reaction followed by gradual slow-down. The kinetics were affected by solution pH, the presence of co-solutes, metal oxide surface properties, and antibacterial structural characteristics. Because of this complexity, the reaction kinetics were characterized only during the initial stage by a pseudo-first-order decay model to yield the initial reaction rate constants (k_{init}) (initial reaction rate divided by initial concentration); decay of antibacterials did not follow the first-order kinetics (or any other order) in the later stage. Such complicated reaction kinetics were also reported by others in Mn oxide-mediated oxidation of organics (Stone, 1987b; Laha and Luthy, 1990; Klausen et al., 1997; Nico and Zasoski, 2001; Shin and Cheney, 2004; Rubert and Pedersen, 2006; Wang and Stone, 2006). Some characterized the reaction kinetics by the initial reaction rate approach (Stone, 1987b; Laha and Luthy, 1990; Zhang and Huang, 2003, 2005b, a) as ours did, whereas others fitted the kinetic data by empirical or semi-empirical equations (Nico and Zasoski, 2001; Rubert and Pedersen, 2006). Based on the experimental results (*i.e.*, kinetic

data, reactive site identification, and extensive product characterization) and the literature, reaction pathways have been proposed for phenolic, FQ and ANO antibacterials in our earlier studies (Zhang and Huang, 2003, 2005b, a). All of the reactions follow a general scheme in which the reaction begins with formation of a precursor complex between the antibacterial and the surface-bound Mn^{IV}, followed by oxidation of the precursor complex. Either precursor complex formation or electron transfer within the precursor complex is likely rate-limiting for the overall reaction.

Despite the elucidation of reaction pathways, the reaction kinetics were not fully understood because the initial reaction rate approach excluded evaluation of the kinetic data at the later stage. Adopting rate equations from previous studies is difficult because most studies focused on reductive dissolution of Mn oxides by using an excess amount of simple organic reductants and the kinetics were monitored by the generation of Mn^{2+}(aq) over time (Stone, 1987b; Laha and Luthy, 1990; Nico and Zasoski, 2001; Wang and Stone, 2006). This is contrary to a focus on the oxidative transformation of trace antibacterials by soil Mn oxides where Mn oxides are in excess of the organic contaminant. To gain more insight into the surface reaction kinetics involving antibacterials and Mn oxides, development of a kinetic model that can describe the entire reaction course is imperative. The objectives of this work were to (i) develop a kinetic model for the oxidation of antibacterials by Mn oxides based on the previously identified reaction mechanisms; and (ii) investigate the effect of reaction conditions on the kinetics based on the model. As will be shown, we have developed a kinetic model (referred to as the MnOII model) that is capable of describing the entire reaction kinetics of 21 organic compounds with MnO_2 in well-defined systems. Although the current model is not yet a predictive tool for real systems, it offers a significant improvement in the ability to evaluate the

kinetics of MnO_2-mediated oxidation reactions. Mechanistic implications of the kinetic modeling of our experimental data are also discussed.

3.2 Materials and Methods

3.2.1 Chemical Reagents

Except for TCs, sources and preparation of stock solutions for the studied compounds were described previously (Zhang and Huang, 2003, 2005b, a). TTC, OTC and CTC were obtained from Sigma at 90-98% purity. Other employed chemicals were of at least 97% purity and were used without further purification. Unless otherwise specified, all other reagents used (e.g. buffers, ion strength agents, acids, etc.) were obtained from Fisher Scientific, Acros or Aldrich. All reagent solutions were prepared using water obtained from a Milli-Q Ultrapure Gradient A10 (Millipore - Billerica, MA) purification systems. Stocks of TCs were prepared in methanol at 1.6 mM, protected from light, stored in -15 ºC freezer, and used within a month of preparation. Throughout the experiment, acetate (pH 5) and 2-(cyclohexylamino)ethanesulfonic acid (CHES) (pH 9) buffers were used to maintain the reaction solution pH. NaCl salt was utilized to control ionic strength. Manganese dioxide (δ-MnO_2, similar to the naturally occurring birnessite) was synthesized using $KMnO_4$ and HCl based on the method by Murray (1974). Characterization of this MnO_2 was reported previously (Zhang and Huang, 2003).

3.2.2 Kinetic Experiments

The reaction setup for phenols, FQs and ANOs was described previously (Zhang and Huang, 2003, 2005b, a). Similar setup was used for TCs: batch kinetic studies (with 20–80 μM of parent organic and 0.2–1.2 mM of MnO_2) were conducted in 60 mL screw-cap amber glass bottles with Teflon septa, under constant stirring at 22 ^{o}C. Reaction pH was maintained using 10 mM of acetate (pH 4-5), 4-morpholinepropanesulfonic acid (MOPS) (pH 6-8), or 2-(cyclohexylamino)ethanesulfonic acid (CHES) (pH 9) and the corresponding sodium conjugate bases. NaCl (0.01 M) was added to maintain constant ionic strength.

The reactions of phenols, FQs, and ANOs were quenched by addition of an excess amount of ascorbic acid to reductively dissolve MnO_2 particles or by centrifugation (Zhang and Huang, 2003, 2005b, a). For TCs, reaction aliquots were dosed with an excess amount (10 M) of oxalic acid, or were rapidly (< 1.5 s) pushed through a membrane filter holder that housed a pre-wetted 0.22 μm GVWP membrane (Millipore) using a 1 mL plastic syringe. Negligible adsorption of TCs to the membrane was confirmed. In this manner, the concentration of antibacterial measured in the supernatant (after centrifugation) or filtrate corresponds to the unreacted parent compound in the aqueous phase, whereas the concentration measured after ascorbic or oxalic acid addition corresponds to the unreacted parent compound both in the aqueous phase and on the MnO_2 surface. Samples after quenching were acidified to near pH 2 by HCl to improve TCs' analytical results, stored in amber vials at < 5 °C, and analyzed within two days. For each testing parameter, at least two replicate experiments were conducted. Control experiments without Mn oxide showed no significant loss of any of the tested compounds during the reaction periods (typically hours).

3.2.3 Analytical Methods

Phenols, FQs and ANOs were analyzed as described previously (Zhang and Huang, 2003, 2005b, a). TCs were monitored by an Agilent 1100 reverse-phase high performance liquid chromatography (HPLC) system at a flow rate of 1 mL/min with a RX-C18 column (4.6 × 250 mm, 5 μm) and a diode-array UV/Vis detector (275 nm and 365 nm). The mobile phase A consisted of 0.01 M oxalic acid and 10 μM EDTA, while mobile phase B was pure acetonitrile. Gradient elution was run to separate the TCs and their reaction products.

3.3 Results

3.3.1 Kinetic Model

On the basis of the previous studies (Stone, 1987b; Zhang and Huang, 2003, 2005b, a) and new results with TCs, we propose the following mechanism for the reactions between antibacterials (denoted as ArXH, X = O or N) and Mn oxides (denoted as $>Mn^{IV}$).

$$>Mn^{IV} + ArXH \underset{k_{-1}}{\overset{k_1}{\rightleftharpoons}} (>Mn^{IV}, ArXH) \quad (1)$$

$$(>Mn^{IV}, ArXH) \underset{k_{-2}}{\overset{k_2}{\rightleftharpoons}} (>Mn^{III}, ArX\bullet) + H^+ \quad (2)$$

$$(>Mn^{III}, ArX\bullet) \underset{k_{-3}}{\overset{k_3}{\rightleftharpoons}} >Mn^{III} + ArX\bullet \quad (3)$$

$$>Mn^{III} \xrightarrow{\text{fast}} >Mn^{II} \quad (4)$$

$$ArX\bullet \xrightarrow{\text{fast}} \text{products} \quad (5)$$

For the redox reaction to occur, formation of a precursor complex between the organic reductant and the oxide surface is necessary (reaction 1). Electron transfer within the precursor complex

occurs next (reaction 2), generating $>Mn^{III}$ and organic radical species (reaction 3). Due to the highly unstable nature, $>Mn^{III}$ may react with neighboring species such as ArX•, ArXH and/or $>Mn^{III}$ to form the more stable $>Mn^{II}$ species; organic radicals further oxidize or combine to form products (reactions 4–5). The precursor complex formation or electron transfer is likely the rate-limiting step.

Assuming that (i) back electron transfer is negligible ($k_2 >> k_{-2}$), and (ii) consumption rate of the precursor complex is high (reactions 3-5 are fast), we get:

$$\frac{d[(>Mn^{IV}, ArXH)]}{dt} = k_1[>Mn^{IV}][ArXH] - k_{-1}[(>Mn^{IV}, ArXH)] - k_2[>Mn^{IV}, ArXH] \quad (6)$$

The total reactive surface sites (S_{rxn}) that oxidized the parent antibacterial (*i.e.*, a two-electron transfer process (Zhang and Huang, 2003, 2005b, a) can be expressed as:

$$S_{rxn} = [>Mn^{IV}] + [(>Mn^{IV}, ArXH)] + [(>Mn^{III}, ArX•)] + [>Mn^{III}] + [>Mn^{II}] \quad (7)$$

The concentration of ($>Mn^{III}$, ArX•) should be very low because its generation rate is much slower than its consumption rate. The instability of $>Mn^{III}$ also leads to its negligible concentration. Because two electrons were transferred from the antibacterial to MnO_2 in the apparent loss of the parent antibacterial, the yielded $>Mn^{II}$ concentration can be expressed below:

$$[>Mn^{II}] = C_0 - C \quad (8)$$

where C_0 (in μM) and C (in μM) are the concentrations of the parent antibacterial at time zero and time *t*, respectively. Note that additional electron transfers that may occur to result in further oxidation of the parent antibacterial and/or its products and re-oxidation of the generated Mn^{2+} by Mn^{IV} surfaces are excluded from eqs 7 and 8 because they do not affect the apparent rate of loss of the parent antibacterial. Variables C_0 and C can be obtained from experimental data.

Variables S_{rxn} and k can be determined by data fitting. Substituting eq 8 into eq 7 in which [(>Mn^{III}, ArX•)] and [>Mn^{III}] are neglected, we obtain:

$$[>Mn^{IV}] = S_{rxn} - (C_0 - C) - [(>Mn^{IV}, ArXH)] \quad (9)$$

Because reactions 1 and 2 are relatively slower than reactions 3-5, we can apply the pseudo-steady-state assumption to the formed precursor complex (>Mn^{IV}, ArXH), *i.e.*,

$$\frac{d[(>Mn^{IV},ArXH)]}{dt} = k_1[>Mn^{IV}][ArXH] - k_{-1}[(>Mn^{IV},ArXH)] - k_2[(>Mn^{IV},ArXH)] = 0 \quad (6b)$$

Substituting eq 9 into eq 6b, we get:

$$[(>Mn^{IV},ArXH)] = \frac{k_1[S_{rxn} - (C_0 - C)]}{k_1 C + k_{-1} + k_2} \quad (10)$$

The oxidation rate of antibacterials can be expressed as follows:

$$-\frac{dC}{dt} = k_1[>Mn^{IV}]C - k_{-1}[(>Mn^{IV},ArXH)] \quad (11)$$

Substituting eqs 9 and 10 into eq 11, we obtain:

$$-\frac{dC}{dt} = \frac{k_1 k_2[S_{rxn} - (C_0\text{-}C)]C}{k_1 C + k_{-1} + k_2} \quad (12)$$

When precursor complex formation is much faster than electron transfer, assuming $k_1C >> k_{-1} + k_2$, eq 12 can be simplified as:

$$-\frac{dC}{dt} = k_2[S_{rxn} - (C_0 - C)] = k'[S_{rxn} - (C_0 - C)] \quad \text{where } k' = k_2 \text{ in unit of time}^{-1} \quad (13)$$

The analytical solution of eq 13 is:

$$C = (C_0 - S_{rxn}) + S_{rxn}e^{-k't} \quad (14)$$

In contrast, when precursor complex formation is much slower than electron transfer, assuming $k_1C << k_{-1} + k_2$, eq 12 can be simplified as:

$$-\frac{dC}{dt} = \frac{k_1 k_2 [S_{rxn} - (C_0 - C)]C}{k_{-1} + k_2} = k''[S_{rxn} - (C_0 - C)]C$$

$$\text{where } k'' = \frac{k_1 k_2}{k_{-1} + k_2} \text{ in unit of conc.}^{-1}\text{time}^{-1} \quad (15)$$

The analytical solution of eq 15 is:

$$C = \frac{S_{rxn} - C_0}{\frac{S_{rxn}}{C_0} e^{k''(S_{rxn} - C_0)t} - 1} \quad (16)$$

We call this kinetic model the MnOII model. Eq 14 with electron transfer the rate-limiting step is called MnOII(i) model; eq 16 with complex formation the rate limiting step is called MnOII(ii) model. Appropriate rate-limiting steps will be applied to different groups of antibacterials. The rate constant *k'* (in h^{-1}) or *k"* (in $h^{-1} \cdot M^{-1}$) and the total reactive surface sites S_{rxn} (in $\mu mol \cdot L^{-1}$ solution) can be obtained by fitting kinetic data to this model.

3.3.2 Model Comparison and Kinetic Fitting

A common feature is shared by MnOII(i) and MnOII(ii): reaction reaches a plateau as $t \rightarrow \infty$, *i.e.*, C approaches a plateau concentration $C_e = C_0 - S_{rxn}$. Visually, the main difference between MnOII(i) and MnOII(ii) is the rate at which the fitting line reaches plateau (Figure 3.1). If all conditions are the same, the rate at which model fits reach plateau is MnOII(i) > MnOII(ii). When S_{rxn} value is low or *k* is high, the two fits overlap. In addition, higher S_{rxn} or *k* corresponds to a higher rate or a lower C_e.

It appears that all data fit well by either model with $R^2 > 0.91$ (Table 3.2). Note the fact that reaction kinetics can fit by a certain model does not necessarily mean that the reaction mechanism that the model is based on applies to that system. MnOII(i) was chosen to fit the loss

of phenols, ANOs, FQs and their structurally related compounds because of (i) their significant adsorption to MnO_2 (*e.g.*, > 40% adsorbed at pH 5 for triclosan and CIP and 14% for CDX, determined by the difference between the two quenching methods (see Materials and Methods) that indicates a fast precursor complex formation, and (ii) a delayed release of soluble Mn^{2+} ions that indicates a slow electron transfer reaction (Zhang and Huang, 2003, 2005b, a). In contrast, MnOII(ii) was chosen to fit the reaction kinetics of TCs because (i) only negligible amounts of adsorbed but unreacted TCs on MnO_2 surface could be detected (about 1% for CTC, 3-6% for TTC and 3–7% for OTC, determined by the difference between the two quenching methods, and (ii) soluble Mn^{2+} ions quickly formed without a lag phase (Figure 3.2), indicating that the electron transfer step occurs immediately after precursor complex formation. Both phenomena suggest that precursor complex formation is the rate-limiting step in the oxidation of TCs by MnO_2. These also mean that k_2 (electron transfer) is likely much larger than k_{-1} (desorption) in the MnOII(ii) model. Therefore, *k"* essentially approaches k_1 (adsorption).

The C_e value can be estimated from the kinetic trend in the later stage. By setting a fixed S_{rxn} based on the estimated C_e value (*i.e.*, $S_{rxn} = C_0 - C_e$), the experimental data were fit to the MnOII model using SigmaPlot program (version 9.01, Systat Software, Inc.) to yield the only fitting parameter *k* (*k'* for phenols, ANOs, and FQs and *k"* for TCs). Good fitting ($R^2 > 0.93$) was obtained for all data collected for a wide range of compounds and two different Mn oxides (MnO_2 and MnOOH) (Tables 3.1-3.3; Figure 3.3). The above single-parameter fitting is considered more meaningful than two-parameter fitting (*i.e.*, both S_{rxn} and *k* as the fitting parameters) despite of the slightly lower R^2 values.

3.3.3 Effect of Reaction Conditions

The kinetic fitting was evaluated for the influence of reactant concentration, solution pH, and the presence of co-solutes for triclosan, ciprofloxacin (CIP), carbadox (CDX), and TTC as the representatives for the four structural classes of antibacterials.

3.3.3.1 Effect of Reactant Loading

Experiments with varying antibacterial loadings (employed concentration at t = 0) but a fixed MnO_2 loading or with varying MnO_2 loadings but a fixed antibacterial loading were conducted at pH 4 (for CDX) or pH 5 (for triclosan, CIP and TTC) to assess the effect of each reactant on the kinetics. The obtained kinetic parameters (S_{rxn} and k) were plotted against antibacterial loading and MnO_2 loading in Figures 3.4 and 3.5.

As antibacterial loading was increased, S_{rxn} increased proportionally (inserts in Figure 3.4) except at the highest loading of CIP and CDX (inserts in Figure 3.5). No apparent relationship was observed for k' versus antibacterial loading for triclosan, CDX and CIP (Figures 3.4 a-c); k' values were roughly constant if considering the experimental errors. In contrast, a very different trend was observed with TTC where k" decreased significantly with higher TTC loading (Figure 2d). As MnO_2 loading was increased, both S_{rxn} and k increased for all four compounds (Figures 3.5). S_{rxn} increased to a plateau that approached the employed antibacterial initial concentration (C_0) (inserts in Figures 3.5) with only one exception (when $[MnO_2]_{t=0}$ was 250-fold in excess of triclosan, S_{rxn} decreased slightly).

3.3.3.2 Effect of pH

Solution pH markedly affected the reaction rate constants for all compounds with smaller *k* at higher pH (Figure 3.6). Approximately linear relationships between log(*k'*) or log(*k''*) and pH was obtained for triclosan, CDX (except for the last data point), and TTC (slope of -0.33 to -0.46, R^2 = 0.76-0.98) (Figure 3.6 a, c and d). Log(*k'*) of CIP also decreased when pH increased from 5 to 6 but stayed approximately constant from pH 6 to 8 (Figure 3.6b). When plotting S_{rxn} against pH (inserts in Figure 3.6), S_{rxn} decreased as pH was increased for all four antibacterials.

3.3.3.3 Effect of Co-Solutes

The effects of co-solutes on the oxidation kinetics by MnO_2 were evaluated for triclosan and TTC (Table 3.4). Compared to the *k'* in the absence of co-solutes, the addition of Mn^{2+}, Ca^{2+}, Zn^{2+}, and natural organic matter (NOM) all lowered the reaction rate constant of triclosan; the inhibitory effect increased as the co-solute concentration was increased. Mn^{2+} had the strongest inhibitory effect, followed by NOM, Zn^{2+}, and then Ca^{2+}. Interestingly, addition of theses co-solutes caused only slight decrease in S_{rxn} even when *k'* was decreased significantly. For TTC, *k''* decreased significantly with an increasing amount of added Mn^{2+}. Compared to Mn^{2+}, addition of Ca^{2+}, Mg^{2+}, and NOM resulted in only slightly smaller *k''* and the inhibitory effect did not increase appreciably even when these co-solute concentrations were increased significantly. Addition of an increasing amount of Mn^{2+} resulted in significant decrease in S_{rxn} while addition of Ca^{2+}, Zn^{2+} and NOM had negligible effects on the total reactive surface sites of TTC.

3.4 Discussion

For all four groups of antibacterials, the total reactive surface sites S_{rxn} increased as the MnO_2 loading increases (inserts in Figure 3.5). However, S_{rxn} increased eventually to a maximum that was close to the employed antibacterial loading C_0 (inserts in Figure 3.5). The fact that S_{rxn} could not exceed C_0 is understandable since C_0 was the maximum amount of parent antibacterial that could be oxidized in the initial two-electron transfer process. The trend in Figure 3.5 inserts also implies that the number of available surface sites changed from being limited at low MnO_2 loading (the curves before reaching the plateau) to being in excess at high MnO_2 loading (the curves at the plateau). Comparison of the S_{rxn} values to the lower MnO_2 loadings where the available surface sites appeared limited suggests that the available surface sites account for only a small fraction (~1-10%) of the total MnO_2 mass. At a fixed MnO_2 loading, S_{rxn} increased with higher C_0 (inserts in Figure 3.4); this is consistent with the expectation that more antibacterial can occupy the surface active sites to undergo redox reaction. However, this S_{rxn} increase was eventually limited by the total available sites as indicated in the cases of CIP and CDX (Figure 3.4 b and c inserts). Solution pH affects the speciation of MnO_2 surface (pH_{zpc} = 3.4 – 3.76 (Murray, 1974; Sahai and Sverjensky, 1997)) and antibacterial (pK_a values in Table 3.1). Within the studied range of pH 4-9, MnO_2 surface is negatively charged, whereas, depending on their pK_a values, the antibacterials may change from positively charged, neutral (or zwitterion), to negatively charged as pH increases especially for CIP and TTC. The S_{rxn} is expected to decrease at higher pH because of (i) less electrostatic attraction between the surface and the antibacterial species, and (ii) stronger competition by OH^- with the antibacterial for coordination with surface-bound Mn^{IV}. The results that S_{rxn} decreased when pH was increased (inserts in Figure 3.6) are consistent with the expectation.

It has been assumed that electron transfer within the surface complex is rate-limiting in the oxidation of phenols, FQs and ANOs by MnO_2 (*i.e.,* MnOII(i) model and *k'*). The rate constant of electron transfer will not be affected by organic reductant concentration (*i.e.,* C_0). As expected, the *k'* values were roughly constant regardless of antibacterial loading (Figure 3.4 a-c). Increase in the oxidizing power of MnO_2 will enhance the rate of electron transfer, or vice versa. The *k'* value increased when MnO_2 loading was increased (Figures 3.5); it may be possible that a greater amount of MnO_2 in the system could maintain the relative proportions of Mn(II), Mn(III) and Mn(IV) within the oxide that yielded higher oxidizing power than in the case of lower MnO_2 loading (Stone and Morgan, 1984a; Stone, 1987b). Solution pH affects the reduction potential of MnO_2 (eq 19 (ref: Stumm and Morgan (1996)) and antibacterial (when proton is involved in its oxidation).

$$MnO_{2(s)} + 4\ H^+ + 2\ e^- = Mn^{2+}{}_{(aq)} + 2\ H_2O, \qquad E_H = E_H^\circ + 0.0296 \cdot \log \frac{\{MnO_2\}\{H^+\}^4}{\{Mn^{2+}\}} \qquad (19)$$

The inverse linear relationship between log(*k'*) and pH for triclosan and CDX (Figure 3.6 a and c) suggests that the decrease in *k'* is most likely due to decrease in the reduction potential of MnO_2 at higher pH. The relationship between log(*k'*) and pH is more complicated for CIP (Figure 3.6b), which may be related to different acid-base behaviors of the reactive functional groups (*i.e.*, N in FQs vs. O in the other antibacterials) that affect their ability to undergo oxidation.

It has been assumed that surface complex formation is rate-limiting in the oxidation of TCs by MnO_2 (*i.e.,* MnOII(ii) model and *k"*). The rate of surface complex formation (*i.e.,* adsorption) will be affected by sorbent concentration (*i.e.,* S_{rxn}), sorbate concentration (*i.e.,* C_0), and solution conditions such as pH. When sorbent concentration and pH were constant, the *k"* value decreased when TTC loading was increased (Figure 3.4d). Decrease in adsorption rate at higher sorbate concentrations with a fix amount of sorbent has been shown previously (Zou et al., 2006).

The *k"* decreases because a higher TTC concentration generates greater self-competition for the same number of surface sites and slows the overall adsorption rate. When sorbate concentration and pH were constant, the *k"* value increased when MnO_2 loading was increased (Figure 3.5d), consistent with the expectation that adsorption rate of TTC would be faster with higher S_{rxn}. An inverse linear relationship was observed between log(*k''*) and pH for TTC (Figure 3.6d). The pH influences adsorption rates most likely through its impact on S_{rxn}. As discussed earlier, increase in pH decreases S_{rxn} and thus leads to slower adsorption rates of TTC to MnO_2.

The presence of co-solutes decreases the reaction rates of triclosan and TTC with MnO_2 by varying degrees (Mn^{2+} > NOM >> Zn^{2+} > Ca^{2+} for triclosan, and Mn^{2+} >> NOM > Ca^{2+} > Mg for TTC) (Table 3.4). Similar trend was observed by the initial reaction rate k_{init} of triclosan in our previous study and was attributed to a decreased number of active surface sites in the presence of co-solutes (Zhang and Huang, 2003). However, examination of S_{rxn} in this study reveals that these co-solutes do not compete with triclosan for the same surface sites. Therefore, metal ions, instead of blocking surface sites as believed earlier, may actually decrease the overall oxidation state of the oxide by adsorbing to the surface and slows electron transfer in the oxidation of triclosan. NOM can reactively adsorb to oxide surfaces generating $>Mn^{II}$ and thus slows the electron-transfer reaction (Lovley et al., 1996). For TTC, the constant S_{rxn} despite increasing [Ca^{2+}], [Mg^{2+}], or [NOM] suggests that these co-solutes do not compete with TTC for the same surface sites, and they affect the adsorption rate of TTC to MnO_2 only mildly. Note that complexation of TTC with Ca^{2+} or Mg^{2+} at the employed pH 5 conditions is negligible (Ohyama and Cowan, 1995; Tongaree et al., 1999). In contrast, the significant decrease in S_{rxn} with increasing [Mn^{2+}] indicates that Mn^{2+} competes with TC for the same surface sites, resulting in slower adsorption of TTC to MnO_2 surface and hence lower *k''*.

Evidently, all the experimental results support the respective rate-limiting step for the reactions of phenols, FQs, and ANOs (*i.e.*, electron transfer) versus for those of TCs (*i.e.*, precursor complex formation) with MnO_2. For MnOII(i), the reaction eventually reached a plateau because most of the fast reactive sites on the MnO_2 were reduced and additional electron transfer needed to involve other less reactive sites and thus the parent antibacterial degradation rate became very slow. For MnOII(ii), while the surface reactive sites were being exhausted due to redox reaction, the concentration gradient between the bulk organic and the surface-bound organic decreased to a level where the adsorption rate became very slow.

The parameters k and S_{rxn} can be used to compare the reaction kinetics of different antibacterials provided that the experiments employ the same pH and $[MnO_2]_{t=0}$ in comparing k' or employ the same pH, $[MnO_2]_{t=0}$ and $[antibacterial]_{t=0}$ in comparing k'' and S_{rxn}. Based on these constraints, the data in Table 3.3 allows comparing k' or k'' within the same structural group, k' of phenol and ANO groups, and S_{rxn} in the TC group. The comparisons indicate that phenols are more reactive to MnO_2 than ANOs. For compounds within the same structural group, the relative reactivity determined by k' (*e.g.*, CIP ~ OFL ~ ENR ~ NOR > LOM > PIP) are consistent with the assessment we reported earlier (Zhang and Huang, 2003, 2005b, a). The data of TCs indicates that the three antibacterials have similar total reactive surface sites (S_{rxn}) but different adsorption rates (k'') to MnO_2. As discussed earlier, surface complex formation is the slowest step in the reactions of TCs probably because the electron transfer step is rather fast in these cases. The hypothesized more rapid redox reaction of TCs with MnO_2 is corroborated by the observation that TCs are less stable than the other antibacterials even in the absence of MnO_2 (instability: CTC > TTC > OTC in time-extended experiments), indicating higher reactivity of TCs. If the degradation rate of MnO_2 surface-bound TCs follows the same trend of CTC > TTC

> OTC, the faster depletion of surface-bound antibacterial will render a greater concentration gradient between the antibacterial in the bulk solution and on the surface and result in faster adsorption. This may explain the observed order of adsorption rate constants CTC > TTC > OTC.

Compared to the past studies, the MnOII model significantly improves the ability to fully evaluate in depth the reaction kinetics of a wide range of organic compounds (antibacterials and non-antibacterials) with MnO_2 using the two independent parameters (*i.e.*, total reactive surface sites S_{rxn} and rate constant *k'* for the electron-transfer reaction or *k"* for precursor complex formation) to gain mechanistic insight. To the authors' knowledge, no prior studies have developed a mathematic model to describe the surface reaction kinetics of antibacterials with manganese oxides nor demonstrated the versatility of a kinetic model for the reactions of such a diverse range of organic structures with Mn oxides. Further development is, however, needed to make the MnOII model a better predictive tool and broaden its applicability to real systems. In applying this model, it is recommended to monitor the reaction until it reaches the plateau state (*i.e.,* C approaches C_e) to accurately determine the total reactive surface sites (S_{rxn}) parameter from the experimental data.

Table 3.1 Structures and pKa values of antibacterials and structurally related compounds examined in this study.

Phenolic compounds	**Structure**	**pK_a (ref)**
Triclosan	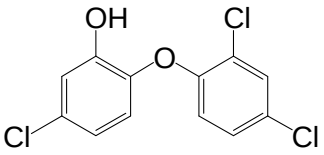	7.99[a]
Chlorophene	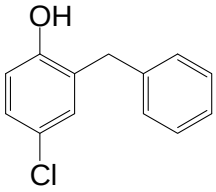	9.96[a]
2-Methyl-4-chlorophenol	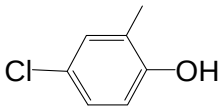	9.76[a]
2,4-Dichlorophenol	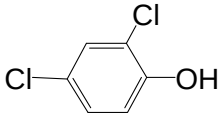	7.96[a]
Phenol	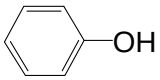	10.0[a]
3-Chlorophenol	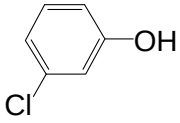	9.18[a]
Aromatic *N*-oxides	**Structure**	**pK_a (ref)**
Carbadox (CDX)	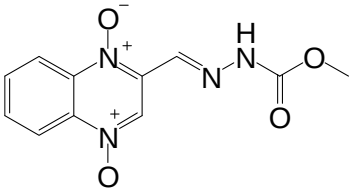	9.61[b]
Quinoline *N*-oxide (QNO)	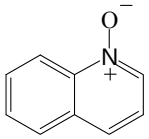	Not Applicable
Quinoxaline *N*-oxide (QXO)	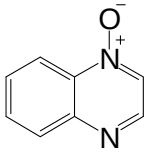	Not Applicable

Table 3.1 (Continued)

Aromatic *N*-oxides	**Structure**	**pK_a (ref)**
Quindoxin (QDX)	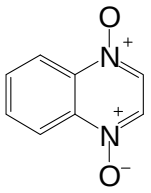	Not Applicable

Fluoroquinolones	**Structure**	**pK_a (ref)**
Ciprofloxacin (CIP)	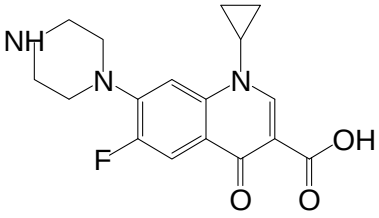	5.46, 7.67[c]
Ofloxacin (OFL)	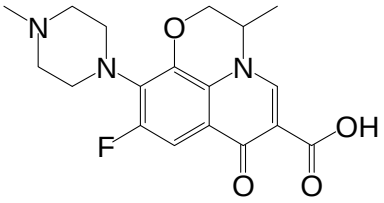	5.41, 7.08[c]
Enrofloxacin (ENR)	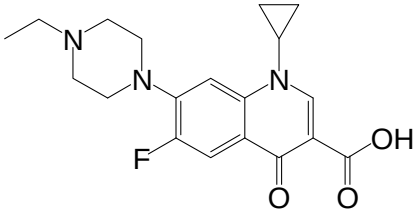	5.46, 7.03[c]
Norfloxacin (NOR)	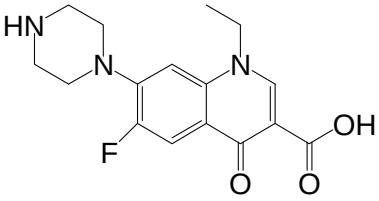	5.46, 7.67[c]
Lomefloxacin (LOM)	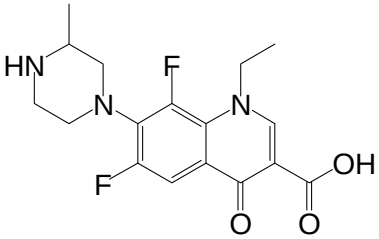	5.38, 7.85[c]

Table 3.1 (Continued)

Fluoroquinolones	**Structure**	**pK_a (ref)**
Pipemidic Acid (PIP)	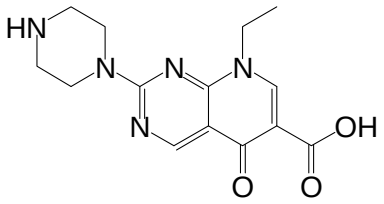	5.20, 6.38[c]
1-Phenylpiperazine (PP)	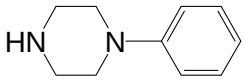	4.49[c]
N-phenylmorpholine (PM)	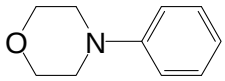	3.32[c]

Tetracyclines	**Structure**	**pK_a (ref)**
Tetracycline (TTC)	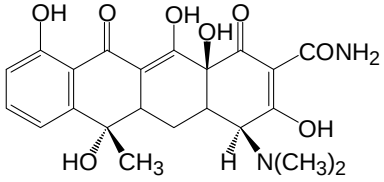	3.32, 7.78, 9.58[d]
Chorotetracycline (CTC)	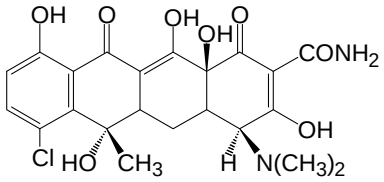	3.22, 7.46, 8.94[d]
Oxytetracycline (OTC)	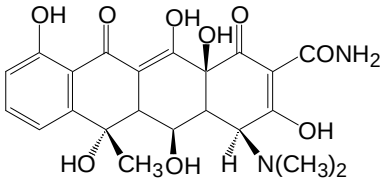	3.33, 7.55, 9.33[d]

[a] from Zhang and Huang (2003)
[b] from Shah et al. (2006)
[c] from Zhang and Huang (2007)
[d] from Qiang and Adams (2004)

Table 3.2 Kinetic fitting of experimental results by MnOII(i) & (ii) models. Both *k* and S_{rxn} were obtained from model fitting. All reactions, unless specified, were performed with MnO_2. (Typical reaction conditions: phenolic compounds and ANOs – 1 mM MnO_2, 10-20 μM organic compound, pH 4; FQs – 1.5 -10 μM FQ, 100 μM MnO_2, pH 5; and TCs – 40 μM TC, 600 μM MnO_2, pH 5.)

	MOII(i)			**MOII(ii)**		
Phenolic compound	k' (h^{-1})	S_{rxn} (μmol L^{-1})	R^2	k'' (M^{-1} h^{-1})	S_{rxn}(μmol L^{-1})	R^2
Triclosan	2.38 ± 0.27	17.73 ± 0.59	0.989	0.14 ± 0.01	20.40 ± 0.77	0.998
Triclosan (with MnOOH)	0.18 ± 0.15	3.41 ± 2.19	0.966	0.01 ± 0.01	4.30 ± 4.02	0.966
Chlorophene	2.04 ± 0.12	11.23 ± 0.21	0.996	0.13 ± 0.03	17.58 ± 3.14	0.990
2-Methyl-4-chlorophenol	2.58 ± 0.17	8.28 ± 0.17	0.992	0.27 ± 0.00	10.37 ± 0.15	0.999
2,4-Dichlorophenol	2.63 ± 0.46	12.38 ± 0.57	0.970	0.16 ± 0.02	12.93 ± 0.54	0.985
Phenol	2.05 ± 0.23	5.67 ± 0.18	0.964	0.25 ± 0.02	5.87 ± 0.15	0.984
3-Chlorophenol	0.45 ± 0.05	4.91 ± 0.19	0.993	0.03 ± 0.00	5.08 ± 0.20	0.995
Aromatic *N*-oxides (ANOs)						
Carbadox (CDX)	1.99 ± 0.16	4.13 ± 0.12	0.989	0.23 ± 0.01	4.23 ± 0.09	0.995
Quinoline *N*-oxide (QNO)	0.94 ± 0.11	6.39 ± 0.18	0.959	0.12 ± 0.01	6.59 ± 0.19	0.969
Quinoxaline *N*-oxide (QXO)	0.60 ± 0.07	8.53 ± 0.40	0.969	0.08 ± 0.01	8.94 ± 0.61	0.963
Quindoxin (QDX)	1.47 ± 0.29	8.37 ± 0.49	0.921	0.22 ± 0.05	8.90 ± 0.61	0.944
Fluoroquinolonic (FQs)						
Ciprofloxacin (CIP)	1.15 ± 0.26	0.36 ± 0.04	0.965	1.42 ± 0.90	0.62 ± 0.30	0.960
Ofloxacin (OFL)	2.99 ± 0.24	0.44 ± 0.01	0.985	5.02 ± 0.81	0.49 ± 0.03	0.978
Enrofloxacin (ENR)	9.65 ± 0.74	1.23 ± 0.02	0.977	9.31 ± 0.39	1.28 ± 0.01	0.996
Norfloxacin (NOR)	4.17 ± 0.48	1.24 ± 0.04	0.966	3.45 ± 0.37	1.41 ± 0.05	0.989
Lomefloxacin (LOM)	1.79 ± 0.10	0.71 ± 0.02	0.994	1.28 ± 0.07	0.74 ± 0.02	0.996
Pipemidic Acid (PIP)	0.68 ± 0.19	2.14 ± 0.28	0.912	0.07 ± 0.02	2.23 ± 0.36	0.927
1-Phenylpiperazine (PP)	9.22 ± 0.28	12.16 ± 0.09	0.999	0.12 ± 0.11	82.48 ± 0.72	0.998
N-phenylmorpholine (PM)	1.24 ± 0.11	7.10 ± 0.24	0.983	0.13 ± 0.02	8.69 ± 0.54	0.991
Tetracyclines (TCs)						
Tetracycline (TTC)	85.16 ± 12.98	35.74 ± 1.01	0.958	3.33 ± 0.42	36.66 ± 0.73	0.983
Chorotetracycline (CTC)	173.3 ± 9.01	37.63 ± 0.25	0.997	10.05 ± 0.55	38.02 ± 0.19	0.999
Oxytetracycline (OTC)	31.23 ± 6.35	36.29 ± 0.92	0.958	1.19 ± 0.21	37.42 ± 0.76	0.981

Notes:

- The model fitting was applied to the kinetic data of phenols, FQs, and ANOs obtained by ascorbic acid quenching and the kinetic data of TCs obtained by filtration quenching. In the case of TCs, model fits to data collected by the two

quenching methods were quite comparable (see Table S3); however, greater experimental errors were found with oxalic acid quenching. Oxalic acid does not reduce MnO_2 as quickly as ascorbic acid but was used for TCs because ascorbic acid interferes with TCs analysis. The greater errors are probably because (i) the time required to completely dissolve MnO_2 varied due to the different amount of MnO_2 employed particularly at the early stage of reaction, and (ii) a large volume of oxalic acid addition was needed.

- For phenols, FQs and ANOs, the experiments were conducted in 2-3 replicates. The parent compound concentrations measured at a given time in the replicate experiments were averaged. A total of 7 to 9 data points (each was an averaged value from the replicate experiments) were used to fit the kinetic equation. For TCs, the experiments were conducted in duplicate. The *k″* value was obtained by fitting the 7 to 9 data points collected in one of the duplicate experiments to the kinetic equation. The duplicate experiments yielded very comparable *k″* values.

- A ± B: A is the estimated value of *k* after regression analysis. B is the standard error of the mean of the specific range, as defined by $\frac{s}{\sqrt{n}}$, where s is standard deviation and n is number of data points.

Table 3.3 Model fitting parameters for the reactions of antibacterials and related compounds with Mn oxide in this study. *k'* and *k"* are obtained from model fitting, C_0, C_e and S_{rxn} are obtained from the experimental data.

Phenolic compound	C_0 (μmol L^{-1})	C_e (μmol L^{-1})	$S_{rxn}=C_0-C_e$ (μmol L^{-1})	k' (h^{-1})	R^2
Triclosan	21.07	2.35	18.72	2.06 ± 0.18[a]	0.983
Chlorophene	13.06	1.29	11.77	2.11 ± 0.07	0.997
2-Methyl-4-chlorophenol	9.48	1.49	7.99	2.24 ± 0.05	0.997
2,4-Dichlorophenol	19.33	6.70	12.63	1.97 ± 0.20	0.976
Phenol	9.26	3.79	5.47	1.31 ± 0.10	0.965
3-Chlorophenol	17	14.02	2.98	1.20 ± 0.14	0.976

Aromatic *N*-oxides (ANOs)	C_0 (μmol L^{-1})	C_e (μmol L^{-1})	$S_{rxn}=C_0-C_e$ (μmol L^{-1})	k' (h^{-1})	R^2
Carbadox (CDX)	9.14	4.67	4.47	1.00 ± 0.06	0.988
Quinoline *N*-oxide (QNO)	9.22	3.95	5.27	0.93 ± 0.04	0.993
Quinoxaline *N*-oxide (QXO)	10.22	3.40	6.82	1.16 ± 0.12	0.956
Quindoxin (QDX)	9.07	1.52	7.55	1.19 ± 0.11	0.968

Fluoroquinolonic (FQs)	C_0 (μmol L^{-1})	C_e (μmol L^{-1})	$S_{rxn}=C_0-C_e$ (μmol L^{-1})	k' (h^{-1})	R^2
Ciprofloxacin (CIP)	0.71	0.20	0.51	2.99 ± 0.29	0.949
Ofloxacin (OFL)	0.70	0.22	0.48	3.10 ± 0.17	0.984
Enrofloxacin (ENR)	0.81	0.20	0.61	3.28 ± 0.19	0.978
Norfloxacin (NOR)	1.45	0.14	1.31	2.95± 0.27	0.941
Lomefloxacin (LOM)	1.55	0.83	0.72	1.73 ± 0.05	0.994
Pipemidic Acid (PIP)	10.65	8.38	2.27	1.19 ± 0.10	0.961
1-Phenylpiperazine (PP)	10	0.30	9.70	3.44 ± 1.83	0.952
N-phenylmorpholine (PM)	10	2.35	7.65	1.29 ± 0.06	0.977

Table 3.3 (Continued)

Tetracyclines (TCs)	C_0 (μmol L^{-1})	C_e (μmol L^{-1})	$S_{rxn}=C_0-C_e$ (μmol L^{-1})	k'' (M^{-1} h^{-1})	R^2
Tetracycline (TTC)	40	1.01	38.99	2.80 ± 0.40	0.966
Chorotetracycline (CTC)	40	1.65	38.35	9.67 ± 0.54	0.998
Oxytetracycline (OTC)	40	0.80	39.20	0.98 ± 0.17	0.972

Typical reaction conditions: phenolic compounds and ANOs – 1.0 mM MnO_2, 10 μM organic compound, pH 4; FQs – 1.5 μM FQ, 0.1 mM MnO_2, pH 5; and TCs – 40 μM TC, 0.6 mM MnO_2, pH 5.

[a] A ± B: A is the estimated value of *k* after regression analysis. B is the standard error of the mean of the specific range, as defined by $s/\sqrt{n}$, where s is standard deviation and n is number of data points (n = 7-9). Each data point (*i.e.*, C at time t) was collected from average of or verified by 2-3 replicate experiments.

Table 3.4 (a) *k'* and S_{rxn} for triclosan oxidation[a], and (b) *k''*and S_{rxn} for TTC oxidation[b] by MnO_2 in various aqueous compositions.

(a)	Co-Solute M^{2+}(%)[c]	*k'* (h^{-1}) *k'*(Mn^{2+})	*k'*(Ca^{2+})	*k'*(Zn^{2+})	Co-Solute NOM (mg L^{-1})	*k'* (h^{-1}) *k'*(NOM)
	0	2.35 ± 0.06	1.83 ± 0.11	1.82 ± 0.06	0	1.69 ± 0.09
	0.1	2.36 ± 0.04	-	1.73 ± 0.04	5	1.55 ± 0.09
	0.5	2.36 ± 0.09	1.80 ± 0.09	1.51 ± 0.08	10	1.21 ± 0.04
	1	1.99 ± 0.07	1.90 ± 0.07	1.71 ± 0.12	15	0.80 ± 0.05
	5	1.46 ± 0.06	1.76 ± 0.07	1.46 ± 0.06		
	10	0.95 ± 0.09	1.64 ± 0.09	1.17 ± 0.07		
	Co-Solute M^{2+}(%)[c]	**S_{rxn} (μmol L^{-1}) S_{rxn}(Mn^{2+})**	**S_{rxn}(Ca^{2+})**	**S_{rxn}(Zn^{2+})**	**Co-Solute NOM (mg L^{-1})**	**S_{rxn} (μmol L^{-1}) S_{rxn}(NOM)**
	0	12.64	10.22	8.80	0	11.00
	0.1	11.48	-	8.94	5	10.82
	0.5	11.39	9.67	8.74	10	10.64
	1	11.94	9.85	8.74	15	10.01
	5	11.18	9.73	8.41		
	10	10.57	9.82	7.75		
(b)	**Co-Solute M^{2+}(%)[b]**	***k"* (M^{-1} h^{-1}) *k"*(Mn^{2+})**	***k"*(Ca^{2+})**	***k"*(Mg^{2+})**	**Co-Solute NOM (mg L^{-1})**	***k"* (M^{-1} h^{-1}) *k"*(NOM)**
	0[d]	0.48 ± 0.116	1.44 ± 0.25	2.02 ± 0.23	0[d]	5.05 ± 0.15
	6.7	0.11 ± 0.019	1.30 ± 0.23	1.83 ± 0.21	1	3.56 ± 0.10
	16.7	0.06 ± 0.009	0.94 ± 0.16	1.88 ± 0.22	5	4.59 ±0.16
	33.3	0.03 ± 0.004	0.61 ± 0.12	1.36 ± 0.15	10	3.72 ± 0.15
	50	0.03 ± 0.004	1.04 ± 0.16	1.53 ± 0.17	20	3.21 ± 0.27
	Co-Solute M^{2+}(%)[ab]	**S_{rxn} (μmol L^{-1}) S_{rxn}(Mn^{2+})**	**S_{rxn}(Ca^{2+})**	**S_{rxn}(Mg^{2+})**	**Co-Solute NOM (mg L^{-1})**	**S_{rxn} (μmol L^{-1}) S_{rxn}(NOM)**
	0	38.20	38.17	36.41	0	38.21
	6.7	37.20	38.00	35.74	1	38.07
	16.7	34.22	37.96	35.57	5	38.08
	33.3	35.35	37.72	34.54	10	37.85
	50	31.25	37.83	35.12	20	38.13

[a] Reaction conditions: 10 μM triclosan, 100 μM MnO_2, pH 5. [b] Reaction conditions: 40 μM TTC, 600 μM MnO_2, pH 5. [c] % of the initial MnO_2 concentration. [c] The difference in *k"* in the controls is likely caused by aging of MnO_2 because the different experiments were conducted over a 9-month period.

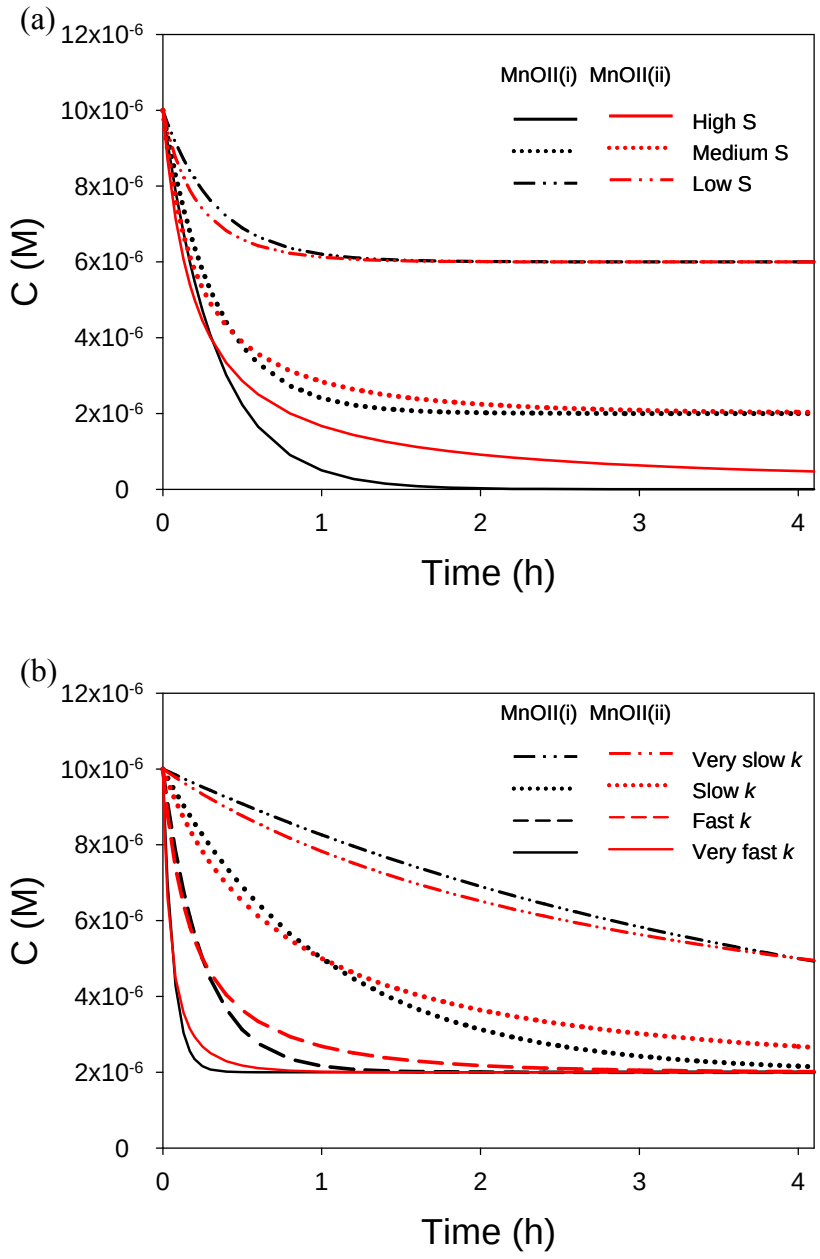

Figure 3.1 Sensitivity analysis of the kinetic models by changing the fitting parameter a) S_{rxn} or b) k. Fitting parameters: $C_0 = 1 \times 10^{-5}$ M in all cases;
a) k' = 3 h^{-1} for MnOII(i), k" = 5×10^5 h^{-1}-M^{-1} for MnOII(ii), $S_{rxn} = 1 \times 10^{-5}$, 8×10^{-6} and 4×10^{-6} M; b) $S_{rxn} = 8 \times 10^{-6}$ M, k' = 0.24, 0.98, 3.92, 15.69 h^{-1} for MnOII(i), k" = 3.60×10^4, 1.44×10^5, 5.75×10^5, 2.30×10^6 h^{-1}-M^{-1} for MnOII(ii).

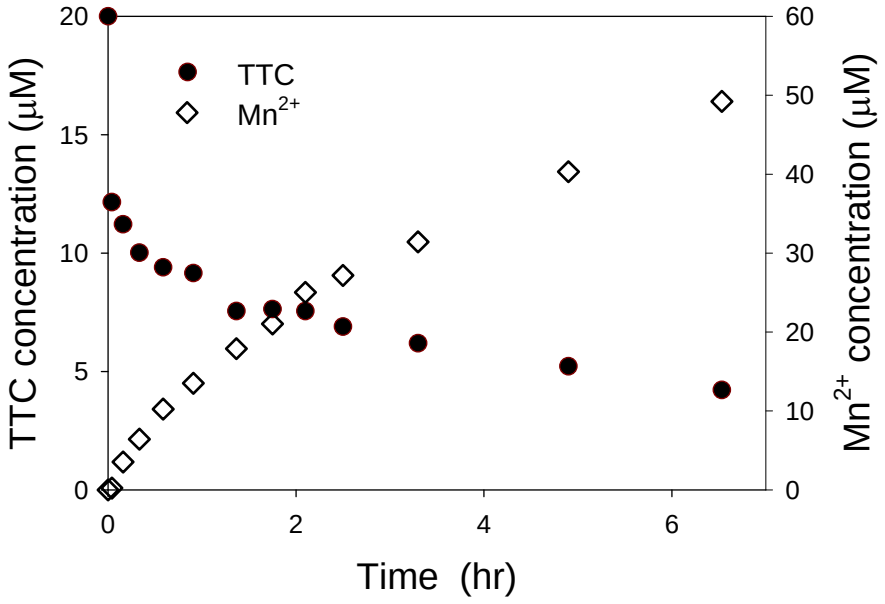

Figure 3.2 Rapid generation of Mn^{2+} was observed in parallel to the loss of TTC. Reaction conditions: $[MnO_2]_0 = 0.1$ mM, $[TTC]_0 = 20$ μM, pH = 5, T = 25 °C.

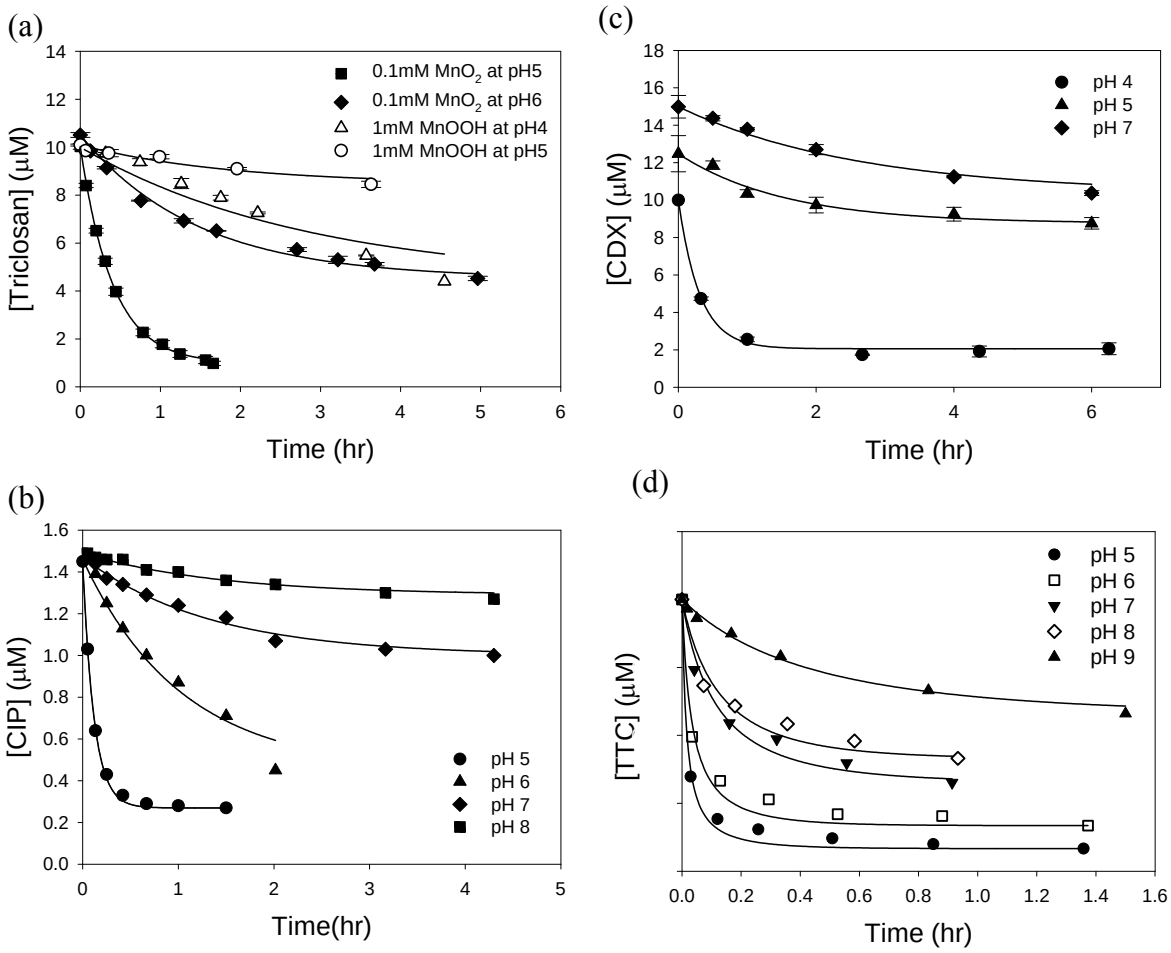

Figure 3.3 Example kinetic results and model fits: (a) Triclosan, (b) CIP, (c) CDX, and (d) TTC. Reaction conditions: (a) $[Triclosan]_0$ = 10 μM; (b) $[CIP]_0$ = 1.5 μM, $[MnO_2]_0$ = 0.1 mM; (c) $[CDX]_0$ = 10-15 μM, $[MnO_2]_0$ = 1.0 mM; (d) $[TTC]_0$ = 40 μM, $[MnO_2]_0$ = 0.6 mM.

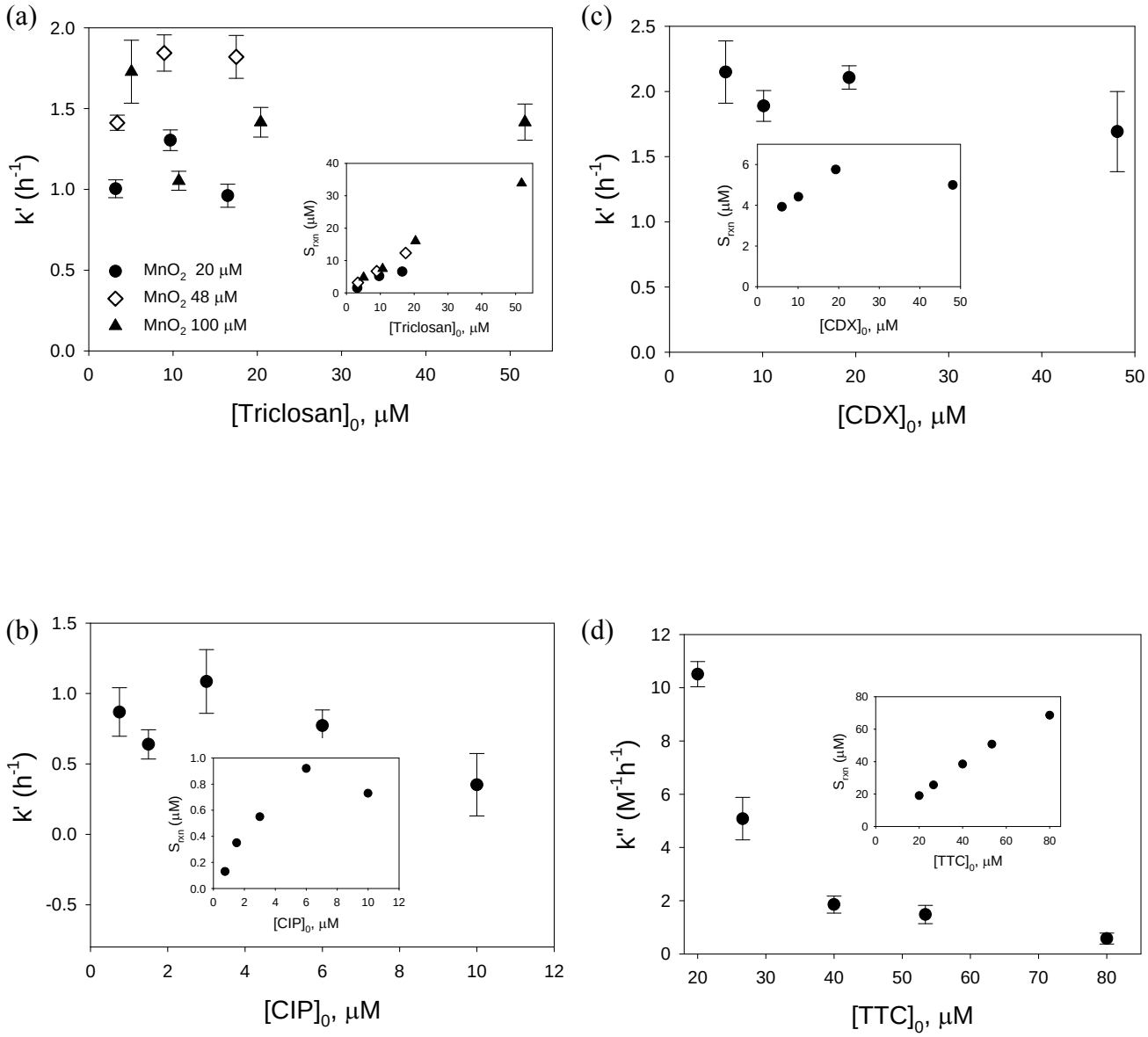

Figure 3.4 Effect of antibacterial loading on *k* and S_{rxn}: (a) Triclosan, (b) CIP, (c) CDX, and (d) TTC. (Reaction conditions: (a) pH 5;; (b) pH 5, $[MnO_2]_0$ = 100 μM; (c) pH 4, $[MnO_2]_0$ = 1 mM; (d) pH 5, $[MnO_2]_0$ = 0.6 mM)

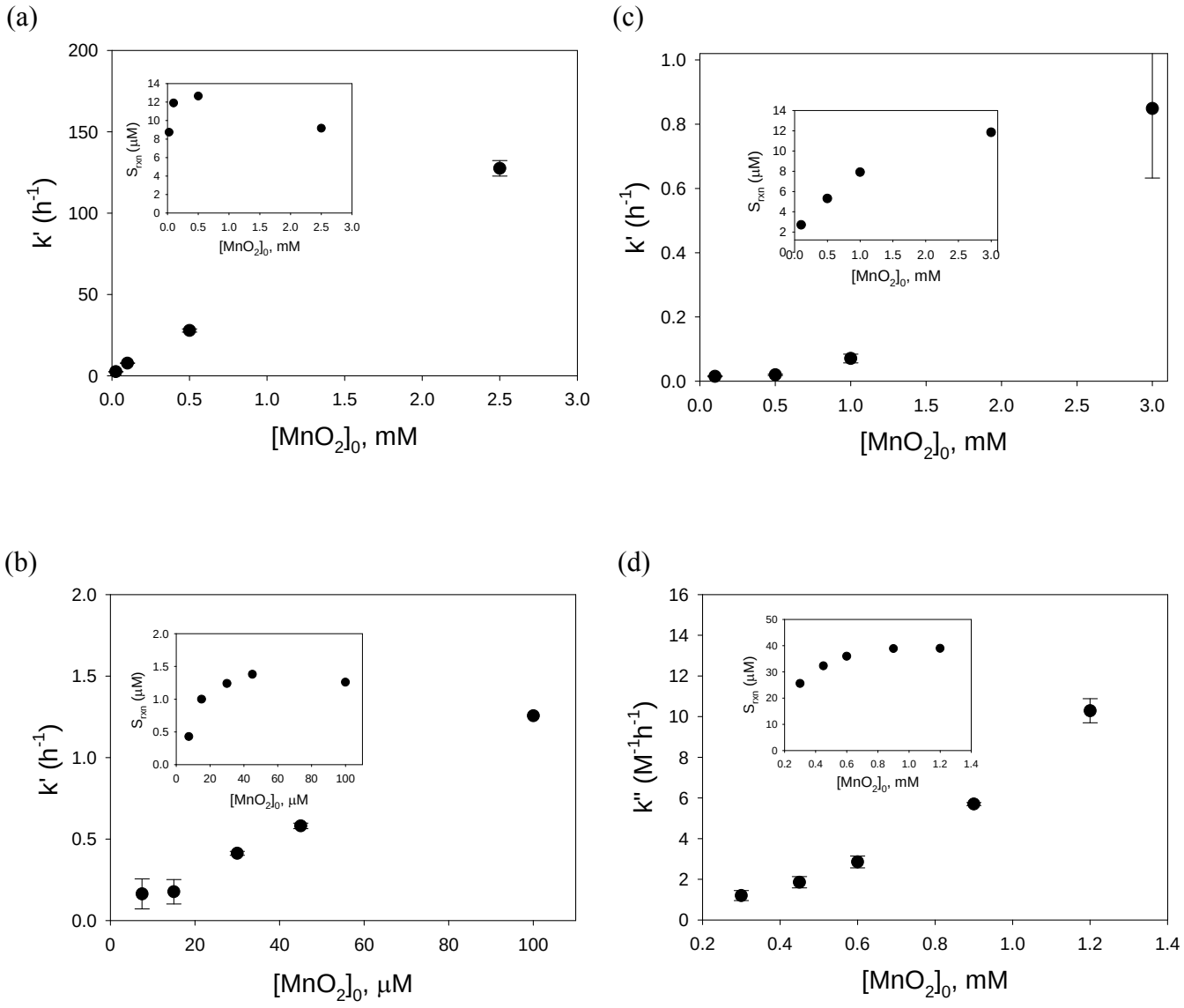

Figure 3.5 Effect of MnO_2 loading on *k* and S_{rxn}: (a) Triclosan, (b) CIP, (c) CDX, and (d) TTC. (Reaction conditions: (a) $[Triclosan]_0$ = 10 µM, pH 5; (b) $[CIP]_0$ = 1.5 µM, pH 5; (c) $[CDX]_0$ = 10 µM, pH4; (d) $[TTC]_0$ = 40 µM, pH 5)

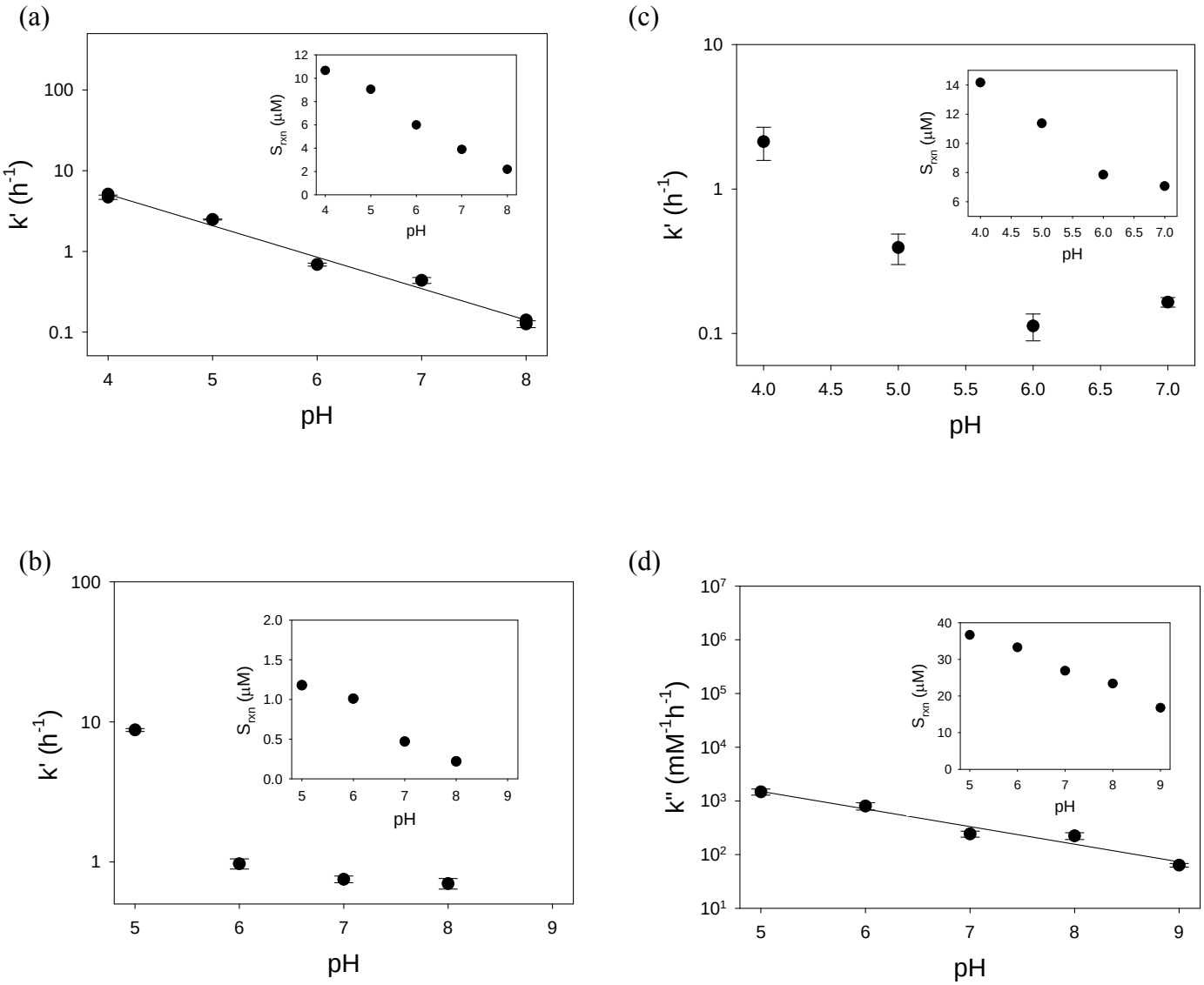

Figure 3.6 Effect of pH on *k* and S_{rxn}: (a) Triclosan, (b) CIP, (c) CDX, and (d) TTC. (Reaction conditions: (a) $[Triclosan]_0$ = 10 μM, $[MnO_2]_0$ = 0.1 mM; (b) $[CIP]_0$ = 1.5 μM, $[MnO_2]_0$ = 100 μM; (c) $[CDX]_0$ = 10 μM, $[MnO_2]_0$ = 1 mM; (d) $[TTC]_0$ = 40 μM, $[MnO_2]_0$ = 0.6 mM)

CHAPTER 4

TRANSFORMATION OF TETRACYCLINE ANTIBIOTICS BY MANGANESE OXIDE

4.1 Introduction

A wide range of antibiotics are used in large quantities in human and veterinary medicine. In addition, many antibiotics are used at sub-therapeutic levels to prevent epidemics and increase the growth rate and weight gain in livestock for food production. A large percentage of the administered antibiotics are excreted from the treated hosts, and subsequently contaminate the environment via various routes. The occurrence of antibiotics in water (Hirsch et al., 1999) and soil (Thiele-Bruhn, 2003) merits concern because of the possibility to foster development of antibiotic-resistant bacteria and cause other potential adverse health effects to humans (Barrett, 2005; Chapin et al., 2005). Among antibiotics, the environmental fate of tetracyclines (TCs) merit great attention because they have been used extensively to treat humans for several decades and account for over 60% of antibiotics used in animal feed (Ungemach Fritz et al., 2006). Among TCs, tetracycline (TTC), oxytetracycline (OTC) and chlorotetracycline (CTC) (Figure 1.1) are used widely in nutrition and feed additives throughout the agricultural sector. In the environment, TCs have been found at concentrations ranged from 0.07 to1.34 μg/L in surface water samples(Lindsey et al., 2001), 86.2 to 198.7 μg/kg in soil samples (Hamscher et al., 2002), 4.0 mg/kg in liquid manure samples (Hamscher et al., 2002), and higher than 3 μg/L in 90% of the farm lagoon samples (Zhu et al., 2001). The occurrence of tetracycline resistance genes in waste lagoons and groundwater has also been reported

(Chee-Sanford et al., 2001). To more accurately assess the risks of TC residues, a better understanding of their environmental fate is critical.

TCs possess complicated ring systems and are amphoteric molecules with multiple ionizable functional groups (Figure 1.2). Past research has shown that TCs are susceptible to various transform reactions including isomerization, dehydration, substitution, and oxygenation in metabolic and abiotic processes (Walton et al., 1970; Liang et al., 1998). For example, TCs can undergo reversible epimerization under certain acidic conditions at position C4 to form the corresponding 4-epi-TCs; the only difference between TCs and their epimers is the -$N(CH_3)_2$ group's position (Figure 1.2). At acidic conditions, acid-catalyzed dehydration may also occur to yield anhydro-tetracyclines (anhydro-TCs) by losing a H_2O at position C6, which exhibit higher cytotoxicity than the parent TCs (Klimova and Ermolova, 1976). TTC was reported to be relatively stable in 0.03 N HCl and its epimerization and acid-catalyzed dehydration are insignificant (McCormick et al., 1957). In contrast, TTC degrade rapidly to form epi-TTC and anhydro-TTC in the presence of phosphoric acid or citric acid. The phosphoric acid and citric acid likely act as a proton conductor in facilitating the above transformations (Walton et al., 1970; Sokoloski et al., 1977). At alkaline pH, the hydroxyl group at C6 of TCs cleaves readily to from their respective iso-tetracyclines (iso-TCs) (Waller et al., 1952).

Environmental processes of TCs including photolytic degradation (Sanniez and Pilpel, 1980; Moore et al., 1983; Oka et al., 1989; Olack and Morrison, 1991; Miskoski et

al., 1998), biotransformation (Aga et al., 2005; Arikan et al., 2006), and strong interactions with mineral surfaces and organic matter (Figueroa et al., 2004; Kulshrestha et al., 2004; Sassman and Lee, 2005; Pils and Laird, 2007) have been well studied. The existence of TC radical in the photoreaction was confirmed and a quinine product was observed (Moore et al., 1983). Structural alteration at the A ring of TCs was suggested for the photo-reaction products (Moore et al., 1983; Olack and Morrison, 1991). Several metabolic products of TCs were found in manure-containing matrices, such as isomerization products (epi-TCs) and dehydration products (anhydro-TCs, α-apo-OTC and β-apo-OTC) (Loke Marie et al., 2003; Aga et al., 2005; Arikan et al., 2006). The formation of α-apo-OTC and β-apo-OTC possibly occurs under acidic conditions (Halling-Sorensen et al., 2002). For the interactions with metal oxides, Rubert and Pedersen reported that MnO_2 can readily degrade several TCs including CTC, TTC, OTC, rolitetracyline and meclocycline (Rubert and Pedersen, 2006). Manganese oxides/hydroxides, commonly present in soils and sediments as colloidal particles or coatings on other minerals, are among the most important natural oxidants in soils (Li et al., 2003). The ability of Mn oxides to oxidatively transform organic contaminants has been demonstrated with a wide range of organic structures (Stone, 1987; Ukrainczyk and McBride, 1993; Li et al., 2003) and with several other groups of antibiotics (Zhang and Huang, 2003, 2005b, a). Rubert and Pedersen (Rubert and Pedersen, 2006) focused on the evaluation of the reaction kinetics of OTC with MnO_2; however, the transformation of OTC by MnO_2 was not characterized. Different from their study, the objective of the work presented here was to compare the reaction kinetics of three TCs (TTC, OTC, CTC) with MnO_2 using a new kinetic model developed in Chapter 3, assess the impact of metal

ion co-solutes on the reaction kinetics, evaluate the transformation products, and propose dominant transformation pathways.

4.2 Experimental Section

4.2.1 Chemicals

TTC, OTC and CTC were obtained from Sigma at 90-98% purity. Other employed chemicals were of at least 97% purity and were used without further purification. Unless otherwise specified, all other reagents used (e.g. buffers, ion strength agents, acids, etc.) were obtained from Fisher Scientific, Acros or Aldrich. All reagent solutions were prepared using water obtained from a Milli-Q Ultrapure Gradient A10 (Millipore - Billerica, MA) purification systems. Stocks of TCs were prepared in methanol at 1.6 mM, protected from light, stored in -15 ºC freezer, and used within a month of preparation. Throughout the experiment, acetate (pH 5) and 2-(cyclohexylamino)ethanesulfonic acid (CHES) (pH 9) buffers were used to maintain the reaction solution pH. NaCl salt was utilized to control ionic strength. Manganese dioxide (δ-MnO_2, similar to the naturally occurring birnessite) was synthesized using $KMnO_4$ and HCl based on the method by Murray (1974). Characterization of this MnO_2 was reported previously (Zhang and Huang, 2003).

4.2.2 Kinetic Experiments

Batch kinetic studies (with 40 μM of TCs and 0.6 mM of MnO_2) were conducted in 60 mL screw-cap amber glass bottles with Teflon septa, under constant stirring at 22 ^oC. Reactions were initiated by adding a certain amount of the TC reactant stock to solutions containing MnO_2, 10 mM buffer, and 0.01M NaCl as constant ionic medium. In the studies of the co-solute effect, the TC antibiotic was pre-mixed with Ca^{2+} or Mg^{2+} before being added to solutions containing MnO_2. Samples aliquots were taken from the reactors at proper time intervals. The supernatant was separated from MnO_2 particles by filtration and analyzed with high performance liquid chromatography (HPLC). As mentioned in Introduction, TCs are relatively stable in HCl. All samples were acidified by adding 5 μL concentrated HCl for preservation and improved analytical results. The samples were stored in amber vials at < 5 °C and analyzed within a couple of days. For each testing parameter, at least two or three replicate experiments were conducted. Control experiments without Mn oxide showed no significant degradation (< 5 %) of any of the tested compounds during the reaction periods (typically within 12 hours).

4.2.3 Analysis of TCs and Mn^{II} Ions

Analyses of TCs were carried out on an Agilent 1100 reverse-phase HPLC system with a Zorbax RX-C18 column (4.6 × 250 mm, 5 μm), an injection volume of 100 μL and a diode-array UV/Vis detector at a flow rate of 1 mL/min. TCs were detected at 275 nm and 365 nm. The mobile phase A consisted of 0.01 M oxalic acid and 10 μM EDTA,

while mobile phase B was pure acetonitrile. The gradient was as follows: 0−3 min 96% A and 4% B; 3−10 min a linear gradient to 73.7% A and 26.3% B; 10.0−19.0 min 73.7% A and 26.3% B; and 19.0−25.0 min linear gradient to 96% A, and 4% B. This final mixture was maintained for the remainder of the 30.0 minutes. Mn^{II} concentration was measured by ICP-AES (ICAP 61E Trace Analyzer, MA USA); all samples were filtered by pre-wetted 0.22 μm membranes (Millipore, GVWP) and acidified to contain 1 % nitric acid prior to analysis.

4.2.4 Product Identification

To identify reaction intermediates and products, reaction suspensions were filtered after at least 75% of the parent TC compound had transformed. Samples were concentrated 100 times by a blowdown device with pure N_2 gas. All mass spectrometric measurements were performed on an Agilent 1100 HPLC/DAD/MSD system equipped with an electrospray ionization source. The separation was performed by a Zorbax SB-C18 column (2.1×150mm, 5 μm) at a flow rate of 0.2 mL/min with the same mobile phases describe above. MS analysis was conducted by positive electrospray ionization at both low and high fragmentation voltages (110 and 250 eV) to yield optimal low and high fragmentation patterns with a mass scan range of m/z 50-1000. The drying gas was at 10 L/min at 350°C, the nebulizer pressure 25 psig, and the capillary voltage 4000 V.

4.3 Results and Discussion

4.3.1 Kinetics of Oxidation of TCs by MnO_2.

Rapid loss of TTC, CTC and OTC was observed in the presence of MnO_2. Figure 4.1 shows a typical time course of degradation of TCs with MnO_2 and a rapid formation of soluble Mn^{2+} ions without a lag phase. The fact that Mn^{2+} was the final stable reduction product and continued accumulating confirmed the oxidation of TCs by MnO_2. Among the three TCs, CTC showed the highest reactivity followed by TTC and then OTC, consistent with the observation by Rubert and Pedersen (2006).

The reaction kinetics of TC with MnO_2 were complicated and apparently deviated from pseudo-first-order decay and could not fit any typical rate equation. A new MnO_2 surface kinetic model was developed in our previous study to describe the reactions of various antibacterials and related organic compounds with MnO_2 (Chapter 3). In this model, either the precursor complex formation or electron transfer within the precursor complex is the rate-limiting step for the overall reaction. The MnOII(ii) model with the surface complexation formation (*i.e.,* adsorption) as the rate-limiting step was applied to the reactions of TCs with MnO_2 because of two reasons: (1) there was no delay in forming Mn^{2+} after the reaction was initiated (Figure 4.1), and (2) only a negligible amount of absorbed but unreacted TCs was accumulated on the MnO_2 surfaces. These observations indicated rapid electron transfer immediately after the molecules of TCs adsorb onto the MnO_2 surfaces. The MnOII(ii) model describes the loss of the parent TC compound in the presence of MnO_2 by the differential equation (1):

$$-\frac{dC}{dt} = k''[S_{rxn} - (C_0\text{-}C)]C \qquad (1)$$

and the equation (2) is the analytical solution of the equation (1):

$$C = \frac{S_{rxn} - C_0}{\frac{S_{rxn}}{C_0} e^{k''(S_{rxn} - C_0)t} - 1} \qquad (2)$$

where C_0 (in μM) and C (in μM) are the concentrations of the TC antibiotic at time zero and time *t*, respectively, k'' (in μM-h^{-1}) is the second-order reaction rate constant, and S_{rxn} (in μM) represents the total reactive surface sites that oxidized the parent antibacterial (*i.e.*, a two-electron transfer process). The MnOII(ii) model characterizes the kinetics parent antibiotic loss by two independent parameters, the reaction rate constant (k'') and the total reactive surface sites (S_{rxn}). Based on the MnOII(ii) model, the reaction reaches a plateau as $t \rightarrow \infty$, *i.e.*, the antibiotic concentration (C) eventually decreases to a constant value $C_e = C_0 - S_{rxn}$. Therefore, S_{rxn} value was estimated from the kinetic trend in the later stage of the experimental results (*i.e.*, $S_{rxn} = C_0 - C_e$). By setting a fixed S_{rxn}, the experimental data was fit to the equation (2) using the SigmaPlot program (version 9.01, Systat Software, Inc.) to yield the rate constant *k"* for TCs.

The validity of the MnOII(ii) model and its associated rate-limiting step (*i.e.*, surface complex formation) assumption were further verified by examining the influence of reactant concentration and solution pH on the reaction kinetics (Chapter 3). The impact of varying the initial TC concentration, the initial MnO_2 concentration and solution pH on the obtained kinetic parameters (*k"* and S_{rxn}) were discussed in detail in Chapter 3. Most significantly, the results showed that, when a fixed amount of MnO_2 was employed, increasing the initial TC concentration resulted in decreasing *k"* (*i.e.*, decreasing adsorption rate). This result supported the adsorption rate-limiting step because higher

TC concentration generated greater self-competition for the same number of surface sites and thus slowed the overall adsorption rate (Zou et al., 2006). In addition, both k'' and S_{rxn} increased proportionally with increasing MnO_2 concentration (note that S_{rxn} could not increase to be higher than the maximum level near the total initial TC concentration C_0). The results were consistent with the expectation that a greater number of oxide surface sites facilitated faster adsorption (*i.e.*, surface complex formation) and thus enhanced the reaction rate. The reaction kinetics were highly pH dependent; both the $\log(k'')$ and S_{rxn} decreased linearly as the pH was increased. The decreased S_{rxn} was attributed to the stronger electrostatic repulsion between the increasingly negatively charged TC and the negatively charged MnO_2 surfaces at higher pH conditions. Lower S_{rxn} led to slower adsorption rate and thus lower rate of TC transformation.

Rubert and Pedersen (2006) also studied the reaction kinetics of OTC with MnO_2 extensively; similarly complicated reaction kinetics to what were observed in our study were reported, in which the reactions eventually reached a plateau. The authors evaluated most of their kinetic results by the initial reaction rate approach, *i.e.*, obtaining the r_{init} in $\mu M\text{-}min^{-1}$ during the initial stage of reaction where the kinetics were fitted by the pseudo-first-order decay model. The reaction conditions employed in our study are comparable to those in (Rubert and Pedersen, 2006) (20-80 μM for TCs, 0.3-1.2 mM for MnO_2 and the pH rage of 5.0-9.0 in ours versus 10-200 μM for OTC, 0.49-1.97 mM for MnO_2 and the pH rage of 4.4-10.9 in theirs). In general, both studies show very similar effects of pH and increasing MnO_2 concentration on the reaction rate constant or rate, *i.e.*, $\log(k'')$ decreased linearly with increasing pH and k'' increased with increasing $[MnO_2]$ in our study versus $\ln(r_{init})$ decreased linearly with increasing pH, and r_{init} increased with

increasing [MnO_2] in Rubert and Pedersen (2006). However, Rubert and Pedersen reported that r_{init} increased with increasing [OTC] - a result that may appear in the first look to be contrary to our observation that *k"* decreased with increasing [TTC or OTC]. Note that the initial reaction rate approach captured only the reaction kinetics during the initial 1-1.5 min. In our study, the initial decay rate of TC was also faster when the initial TC concentration was higher. However, the rate at which the reaction reached the plateau was more gradual at higher [TC] and thus lower *k"*.

Note that our experimental results also showed that the generation of Mn^{2+} was 2 to 3 times higher than the amount of parent TC disappearance (Figure 4.1), indicating that multiple 2-electron transfers have occurred. This result indicates that multiple functional groups of TCs may have been oxidized and/or some of the functional groups can undergo multiple steps of oxidation. As will be discussed later, analyses of the oxidation products of TCs have confirmed these possibilities.

4.3.2 Effect of Metal Ion Co-Solutes.

TC molecules contain multiple electron-rich groups such as amines and carbonyls, and therefore can bind to cationic metal ions strongly, especially at neutral to higher pH conditions (Ohyama and Cowan, 1995; Tongaree et al., 1999). This section examines the effect of Mg^{2+} and Ca^{2+} co-solutes on the reaction rate of TTC with MnO_2. The effect was studied at pH 5 and 9. In these experiments, the Mg^{2+} or Ca^{2+} co-solute was pre-mixed with the target TTC and then the mixture was added into the reactor containing MnO_2 to initiate the reaction. The reported stability constants for Mg^{2+} and Ca^{2+} to form $MgHTC^+$ and $CuHTC^+$ complexes (*i.e.*, 1:1 metal:ligand copmlex) with TTC were 14.57

and 14.64, respectively (Ohyama and Cowan, 1995). Indeed, it is possible for two metal ions to complex with one TTC molecule (*i.e.*, 2:1 metal:ligand complex) at high metal ion concentration (Jezowska-Bojczuk et al., 1993; Wessels et al., 1998); however, reported stability constants for 2:1 Mg^{2+} and Ca^{2+} to TTC complexes are not available in the literature. The equilibrium computer program MINEQL+ (Version 4.5) (Schecher and McAvoy, 2001) was used to calculate the complexation of TTC with Mg^{2+} and Ca^{2+} with consideration of only the 1:1 complexes. The complex formation at pH 5 was calculated to be less than 5% of the total TTC for either Mg^{2+} or Ca^{2+} even when the metal ion concentration was 7.5 times higher than the TTC concentration ($[TTC]_0$ = 40 μM, $[Mg^{2+}$ or $Ca^{2+}]_0$ = 0.3 mM). In contrast, 33-93% of TTC was complexed with Mg^{2+} or Ca^{2+} at pH 9; the concentration of the metal complex increases with increasing metal ion co-solute concentration (Table 4.1).

The obtained kinetic parameters (*k"* and S_{rxn}) were plotted against the $[Mg^{2+}$ or $Ca^{2+}]_0$ to $[TTC]_0$ ratio (Figures 4.2 and 4.3). At pH 5, the presence of Mg^{2+} or Ca^{2+} co-solutes caused little decrease in the total reactive surface sites (S_{rxn}) and resulted in only a slight decrease in the reaction rate constant *k"* (Figure 4.2). No significant inhibitory effect could be observed even when the metal co-solute concentration was more than 7 times higher than the TTC concentration. These results suggest that Mg^{2+} and Ca^{2+} ions do not compete with TTC for the same sites on the MnO_2 surfaces and thus had negligible effect on both S_{rxn} and *k"*. At pH 9, however, the presence of the metal co-solutes caused a noticeable decrease in S_{rxn} but an increase in *k"* when a higher metal co-solute concentration was applied (Figure 4.3). We hypothesized that, at pH 9, Mg^{2+} and Ca^{2+} have a stronger tendency to accumulate on the negatively charged MnO_2 surfaces,

leading to fewer available sites to participate in TTC oxidation (*i.e.*, decreased S_{rxn}). On the other hand, these metal co-solutes are able to complex with TTC to form $CaHTC^+$ or $MgHTC^+$ complexes, altering the overall charge of TTC from -1 of its dominant free TTC species at pH 9 (HTC^-) to +1 by metal ion complexation. This positive charge facilitated more rapid favorable adsorption of TTC to the negatively charged MnO_2 surfaces, leading to increase in *k"*.

4.3.3 Transformation Product Analysis.

The reaction mixtures of each of the TC members with MnO_2 were stopped by filtration, and the filtrate was analyzed by HPLC/UV/MS. Table 4.2 summarized the UV absorbance and mass spectral data of TCs and the products that were measured.
The UV analysis was used to complement the MS analysis. Note that the tricarbonylamide (A ring) and the phenolic-diketone (BCD ring) are two separate resonance groups, contributing to two major absorption bends (250-300 nm and 340-380 nm) of TCs' spectra. In general, the A ring chromophore contributes only to the 250-300 nm absorption, whereas the BCD ring chromophore contributes to both absorption bends (McCormick et al., 1957; Wessels et al., 1998; Schneider et al., 2003).

4.3.3.1 TTC Transformation Products

The molecular ion of the TTC parent compound was *m/z* 445 with two major fragments (- 17 and -35 *m/z*) (Table 4.2), indicating the TTC molecule can easily lose a NH_3 and a H_2O to generate $[M+H-NH_3]^+$ and $[M+H-NH_3-H_2O]^+$ fragments. Unlike many other organic compounds reported previously (e.g., Lykkeberg Anne et al. (2004)), TCs

did not form adducts with a sodium ion in the electrospray LC/MS analysis. The molecular ions were identified based on: 1) the results when low fragmentation voltage (110 V) was applied, 2) the $[M+H]^+$ ion as the base peak, and 3) most TCs and products have the same daughter ion pattern – a *m/z* 17 and a *m/z* 18 losses (Table 4.2). The NH_3 loss involves the amino group at the C2 cabonylamine group and the H_2O loss was suggested from the hydroxyl group bound at the C6 atom (Dalmazio et al., 2007).

Analyses of TTC reaction mixtures indicated the presence of primarily ten products with molecular ions of *m/z* 433, 445, 459, 461, 475a, 475b, 847, 849, 875 and 907 (Table 4.2, two products have the same *m/z* ratio 475). With the exception of the products of over *m/z* 847, the products were also short-written as M-12, M, M+14, M+16, M+30a and M+30b, indicating the mass difference relative to the molecular weight of TTC. The *m/z* 445 product with the same *m/z* ratio as parent TTC does not exhibit a $[M+H-NH_3-H_2O]^+$ fragment but a $[M+H-NH_3-CO]^+$ fragment and shows no UV absorptivity at 365 nm, indicating an iso-derivate of TTC formation (Zurhelle et al., 2000). All other products exhibited fragmentation patterns similar to that of TTC, indicating they shared a common base structure with TTC, that is, the basic tetracyclic rings. This typical daughter ion pattern was also applied to identify OTC, CTC and their transformation products.

The *m/z* values of most TTC products were higher than that of TTC, indicating net mass gain of the transformation products. The M+16 and M+14 products, in comparison to TTC, agreed well with previous findings in the MnO_2-oxidized products of phenols (e.g., ref: Ukrainczyk and McBride (1993)). TC molecules are complicated structures with two resonance groups: the phenolic-diketone group at the BCD ring and the tricarbonylamide group at the A ring (Figure 4.4). The phenolic-diketone moiety is

involved in unusual keto-enol tautomerism which cannot be distinguished by LC/MS analysis (Clive, 1968). The same resonance structural features are capable of stabilizing radical formation (Figure 4.5) and make TC molecule susceptible to oxidation. Oxidation of TC may start at O10, O11 or O12 within the phenolic-diketone group and at O1 or O3 within the tricarbonylamide group. Among the above prospective sites, O10 is highly possible to be subject to oxidation (see more discussion later). As illustrated in Figure 4.6 Scheme I, the ring D of TTC structure is a phenol moiety which can readily form a phenoxy radical by one-electron oxidation by MnO_2. The phenoxy radical can be further oxidized by Mn(IV) to result in a hydroquinone product (a net weight gain of 16). The addition of –OH group can occur at either the ortho (C9) or para (C7) position relative to the phenolic -OH group (C10). Considering that the C10-C12 diketone group is the primary site of TTC to react with MnO_2 surface sites to generate the phenoxy radical, the subsequent oxidation of the phenoxy radical by another surface Mn(IV) is more likely to occur on the C9 position right next to C10 (Zhang and Huang, 2005b). Therefore, an ortho-substituted hydroquinone product at the D ring of TTC is proposed in Scheme 1 (Figure 4.6). The hydroquinone moiety can undergo further two-electron oxidation by MnO_2 to form a quinone moiety (overall a net weight gain of 14) (Figure 4.6 Scheme 1). Although oxidation via the O11 or O12 group of TTC by MnO_2 is possible (Figure 4.5), the weak absorbance at 365 nm of all products strongly suggests that an iso-derivative has been formed at TTC's C ring. If the C ring is converted to the iso-structure, resonance stabilization of the radical from O11 and O12 is prohibited. Based on this reason, oxidation from TTC's O11 or O12 group is considered less likely than O10.

Besides the C10-C12 diketone group, the C1-C3 tricarbonylamide group is another site possibly subject to oxygenation. Oxidation of O1 or O3 will result in a radical that can be stabilized by three possible resonance structures, although fewer resonance structures than in the case of O9 oxidation (Figure 4.5). Oxidation of O1 or O3 by MnO_2 will most likely lead to –OH addition at C2 (Figure 4.6 Scheme 2). This proposed product structure agrees with the study by Dalmazio et al. (2007), which investigated the oxidation of TCs by ozone. The authors proposed oxygen insertion at the C11a-C12 double bond in the phenolic diketone system and the C2-C3 double bond in the tricarbonylamide moiety. Combining both oxidation pathways from O10 and O1-O3, formation of a quinone structure at the D ring of TTC plus hydroxylation at C2 will result in a M+30 product (II or III in Figure 4.7a).

4.3.3.2 OTC Transformation Products

Among the three TCs investigated, OTC (*m/z* 461) showed the slowest reaction rate with MnO_2 and the least complicated product formation patterns. Note that the elution of epi-OTC was not observed for OTC standard under reserved-phase HPLC conditions. OTC is less likely to epimerize, compared to TTC and CTC, because the hydroxyl group at C5 forms a hydrogen bond with the $–N(CH_3)_2$ group (Mitscher, 1978). Product analysis show that OTC did not have a product with the same *m/z* ratio as itself and most products retain strong absorbance at 365 nm, indicating that iso-OTC was not formed. Previous studies have reported the lower tendency of OTC for isomerization literature (Waller et al., 1952); it may be possible that the C5-OH of OTC also forms a hydrogen bond with the C6-OH, thus increasing its stability.

The *m/z* values of OTC major products were 386, 447, 477 and 639. The *m/z* 386 was the only even *m/z* product detected, suggesting that a N loss from the parent compound. The *m/z* 447 product, short written as M-14, was tentatively identified as an N-demethyl product of OTC (*i.e.*, a $-CH_3$ group was substituted by a hydrogen atom at N4). This product was proposed based on the following three properties: (1) a loss of 14 unit for the molecular ion, (2) a shorter retention time in reverse-phase HPLC, indicating greater polarity, and (3) similar daughter ion pattern as that of OTC. The same three properties were used by Zurhelle to identify the N-demethyl metabolic products in eggs and the C-N bond cleavage within the $-N(CH_3)_2$ group was proposed (Zurhelle et al., 2000). A similar C-N bond cleavage has also been proposed for the catalytic oxidation of nitrilotris(methylene)phosphonic acid by Mn(II) ions and molecular oxygen (Nowack and Stone, 2000). Therefore, in the case of OTC, we proposed that the positively charged $-N(CH_3)_2$ group is subject to adsorption and oxidation by negatively charged MnO_2 surfaces. As shown in Figure 4.6 Scheme III, the first electron transfer occurs between the methyl group and Mn^{IV} and a methylene radical is generated. This methylene radical can be further oxidized to an iminium cation, which undergoes fast hydrolysis reaction to yield the N-desmethyl derivative and formaldehyde. The *m/z* 477 product showed a 16 unit increase in molecular weight, suggesting OTC may undergo similar oxygen insertion as TTC.

4.3.3.3 CTC Transformation Products

A typical chromatogram of the CTC (*m/z* 479) standard showed four separated peaks, as also reported by Blanchflower et al. (1997). These peaks were identified as CTC, epi-CTC, keto-CTC and enol-CTC. Keto-CTC and enol-CTC are the keto tautomers of CTC and epi-CTC, respectively. Besides these four basic peaks, the *m/z* values of CTC's major products were 479, 445, 465, 467, 495 and 511, short-written as M, M-34, M-14, M-12, M+16 and M+32. The two products (M+16 and M+32) exhibited additional one or two oxygen atomic weight, suggesting that additional oxygens were present in these products possibly via the oxidative transformation Scheme I and II (Figure4.6). The *m/z* 479 product was confirmed to be iso-CTC because it: (1) exhibited a $[M+H-NH_3-CO]^+$ fragment ion, (2) showed no UV absorptivity at 365 nm, and (3) had the same retention time as iso-CTC standard. The *m/z* 465 (M-14) product was identified as N-demethyl-CTC based on the same reasons as those for the *m/z* 447 product for OTC. Besides the M-34 product, all products exhibited the characteristic 3:1 isotopic ratio of $^{35}Cl/^{37}Cl$ for their molecular ions, indicating the chlorine atom was intact. The M-34 product was identified to be TTC because it lacked a Cl atom and had the same retention time and m/z ratio as those of TTC.

The higher molecular weight products of *m/z* 847, 849, 875 and 907 from TTC and m/z 639 from OTC suggest coupling products via radical-radical coupling. Several products including the *m/z* 386 from OTC and the M-12 products from TTC and CTC could not be identified based on the MS data and literature. The above results clearly demonstrated a complicated reaction and product formation mechanism for the oxidation of TCs by MnO_2.

4.3.4 Proposed Transformation Pathways.

Attempts were made to evaluate if the distribution among the oxidation products differed among the TCs. Due to the lack of authentic standards, a rudimentary quantification of the products was performed by using the crude assumption that the mass spectrometric response of the products is the same as that of the parent compounds. The evolution of major products for the three TCs over time was presented in Figure 4.8, and the details are discussed along with proposing transformation schemes of TCs. The likely transformation pathway (Figure 4.7) for each TC compound by MnO_2 is proposed based on the results of reaction kinetics and product identification discussed above, the literature on the isomerization and oxidation of TCs, and the product evolution results.

We hypothesize that the reaction with MnO_2 caused isomerization TTC at the C ring and the isomerized TTC is oxidized by MnO_2 to yield various products (Figure 4.7a). The hydroxylated products (i.e., M+16) were present for all of the three TCs after oxidation by MnO_2 (Figure 4.8). However, the M+16 product yield from TTC (Figure 4.8a) was noticeably higher than from OTC and CTC, and was the dominant product of TTC transformation by MnO_2. Based on the discussion presented in the previous section, TTC is likely to be oxidized initially via the oxidative transformation Scheme I to yield Product IV (Figure 4.7a). Further oxidation of IV then yields the quinone Product I (M+14). Further oxidation at the tricarbonylamide group via the oxidative transformation Scheme II to form the M+30 product (Figure 4.7a, Products II and III). Although two M+30 products were detected, the most plausible structure was proposed in Figure 4.7a. Other possible structures for the M+30 products cannot be determined based on the data.

Figure 4.8b clearly shows that the N-demethyl derivative of OTC (*m/z* 447) is an intermediate. A high abundance appeared at 3-4 hours and significantly decreased after 4 hours along with the formation of the *m/z* 639 product. The presence of a hydroxyl group at C5 conveys some special properties on OTC which makes its chemistry different from that of the other TCs (Mitscher, 1978). The additional hydroxyl group at C5 forms hydrogen bonding with the $-N(CH_3)_2$ at C4 position. Consequently, OTC shows a stronger tendency to absorb on MnO_2 via $-N(CH_3)_2$ group and tends to undergo N-demethyl oxidation pathway (Figure 4.7b) unlike the patterns exhibited by TTC. Also, in contrast to TTC, OTC does not form the iso-derivative product in the reaction with MnO_2. One M+16 product was detected for OTC (Figure 4.8b). We proposed that the oxidation occurred via Scheme II (Figure 4.7b) since structural alteration of OTC in the reaction with MnO_2 tended to involve the A ring, only one M+16 was detected, and M+14 product was found.

Iso-CTC was clearly the most abundant product formed (Figure 4.8c) from the reaction of CTC with MnO_2, consistent with the stronger tendency of CTC than the other TCs to form iso-CTC reported in the literature (Waller et al., 1952). Mn oxide surfaces, by coordinating to the C11 carbonyl group, likely promoted the nucleophilic attack of the C6 –OH group on the C11 carbonyl carbon to yield isomerized product. The iso-CTC showed a significant amount at the first 30 minutes and gradually decreased in concentration, indicating that iso-CTC is an intermediate (Figure 4.8c). Compared to TTC and OTC, the M+16 product yield was much lower for CTC. This may be attributed to the chlorine substitution at C7 of CTC. Due to its electron-withdrawing effect, chlorine substitution generally lowers the tendency of a phenolic moiety toward oxidation

(Ulrich and Stone, 1989). Further oxidation of iso-CTC can occur via both Scheme I and/or II , yielding two possible M+16 (Xa and Xb), M+32 (VII) and M+30 (VIII) products (Figure 4.7c) . The detection of M-14 product for CTC suggests the formation of a N-demethyl derivative (product IX) likely via Scheme III (Gratacos-Cubarsi et al., 2007). Transformation of CTC to TTC is also possible based on the detection of TTC (Figure 4.7a).

The above results show that TCs can undergo multiple oxygenation steps by MnO_2, which is consistent with the Mn^{2+} generation result. The amount of TC transformation can yield 2 to 3 times higher amounts of Mn^{2+} (Figure 4.1), indicating that multiple e-transfers occurred. In summary, the transformation is initiated by formation of a surface complex. The surface promotes isomerization and oxidation of the compounds. The product analysis suggests that the TC molecule has two labile sites (C9 and C2) that can be inserted with oxygen, thus allowing the multiple oxidation steps to occur. .

4.4 Environmental Relevance

Based on the high reactivity of TCs to oxidative and isometric transformation by MnO_2, it is quite likely that TCs will transform in soil-water environment with the presence of MnO_2. The surface complex formation between TCs and MnO_2 controlls the reaction kinetics, along with the influence of water pH and the reactant concentration. Product identification is not only necessary to deduce the mechanisms of TCs oxidation by MnO_2 in solutions but also essential for assessing the potential risk of the transformation products. In the LC/MS analysis, TTC tends to be oxidized via the D ring, CTC is inclined to undergo surface-promoted isomerization, and OTC has a stronger

tendency to yield a N-demethyl derivate. Three TCs showed different reactivities and transformation pathways towards MnO_2. Besides iso-TCs, all other products retained the unchanged tetracyclic ring system and possibly still possess bioactivity (Mitscher, 1978). Mitscher described the molecular structural change of TCs with two principles: (1) the bioactivity of TCs reduces if chemical changes occur at any position in C1-C4 and C10-C12 areas, and (2) the bioactivity is not reduced if chemical changes occur in the rest of the areas (Mitscher, 1978). Therefore, it can be inferred that the bioactivity of Products I and II for TTC may remain the same. In contrast, the rest of the products should therefore be less potent than their respective parent compounds.

This is the first study examining the transformation pathways and products of several TCs by manganese oxide. Manganese oxide not only causes oxidation but also significantly promotes isomerization and substitution for TCs. Several transformation products were identified and the basic tetracyclic structure was not changed significantly. Because of the modest structural change, some of the products may still have the tendency to promote antibiotic-resistant bacteria and raise the concern of potential adverse health and ecological effects of these compounds. The mechanisms and the reaction pathways elucidated in this study provide the basis for predicting the reactivity of TCs in the environemnt. The kinetic results help predict their persistence in the soil-water system; OTC showed more persistence than TTC and CTC. In addition, the oxidation and surface-promoted transformation of TCs may provide an abiotic process in the treatment of wastewater for the detoxification of toxic and bioresistant organic pollutants. Results of this study also warrant further investigation on the potential interactions of TCs with environmentally important minerals and metal species, such as

iron oxides and silica. The mineral surface may promote the isomerization and substitution of TCs, like the surface of MnO_2. This study helps to evaluate the potential risk of antibiotic disruption resulting from these abiotic active materials. It was necessary to study the occurrence and the fate of these antibiotic compounds in the aquatic environment. The role of metal oxides appears to affect the fate and transport of antibiotics and influence their persistence in the environment. Identification of significant transformation products can provide a molecular basis for future studies on the formation of potentially toxic degradation products.

Table 4.1 Metal-TTC complexation percentage. ($[TC]_0$=40 μM, pH 9)

Co-solute / TTC to M^{2+} ratio	Metal-TTC complex (%Total TTC)	
	Mg^{2+} as co-solute	Ca^{2+} as co-solute
	$MgHTTC^+$	$CaHTTC^+$
no M^{2+}	0	0
M^{2+}/TTC= 0.5	33.1	34.7
M^{2+}/TTC= 1	56.3	58.8
M^{2+}/TTC= 3	86.3	88.0
M^{2+}/TTC= 5	92.3	93.4

Table 4.2 Results of LC/UV/MS analysis of the transformation products of TCs by MnO_2

Compound	RT (min)	UV absorbance bend		Short written	m/z (relative intensity)				
		275nm	365nm		MH^+	Daughter ions			
TTC	10.92	strong	strong	M	445	428	410		
Unknown A	5.83	strong	weak	M-12	433	416			
iso-TTC	12.12	strong	weak	M	445	417	400		
I	13.85	strong	weak	M+14	459	442	424	415	398
II	14.53	strong	weak	M+30	475	458	412		
III	14.92	strong	weak	M+30	475	458	412		
IV	16.73	strong	weak	M+16	461	444	426	399	382
Unknown B	20.28	strong	weak		875	449	432		
Unknown C	21.00	medium	weak		907	465	443		
Unknown D	24.25	strong	weak		849	436	419	396	
Unknown E	25.61	strong	weak		847	435			
OTC	8.75	strong	strong	M	461	444	426		
V	7.27	strong	strong	M-14	447	429	412		
VI	10.06	strong	strong	M+16	477	460	433		
Unknown F	14.20	strong	medium		639	331			
Unknown G	15.03	medium	strong		386	369	351	333	
CTC	15.96	strong	strong	M	479	462	444		
VII	10.73	strong	absent	M+32	511	494			
TC	11.06	strong	strong	M-34	445	428	427	410	
keto-CTC	11.59	strong	strong	M	479	462	444		
VIII	12.33	strong	absent	M+30	509	492	465	448	
iso-CTC	13.63	strong	absent	M	479	462	451		
IX	15.22	strong	weak	M-14	465	448	430		
Unknown H	16.76	strong	medium	M-12	467	450	432		
X	20.51	small	absent	M+16	495	478	460	433	416

Note: TTC, CTC, keto-CTC and OTC have C4 epimeric equilibrium. epi-TCs show the same daughter ion patterns in mass spectra and the same UV-Vis spectra with their parent compounds which are not listed in the table.

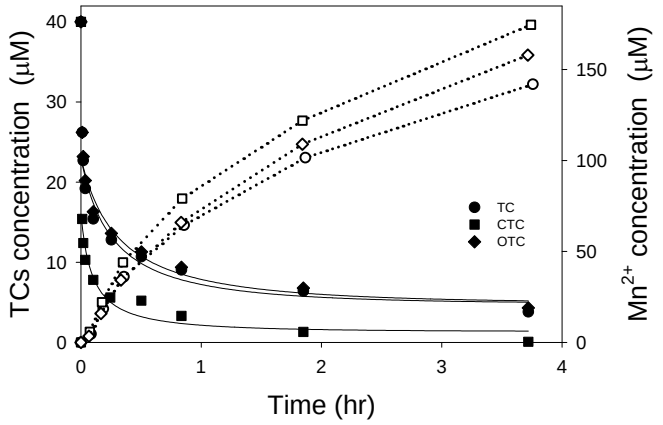

Figure 4.1 Kinetics of TCs transformation (in solid symbols) along with Mn^{2+} generation (in open symbols) by MnO_2. ($[TCs]_0$ = 40 μM, $[MnO_2]_0$ = 0.6 mM, pH 5)

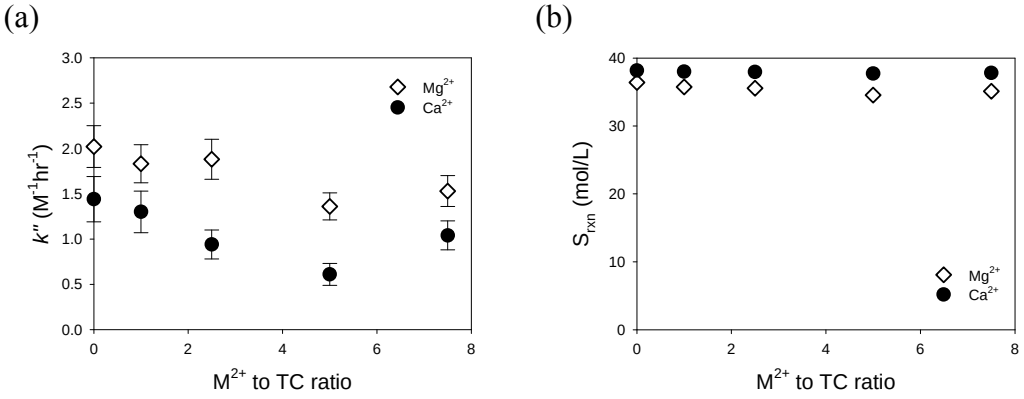

Figure 4.2 Co-solute effect on TC/MnO_2 reaction at pH 5. (a) *k"*; (b) S_{rxn}. ($[TCs]_0$ = 40 μM, $[MnO_2]_0$ = 0.6 mM.)

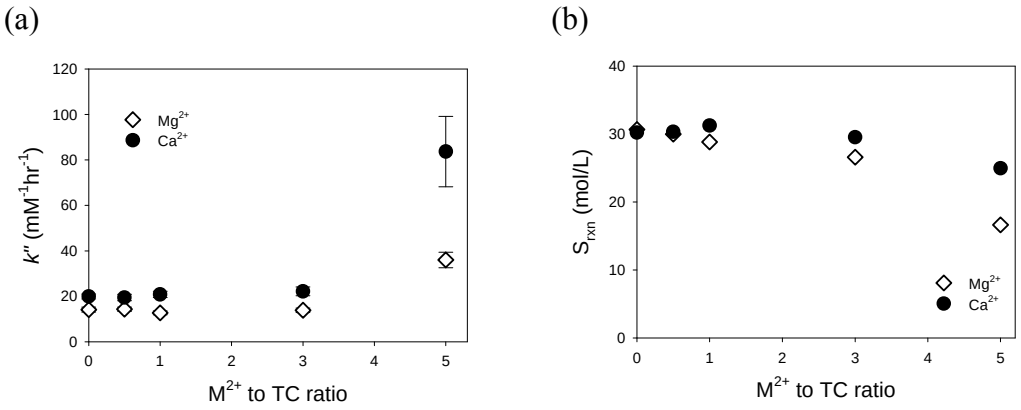

Figure 4.3 Co-solute effect on TC/MnO_2 reaction at pH 9. (a) *k"*; (b) S_{rxn}. ($[TCs]_0$ = 40 μM, $[MnO_2]_0$ = 0.6 mM.)

(a) Resonance of H^+ in the phenolic-diketone group:

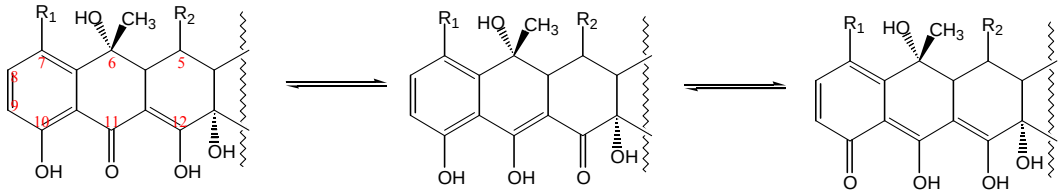

(b) Resonance of H^+ in the tricarbonylamide group:

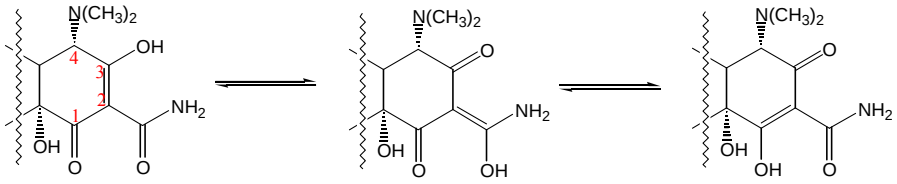

Figure 4.4 Resonance of proton in TC molecule.

a) **Resonance of radical in the phenolic-diketone group:**

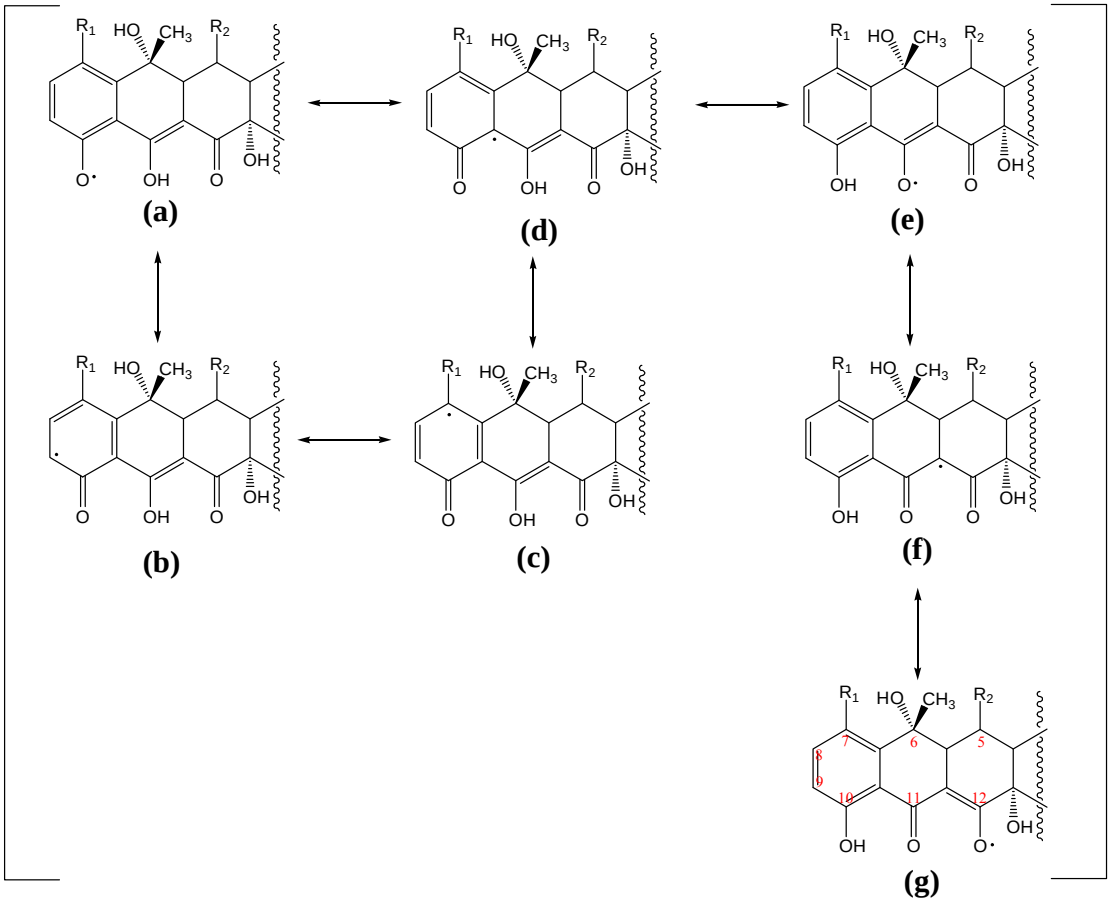

(Oxidation of TC may start as (a), (e) or (g) radical at the phenolic-diketone group)

(b) **Resonance of radical in the tricarbonylamide group:**

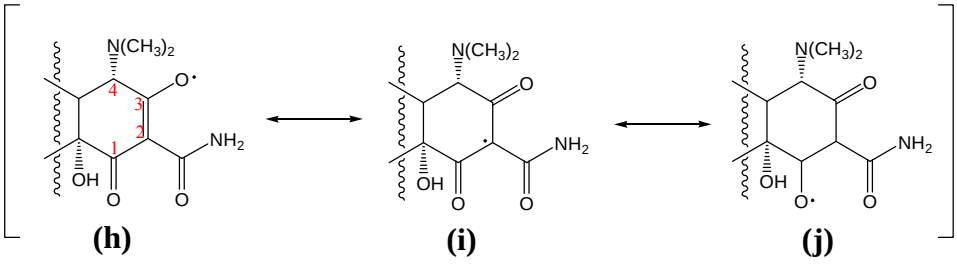

(Oxidation of TC may start as (h) or (j) radical at the tricabonylamide group)

Figure 4.5 Resonance of radical in TC molecule.

Scheme I

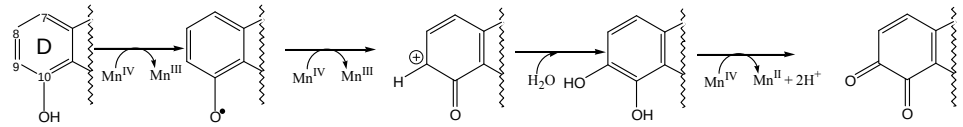

Scheme II

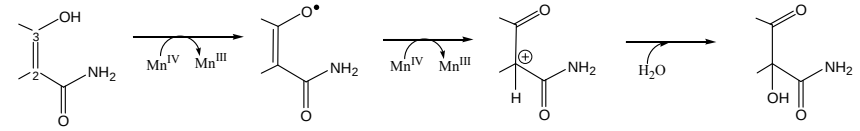

Scheme III

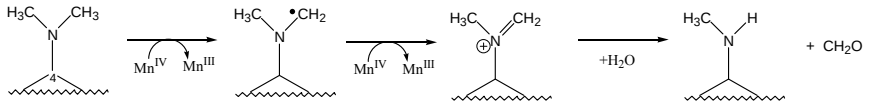

Figure 4.6 Proposed reaction schemes of oxidative transformation pathway of TCs by MnO_2.

(a)TTC

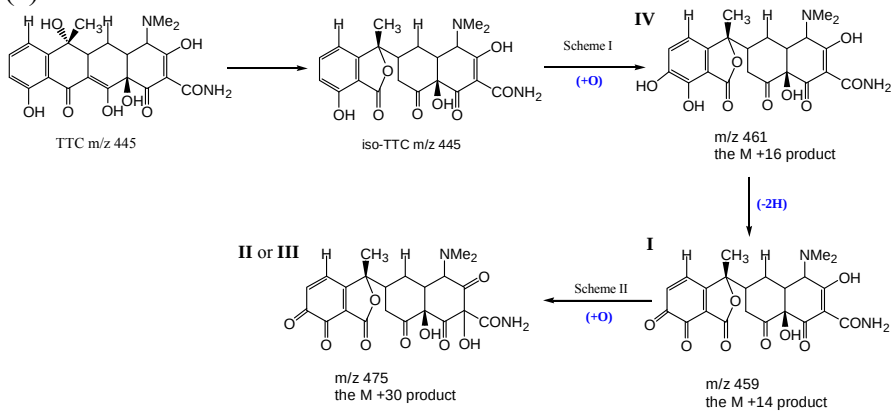

(b)OTC

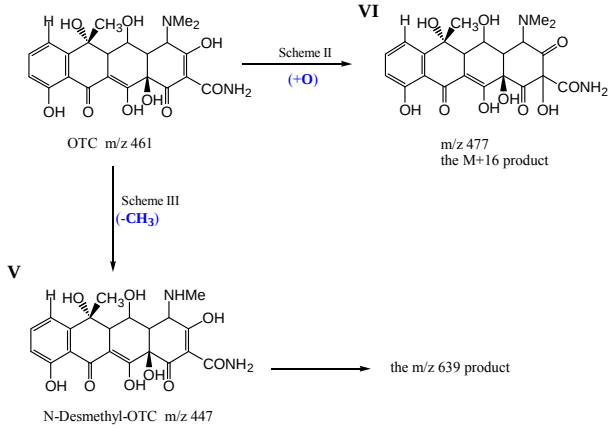

Figure 4.7 Possible reaction schemes for the transformation of TCs by MnO_2: (a) TTC, (b) OTC, (c) CTC.

(c)CTC

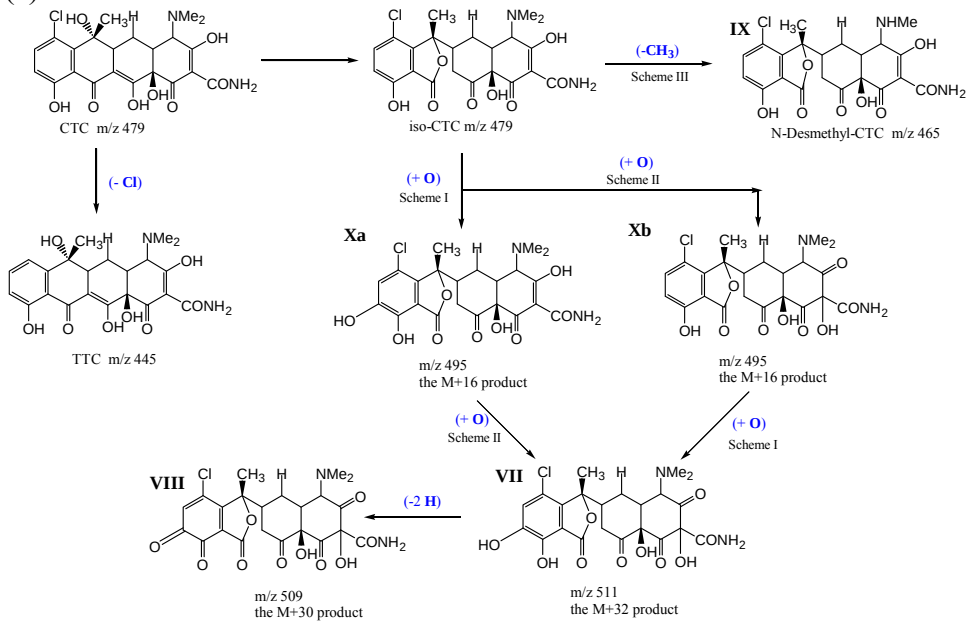

Figure 4.7 (Continued) Possible reaction schemes for the transformation of TCs by MnO2: (a) TTC, (b) OTC, (c) CTC.

(a) TTC

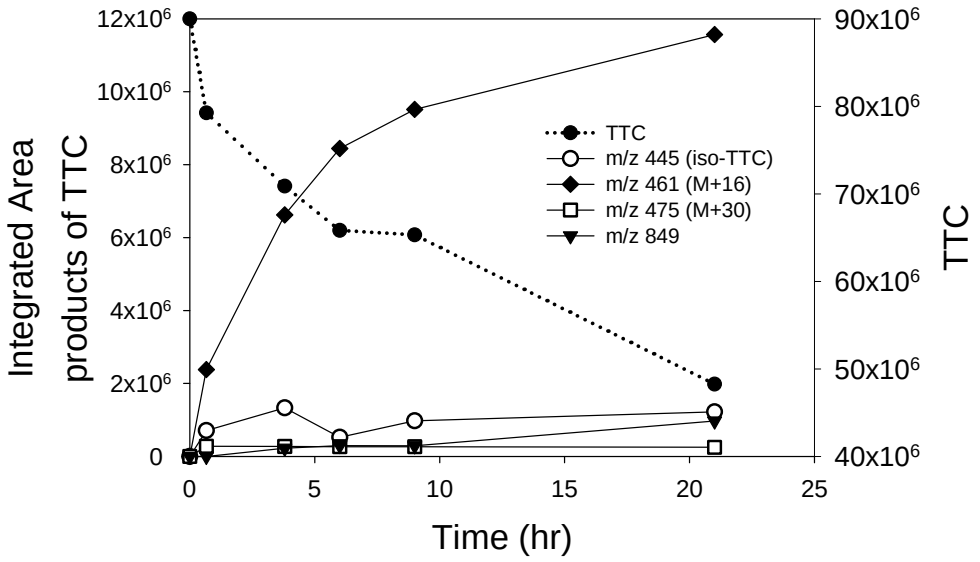

(b) OTC

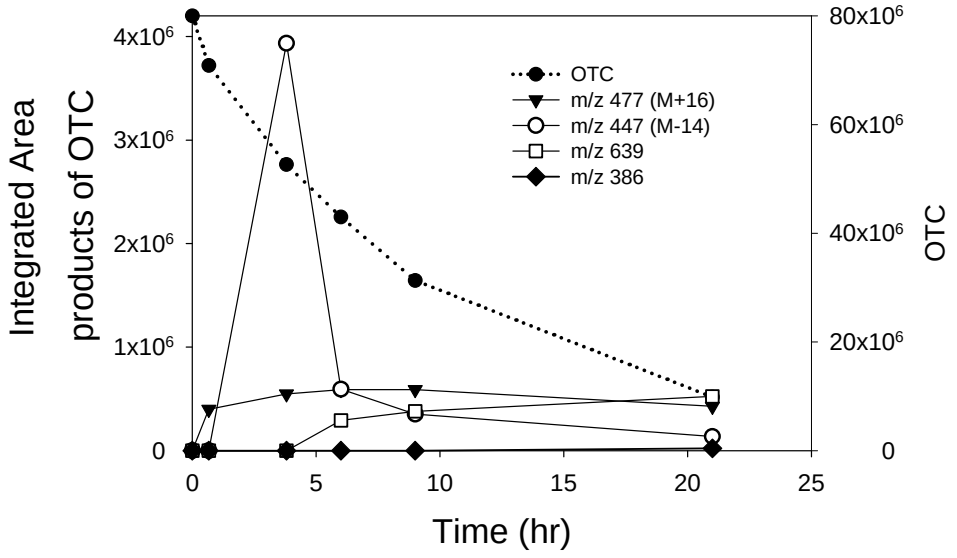

Figure 4.8 Product evaluation from the reaction of TCs with MnO_2 monitored by LC/MS. (a) TTC, (b) OTC, (c) CTC. (Reaction conditions: $[TCs]_0$=40 uM, $[MnO_2]_0$=0.6 mM, pH 5, 22°C)

(c) CTC

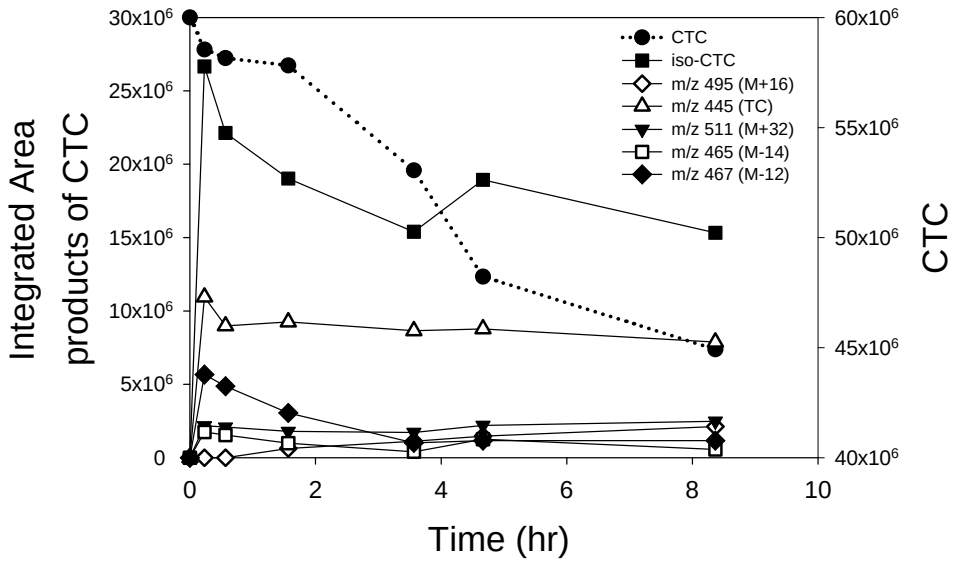

Figure 4.8 (Continued) Product evaluation from the reaction of TCs with MnO_2 monitored by LC/MS. (a) TTC, (b) OTC, (c) CTC. (Reaction conditions: $[TCs]_0$=40 uM, $[MnO_2]_0$=0.6 mM, pH 5, 22°C)

CHAPTER 5

ADSORPTION AND TRANSFORMATION OF TETRACYCLINE ANTIBIOTICS WITH ALUMINUM OXIDE

5.1 Introduction

The occurrence of antibiotics in water (Hirsch et al., 1999) and soil (Thiele-Bruhn, 2003) merit more attention because of the serious dangers of antibiotic-resistant bacteria (Barrett, 2005; Chapin et al., 2005). A large percentage of administered drugs are excreted from treated animals, and are often disseminated mostly via excrements that enter the soil and other environmental compartments. Although the antibiotics given to humans are rarely the same as those given to attention because of their wide range of applications. TCs have been used extensively to treat humans for several decades, are the leading group of antibiotics used in animal feed, and are widely used in aquaculture due to their great therapeutic values (Graslund and Bengtsson, 2001; Ungemach Fritz et al., 2006). The TC family of antibiotics accounts for over 60% of the total antimicrobial usage in agriculture (Ungemach Fritz et al., 2006). The occurrence of TCs in the environment has been the subject of numerous studies. The concentrations of TCs ranged from 0.15 μg/L in ground water and surface water samples (Lindsey et al., 2001), 86-199 μg/kg in soil samples, 4.0 mg/kg in liquid manure (Hamscher et al., 2002), to higher than 3 μg/L in 90% of farm lagoon samples (Zhu et al., 2001). Several metabolic products of TCs were also commonly found in manure-containing matrices, such as isomerization products and dehydration products (Loke Marie et al., 2003; Aga et al., 2005; Arikan et al., 2006). The continuous detection of TCs and their derivatives in the environment has

led to the occurrence of tetracycline resistent genes in waste lagoons and groundwater (Chee-Sanford et al., 2001).

Tetracycline therapy involves mainly the following three members: tetracycline (TTC), oxytetracycline (OTC), and chlorotetracycline (CTC) (Figure 1.1). Tetracycline antibiotics are known to be unstable under certain circumstances. During long-term storage, abiotic transformation may occur via isomerization, dehydration, substitution, and oxygenation (Walton et al., 1970; Liang et al., 1998). Under alkali conditions, the iso-derivatives of TCs form rapidly via a nucleophilic attack of the C6 hydroxyl group at the C11 carbonyl carbon and the bond cleavage at C11-C11a (Figure 1.2). CTC, in particular, shows stronger tendency to undergo this isomerization (Waller et al., 1952). In strong acidic media, TCs can undergo reversible epimerization at position C4 to form the corresponding 4-epi-TCs. and may degrade to form anhydro-tetracyclines (AHTCs) by losing a H_2O at position C6 (Figure 1.2). Studies have shown that some weaker acids such as phosphoric acid and citric acid can accelerate the above acid-catalyzed epimerization and anhydro-TCs formation because they can act as a molecular proton conductor (Walton et al., 1970; Sokoloski et al., 1977; Yuen and Sokoloski, 1977). On the other hand, TTC is relatively stable for long periods in 0.03 N HCl and its epimerization and acid-catalyzed dehydration are insignificant (McCormick et al., 1957). Other environmental transformations of TCs include photolytic degradation (Sanniez and Pilpel, 1980; Oka et al., 1989; Olack and Morrison, 1991; Miskoski et al., 1998) and biotransformation (Kim et al., 2005; Gartiser et al., 2007).

TCs, with ketone, carboxyl, amino, and hydroxyl groups, have been reported to have strong interactions with metal ions (Lambs et al., 1988; Wessels et al., 1998) and mineral surfaces (Kulshrestha et al., 2004; Kim et al., 2005; Sassman and Lee, 2005; Pils and Laird, 2007). In particular, several studies have demonstrated the strong adsorption of TCs with Al oxide surfaces and clays (Gu and Karthikeyan, 2005; Pils and Laird, 2007). Aluminum oxides are the most abundant minerals in the environment that control the mobility and stability of trace contaminants. Due to their high surface area and positive surface charges at neutral pH conditions, Al oxide surfaces can retard the spread of organic contaminants within the surrounding environment. In addition, the Al(III) atom of Al oxides has been reported as an acid center and may catalyze the oxidation (Karthikeyan et al., 1999), dimerization (Sohn et al., 2006), dehydration, and isomerization (Pines and Haag, 1960) of organic compounds. Alumina has been one of the most important catalyst materials in industrial processes because of its intrinsic acidity and catalytic activity (Pines and Haag, 1960). Despite the well recognized strong adsorption of TCs to Al oxides, the potential impact of Al oxide surfaces on the transformation of TCs was not explored. The previous study by Gu and Karthikeyan adopted two different approaches to measure TTC adsorption on aluminum hydrous oxides and reported that more than 20% of TTC was subjected to other reactions besides adsorption (Gu and Karthikeyan, 2005); however, the other reactions were not characterized. As will be shown later, our study found that, after rapid adsorption, aluminum oxide (Al_2O_3) surfaces continuously promoted structural transformation of TCs. The main focus of this study was to elucidate the reaction kinetics of TCs in the presence of Al oxide under different conditions and identify their transformation products.

Overall, the results of this study will improve the ability to properly assess the risks of TC residues in the environment.

5.2 Experimental Section

5.2.1 Chemicals

TTC, OTC and CTC were obtained from Sigma at 90-98% of purity and used without further purification. Standards of AHTCs were synthesized according to the method by Clive (1968), in which TTC, CTC and OTC stock solutions were added separately to 0.2 N H_2SO_4 at 100 °C to generate their corresponding AHTCs. Unless otherwise specified, all other reagents used (*e.g.*, buffers, ionic strength salt, acids, solvents, etc.) were obtained from Fisher Scientific, Acros or Aldrich at > 97% of purity. All reagent solutions were prepared using water obtained from a Millipore Milli-Q Ultrapure Gradient A10 purification system. Stocks of TCs were prepared in methanol at 1.6 mM, protected from light, stored in a -15ºC freezer, and used within a month of preparation. Throughout the experiment, acetate (pH 4 - 5.5), 4-morpholinepropanesulfonic acid (MOPS) (pH 6 - 8), and 2-(cyclohexylamino) ethanesulfonic acid (CHES) (pH 9 - 10) buffers were used to maintain the reaction solution pH. NaCl salt was used to control ionic strength. The aluminum oxide used in this study was Al_2O_3(s) (type C) from Degussa at > 99.6% of purity.

5.2.2 Kinetic Experiments

Batch kinetic studies (with 20 – 110 μM of parent TCs and 0.8 – 3.5 g/L of Al_2O_3) were conducted in 60 mL screw-cap amber glass bottles with Teflon septa. All glassware was soaked in 5 N HNO_3 and thoroughly rinsed with reagent water prior to use. A suspension containing Al_2O_3 particles, 10 mM pH buffer, and 0.01M NaCl was initially prepared, maintained at 22 ^oC in a water bath and constantly stirred by a stir bar on a submersible stirrer. Reaction was initiated by adding a certain amount of the TC stock to the above suspension. Sample aliquots were taken from the reactor at proper time intervals, centrifuged for 20 minutes, and the supernatant added with 5 μL of concentrated HCl (to improve the analytical results of TCs) and analyzed by HPLC. To desorb TCs from the Al_2O_3 surface, one mL of sample aliquot was added with 10 μL of concentrated HCl, shaken for three minutes, and then centrifuged for 20 minutes. Note that TCs are stable in HCl as mentioned earlier. All samples were stored in amber vials at < 5 °C and analyzed within a couple of days. For each testing parameter, at least two or three replicate experiments were conducted. Control experiments without Al oxide showed no significant degradation (< 5 %) of any of the tested compounds during the reaction periods (typically in 24 hours).

5.2.3 Analysis of TCs

Analyses of TCs were carried out on an Agilent 1100 reverse-phase high performance liquid chromatography (HPLC) system with a Zorbax RX-C18 column (4.6 × 250 mm, 5 μm), an injection volume of 100 μL and a diode-array UV/Vis detector at a flow rate of 1 mL/min. TCs were detected at 275 nm and 365 nm. The mobile phase A

consisted of 0.01 M oxalic acid and 10 μM EDTA, while mobile phase B was pure acetonitrile. The gradient was as follows: 0−3 min 96% A and 4% B; 3−10 min a linear gradient to 73.7% A and 26.3% B; 10.0−19.0 min 73.7% A and 26.3% B; and 19.0−25.0 min linear gradient to 96% A, and 4% B. This final mixture was maintained for the remainder of the 30-minute run time.

5.2.4 Product Identification

To identify reaction intermediates and products, reaction suspensions were filtered after > 75% of the parent TC disappeared. All mass spectrometric measurements were performed on an Agilent 1100 HPLC/DAD/MSD system equipped with an electrospray source. The separation was performed by a Zorbax SB-C18 column (2.1 × 150mm, 5 μm) at a flow rate of 0.2 mL/min with two mobile phases as described above. MS analysis was conducted by positive electrospray ionization at both low and high fragmentation voltages (110 and 250 eV) with a mass scan range of *m/z* 50-1000. The drying gas was at 10 L/min at 350 °C, the nebulizer pressure 25 psig, and the capillary voltage 4000 V.

5.3 Results and Discussion

5.3.1 Adsorption and Transformation of TCs in the Presence of Al_2O_3

In the absence of Al_2O_3, the TCs were stable under the experimental conditions and less than 5 % loss of the parent compound was detected after 24 hours. In contrast, significant disappearance occurred in the presence of Al_2O_3 for all three TCs (Figure 5.1a). The dotted and solid lines in Figure 5.1a represent samples with and without acid

(HCl) desorption (see Section 5.2.2), respectively. The TC concentration measured without acid desorption corresponded to the unreacted parent compound in the aqueous phase while the concentration measured with acid desorption corresponded to the unreacted parent compound in the aqueous phase plus the removable portion of the parent compound adsorbed on the Al_2O_3 surface.

The disappearance of TCs in the presence of Al_2O_3 was most rapid in the first 30 minutes, followed by relatively fast loss within 3 hours (Figure 5.1a). After 3 hours the reaction rate slowed appreciably, and the log of TC concentration decreased linearly with time. The initially rapid then slower and continuous disappearance of TCs and detection of transformation products (see discussion later) indicated that both adsorption and transformation of TCs occurred with Al_2O_3. We hypothesized that the initial rapid loss was due to adsorption and the later slower disappearance was related to transformation reaction. The rate of transformation was approximated by conducting linear regression to the linear section of the semi-log plot (Figure 5.1a) and the slope yielded the observed first-order rate constant k_{obs} in hr^{-1}.

The data collected with and without acid desorption showed similar characteristics, *i.e.*, the log([TC]) versus time curves had similar shapes (Figure 5.1a) and the linear regressions on both trendlines yielded comparable k_{obs} values (Table 5.1). For each of these two sets of data, the adsorption extent was estimated by the difference between the initial TC concentration and the intercept of the regression line at t = 0. We call the adsorption determined from the data without acid desorption as the "total adsorption (A_T)", and the adsorption determined by the data with acid desorption the "irreversible adsorption (A_I)". The A_T was in the range of 43-57% and A_I in 15-21% of the total TC

amount. Apparently, HCl acid addition could desorb approximately half of the total adsorbed on the Al_2O_3 surface. In general, TTC and OTC showed comparable adsorption and CTC had higher adsorption. CTC also showed the fastest transformation rate, followed by TTC, and OTC the slowest.

In general, the trends in adsorption and transformation rate among the three TCs of CTC, TTC and OTC obtained in this study are consistent with the results in the literature. The stronger adsorption of CTC than TTC was also observed on soil clays in the study by Pils and Laird (2007). The authors attributed the greater adsorption of CTC to the strong polar-polar interaction between the additional chlorine at C7 and clay. Aga *et al.* (2005) used enzyme-linked immunosorbent assay (ELISA) and LC/MS to study the persistence of tetracycline antibiotics and related products in manure-amended soils and showed that only OTC was in measurable levels in subsurface soils out of CTC, TTC and OTC, suggesting that OTC is more persistent. In our study that investigated the reaction kinetics of TCs with MnO_2, the same reactivity order (CTC > TTC > OTC) as that observed with Al_2O_3 was observed (Rubert and Pedersen, 2006).

5.3.2 Effect of Reaction Conditions

The reaction kinetics were evaluated for the influence of TTC concentration, Al_2O_3 oxide concentration, solution pH, and the presence of oxygen:

5.3.2.1 Reactant Loading Effect

A series of experiments with varying Al_2O_3 loadings but a fixed TTC loading, or with varying TTC loadings but a fixed Al_2O_3 loading, were conducted at pH 5 to assess the effect of each reactant on the reaction kinetics. Loading refers to the initial reactant

concentration employed. When TTC loading was increased from 20 μM to 106 μM at a fixed 1.78 g/L of Al_2O_3 loading, the TTC transformation rate constant k_{obs} decreased with increasing TTC loading (Figure 5.2a). This decreasing trend of k_{obs} is similar to the decrease in adsorption (A_T and A_I) of TTC to Al_2O_3 surfaces at higher TTC concentration (Figure 5.2b). When Al_2O_3 loading was increased from 0.9 to 3.3 g/L, the TTC transformation rate constant k_{obs} increased linearly with increasing Al_2O_3 loading (Figure 5.3a). The adsorption (A_T and A_I) of TTC to Al_2O_3 surfaces also increased almost linearly with increasing Al_2O_3 loading (Figure 5.3b). At a fixed Al_2O_3 loading, the percentage of adsorbed TTC was lower when the TTC concentration was higher indicates that a limited number of sites are available on the Al_2O_3 surfaces for TTC. At a fixed TTC concentration, more surface sites are available at a higher Al_2O_3 loading and thus led to higher adsorption of TTC. The strong correlations between k_{obs} and A_T and A_I suggest that adsorption is crucial for the transformation reaction to occur.

5.3.2.2 pH Effect

The effect of pH was examined at pH 5 to 9 with fixed TTC and Al_2O_3 loadings. As illustrated in Figure 5.4a, maximum k_{obs} was observed at near pH 7, and k_{obs} decreased at pH lower or higher than 7. Similarly, the adsorption (A_T and A_I) of TTC to Al_2O_3 also showed a maximum near pH 7, and the adsorption decreased when the pH was either decreased or increased from 7. These parallel trends again suggest the importance of adsorption in the transformation of TTC by Al_2O_3 surface sites. The pH dependence can be understood by evaluating the charges of TTC and Al_2O_3 surfaces. The zero-point-of-charge (pH_{zpc}) of Al_2O_3 was reported to be 7.5-8.7 (Stumm, 1992). At pH 5-9, the Al_2O_3

surface charge was positive when pH < pH_{zpc} and negative when pH > pH_{zpc}. The dominant species of TTC changed from being positively charged (H_3L^+ at pH < pK_{a1} = 3.32), to neutral or zwitterionic (H_2L^0 at pK_{a1} < pH < pK_{a2} = 7.78), and to negatively charged (HL^- at pH > pK_{a2} = 7.78). Electrostatic repulsion between similar charges of TTC and Al_2O_3 surfaces was greater at either lower pH (positive-positive repulsion) or at higher pH (negative-negative repulsion), thus creating a maximum electrostatic attraction at the intermediate pH range. A similar bell-shaped pH dependence with highest adsorption around pH 7 was also observed by Gu and Karthikeyan in the adsorption of TTC with aluminum hydrous oxide (Gu and Karthikeyan, 2005). The surface complexes of zwitterionic species of TTC was previously suggested by Figueroa *et al.* (2004) as the major contributor to the adsorption mechanism of TTC to model clays.

5.3.2.3 The Presence of Oxygen

Previous studies have reported that Al oxide surfaces can catalyze the oxidation of 1-naphthol by oxygen, in which the $Al(OH)_3$ surfaces were believed to promote the reaction by binding to the transformation product of 1-naphthol (Karthikeyan et al., 1999). To evaluate whether oxygen was involved in the observed transformation of TCs, experiments were also conducted in the absence of oxygen and with constant oxygen purging, respectively. Results show that change in the oxygen content did not have any impact on the adsorption and transformation rate of TCs and their transformation products. Thus, it was concluded that the catalyzed transformation of TCs by Al_2O_3 was not oxidation; instead, dehydration and isomerization catalyzed by Al_2O_3 surfaces are more likely.

5.3.3 Transformation Product Analysis

Reaction mixtures of TTC with Al_2O_3 at pH 5 were stopped by centrifugation after 23 hours (~25% of the parent TTC was transformed). The supernatant was analyzed by HPLC-UV to yield five peaks (Figure 5.5a): epi-TTC (8.94 min), TTC (10.74 min) and three transformation products with longer retention times (16.29, 18.21 and 19.16 min). The UV spectra of the five peaks are shown in Figure 5.6. The supernatant was also analyzed by LC/MS to yield five peaks with molecular ions of *m/z* 445a, 445b, 559a, 559b and 427 (Table 5.2). The two peaks with the same *m/z* 445 are TTC and epi-TTC, and exhibited the same fragmentation pattern with two major fragments M-17 and M-35, corresponding to $[M+H-NH_3]^+$ and $[M+H-NH_3-H_2O]^+$ ions, respectively. Studies have suggested that the NH_3 loss likely involves the amino group at the C2 atom and the H_2O loss from the hydroxyl group bound at the C6 atom (Dalmazio et al., 2007).

The peak at 19.16 min was identified as AHTTC based on the results of both HPLC-UV and LC/MS. The HPLC-UV analysis showed that this peak had similar retention time as the AHTTC standard (Figure 5.5b), and its UV spectrum showed a hypochromic shift from 365 nm to 420 nm similar to that of AHTTC (Gratacos-Cubarsi et al., 2007) (Figures 5.6 and 5.7). The LC/MS analysis showed that the 19.16 min peak had *m/z* 427 (*i.e.*, M-18) and only the $[M+H-NH_3]^+$ but not the $[M+H-NH_3-H_2O]^+$ fragment, confirming that a water was lost from the parent TTC. The longer retention time than that of TTC on the reverse-phase (C18) HPLC chromatography was also expected since removal of the hydroxyl group at the C6 position makes the compound less polar (Gratacos-Cubarsi et al., 2007).

The two peaks at 16.29 and 18.21 min showed very similar UV spectra (Figure 5.6) and the same *m/z* 559 and fragmentation patterns (unknown I and II in Table 5.2), suggesting that they are likely isomers. Both compounds unfortunately showed low ionization efficiency in the electrospray LC/MS, resulting in low signals and difficulty to identify the structures. In general, they both showed a net weight increase by 114 and fragmentation patterns different from those typical of TTC and the other products (*i.e.,* a 17 loss and a 18 loss). Figure 5.6 shows these two unknown products had a significant shift in the 340-380 nm absorption bend compared to TTC and epi-TTC. The A ring and the BCD ring of TCs are two separate resonance systems, contributing to two major absorption bends (250-300 nm and 340-380 nm) of TCs spectra. In general, the A ring chromophore contributes only to the 250-300 nm absorption, whereas the BCD ring chromophore contributes to both absorption bends (McCormick et al., 1957). The sharp shift at 340-380 nm suggests that the BCD ring structure was altered. These two products also did not appear to be related to the pH buffer employed or the presence of oxygen; the product distribution was roughly the same regardless of changing the above conditions.

The generation of products over time was also monitored. Due to the lack of authentic standards and the apparently different ionization efficiency among TTC and some of its products, the product concentration was estimated by HPLC-UV absorbance (275 nm) based on the crude assumption that the UV absorbance of the products at 275 nm is similar to that of TTC (Figure 5.6). As shown in Figure 5.8, the generation of AHTTC and the two unidentified products accompanied the disappearance of TTC over time, further confirming that TTC transformation occurred in the presence of Al_2O_3. Interestingly, the concentration of epi-TTC decreased noticeably during the first 2 hours

but remained at a steady level afterwards. Rapid adsorption to Al_2O_3 surfaces probably contributed to the sharp decrease in the beginning as similar phenomenon was seen with TTC. Epi-TTC differs from TTC only in the position of the A ring's dimethylamine (-$N(CH_3)_2$) group and has similar tendency to convert to its anhydro-from as TTC to AHTTC. A continuous decrease of epi-TTC was observed when epi-TTC the only organic reactant in the reaction with Al_2O_3. The result that epi-TTC concentration did not decrease over time is likely because that epi-TTC was generated from Al_2O_3 surface-promoted epimerization of TTC. The transformation of epi-TTC was counterbalanced by the generation of epi-TTC from TTC.

Aluminum oxides are well known facile catalysts for organic compound transformation because of the intrinsic acidity associated with Al(+III) (Pines and Haag, 1960). The reactions catalyzed by alumina such as dehydration of alcohols and skeletal isomerization are also typically acid catalyzed. The results presented thus far strongly suggest that TTC undergoes acid-promoted transformation in the presence of Al_2O_3. An additional set of experiments was conducted with 40 μM TTC and 0.017 M Al^{3+} in 0.03 N HCl. About 35% of TTC was transformed after 72 hours and significant formation of AHTTC and epi-AHTTC was detected. Note that such transformation did not occur without Al^{3+} because TTC is stable for long periods in 0.03 N HCl at room temperature (McCormick et al., 1957), further confirming that role of Al(III) in promoting the acid-catalyzed transformation of TTC. The Al^{III} on Al_2O_3 surface acts as Lewis acid site and renders dehydration of TTC to AHTTC an easier process. Like phosphate and citric acid, Al^{III} can serve as a molecular proton conductor and facilitate the formation of epimer and dehydration derivatives of TTC (Sokoloski et al., 1977; Yuen and Sokoloski, 1977).

Earlier study by Gu and Karthikeyan (2005) also investigated the adsorption of TTC to Al hydrous oxides; however, the formation of AHTTC and other products was not reported. This may be because the HPLC monitoring time (12 min) was not long enough to observe the products.

The reaction products of CTC (m/z 479) and OTC (m/z 461) were also analyzed by HPLC-UV and LC/MS. For CTC, formation of two M+114 products (unknown III and IV in Table 5.2) was also observed but AHCTC was not detected (Figure 5.5). The most significant product was iso-CTC, identified by matching retention time and the lack of UV absorptivity at 365 nm with a standard, the *m/z* ratio of 479, and the formation of a $[M+H-NH_3-CO]^+$ but not a $[M+H-NH_3-H_2O]^+$ fragment in its MS spectrum (Zurhelle et al., 2000). Compared to TTC and OTC, CTC is particularly prone to form an iso-derivative (Waller et al., 1952). In Chapter 4, we observed that MnO_2 surfaces can promote the formation of iso-derivatives of CTC and TTC. It is likely that the Al_2O_3 surfaces promoted such isomerization of CTC predominantly rather than dehydration. Reacting at the slowest rate, OTC yielded only one transformation product (unknown V in Table 5.2) with the same *m/z* 461 as OTC, and AHOTC was not detected (Figure 5.5). This product is possibly the iso-derivative of OTC since it shows much smaller UV absorptivity at 365 nm in the UV spectrum. While preparing the standards of AHTCs, it required a higher concentration of H_2SO_4 and a longer reaction time for OTC than TTC and CTC to yield the same amount of anhydro derivative, suggesting that the formation of AHOTC is less favorable than those of AHTTC and AHCTC (Clive, 1968). The C6-OH and C5-OH groups of OTC are positioned favorably for hydrogen bond formation,

and such interactions may help stabilize the C6-OH of OTC and lower the tendency to form AHOTC.

5.4 Environmental Relevance

Results from this study clearly show that, while strong adsorption of TCs to Al oxides occurred, the Al oxide surfaces can catalyze transformation of TCs over time. The transformation rate correlates with adsorption extent very well, indicating that adsorption is crucial for the transformation to occur. Among the three TCs examined, the reactivity towards Al oxides followed the order of CTC > TTC > OTC. The surface complex formation between TCs and Al_2O_3 controlled the transformation reaction kinetics along with the influence of water pH and the reactant concentration. Since the adsorption extent was the greatest and the transformation reaction rate the fastest at neutral pH conditions, both processes are likely to occur in the aquatic environment and affect the fate and transport of TC antibiotics.

Al oxide surface sites acting as acid centers apparently can catalyze isomerization and dehydration of TCs. Reaction patterns and product formation, however, depends on the structure of TCs. The formation of AHTTC from TTC promoted by Al_2O_3 merits particular concern because AHTCs in general have high toxicity. Previous studies which examined the effect of TTC and AHTTC on the spleen cells showed that a much lower amount of AHTTC (40 to 100 times lower than those of TTC) can induce the same decrease in the number of the antibody-producing cells (Klimova and Ermolova, 1976). Formation of AHCTC and AHOTC was not observed in this study within 72 hours, likely because that surface promoted formation of iso-CTC was the dominant pathway for CTC, and that the kinetics of AHOTC formation form OTC is comparatively slow than the

other two TC cases. Further studies are needed to evaluate the persistence and fate of AHTTC, and determine the structures and toxicities of several of the unknown products found in this study.

Table 5.1 Regression result from three TCs reaction with Al_2O_3.

Compound	Reaction rate k_{obs}(10^{-3}hr^{-1})		Adsorption (%)		R^2	
	Centrifugation	Acid added before centrifugation	Irreversible	Total	Centrifugation	Acid added before centrifugation
TTC	15.3±1.1	10.9±0.3	18.8±0.9	43.1±1.9	0.991	0.998
CTC	17.5±1.0	17.2±0.9	21.5±2.3	56.9±1.4	0.993	0.994
OTC	6.2±0.9	6.4±0.1	15.8±0.2	44.3±1.6	0.961	0.999

Table 5.2 HPLC chromatogram and mass spectral data for TCs transformation products by Al_2O_3

Compound	RT (min)	UV absorbance peaks wavelength (nm)			Short written	m/z				
						MH^+	Daughter ions			
TTC	11.18		275	365	M	445	428	410		
unknown I	16.74	240	280	385	M+114	559	496	451	437	429
unknown II	18.47	240	280	385	M+114	559	496	451	437	429
AHTTC	19.31		275	430	M-18	427	410			
CTC	15.86		275	375	M	479	462	444		
keto-CTC	11.88		275	360	M	479	462	444		
iso-CTC	13.45		278		M	479	462	451		
unknown III	21.32	240	280	295	M+114	593	530	485	471	
unknown IV	22.94	240	282	395	M+114	593	530	485	471	
OTC	8.90		275	365	M	461	444	426		
unknown V	11.45		280	375	M	461	444			

*TTC, CTC, keto-CTC and OTC have C4 epimeric equilibrium. Epi-TCs which are not listed in the table show the same daughter ion patterns in mass spectra and the same UV-Vis spectra with their parent compounds.

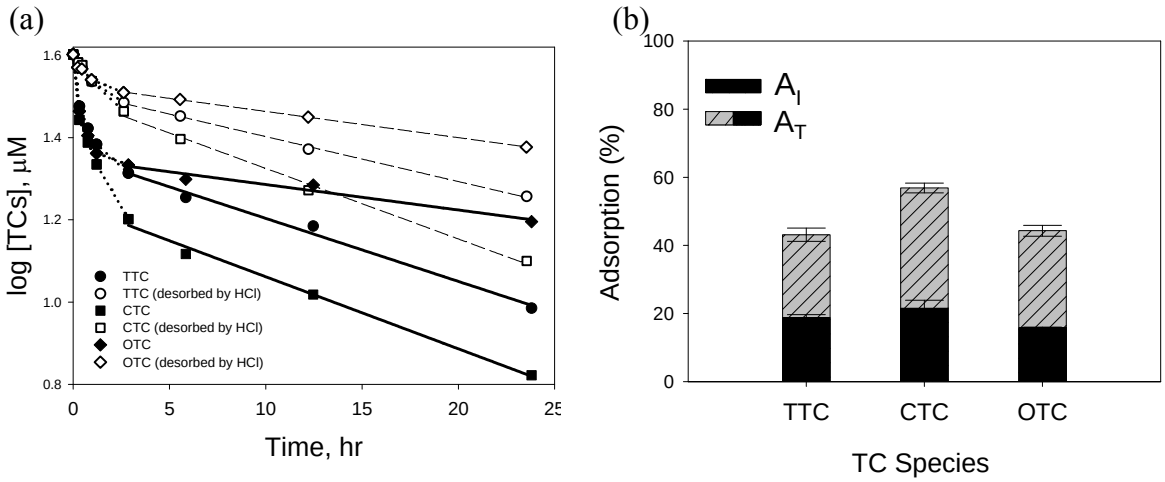

Figure 5.1 Kinetics of TCs removal by Al_2O_3 at pH 5. (a)Semilogarithmic plot is linear after the first 3 hr. (b)Adsorption percentage of TCs determined by two quenched methods. A_I and A_T refer to irreversible adsorption and total adsorption respectively. (Initial total $[TCs]_0$=40 μM, $[Al_2O_3]$=0.17 g/L, pH 5).

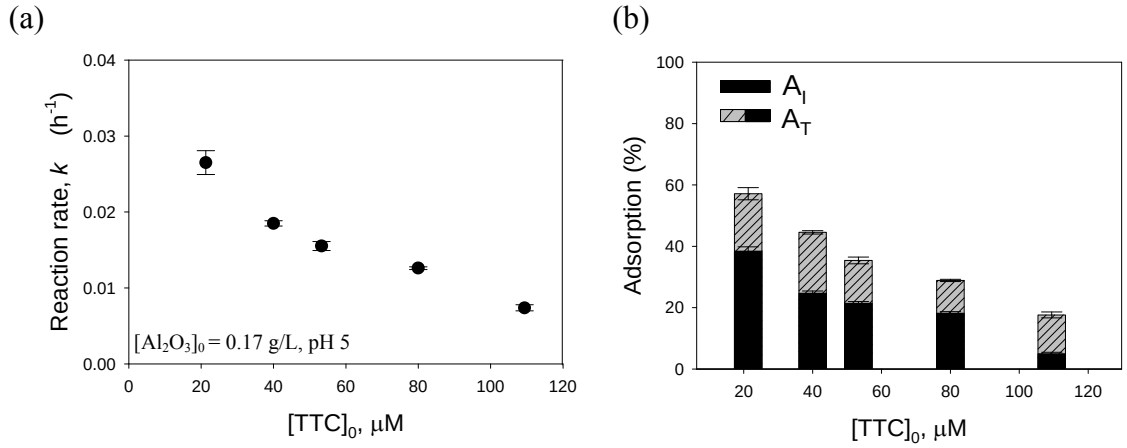

Figure 5.2 Effect of TTC loading on TC transformation kinetics. (a) reaction rate, *k* (b) adsorption.

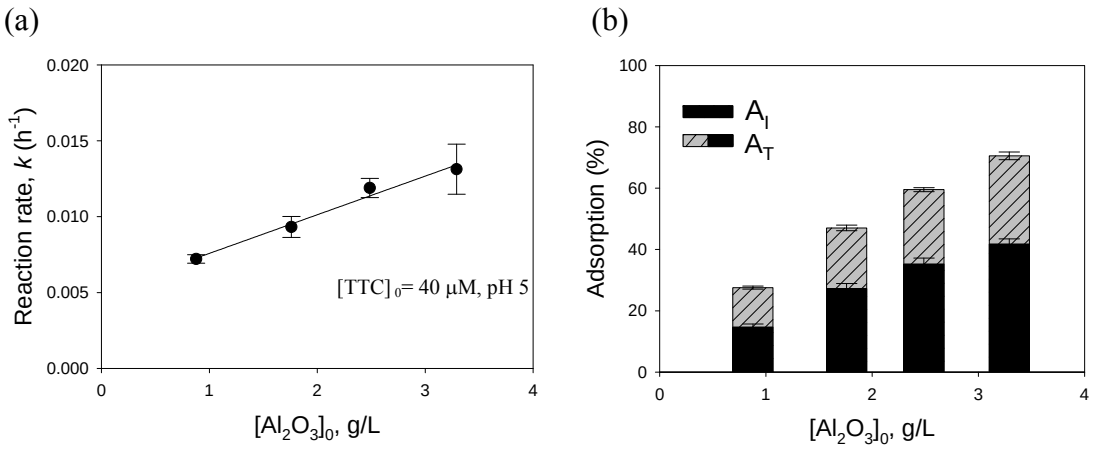

Figure 5.3 Effect of Al_2O_3 loading on TTC transformation kinetics. (a) reaction rate, *k* (b) adsorption.

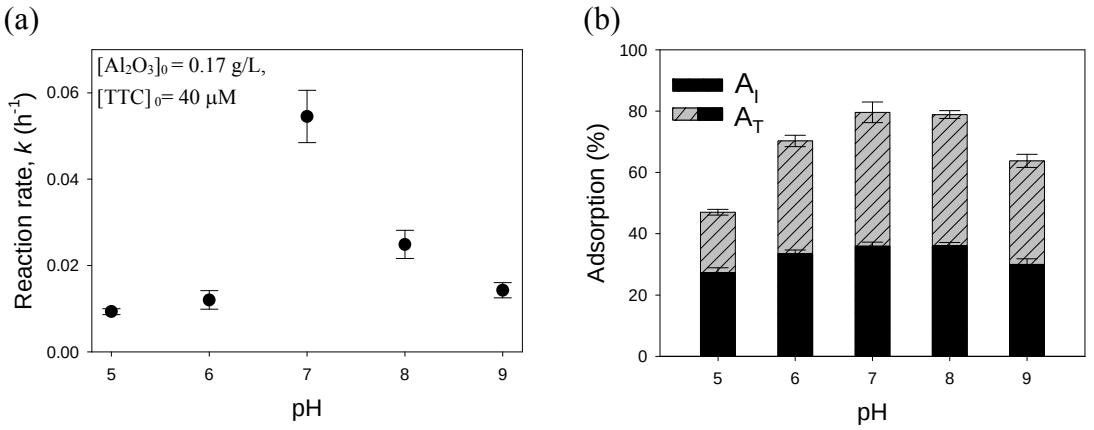

Figure 5.4 Effect of pH on TTC transformation kinetics. (a) reaction rate, *k* (b) adsorption.

(a)

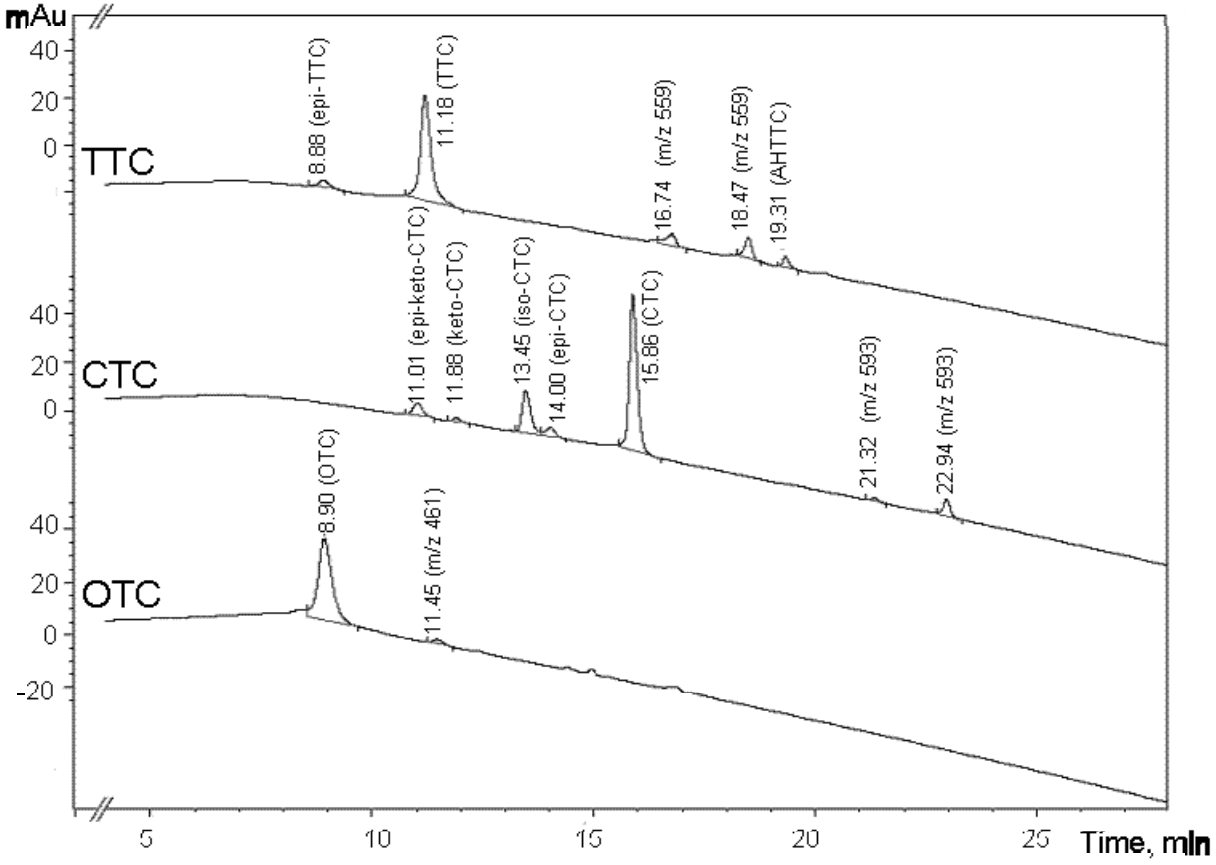

Figure 5.5 HPLC-UV chromatograms of (a) TCs and their transformation products at 275 nm with Al_2O_3 after approximately 25% TCs transformed. ($[TCs]_0$=40 μM, $[Al_2O_3]_0$=0.178 g/L, pH 5) (b) synthesized AHTC standards.

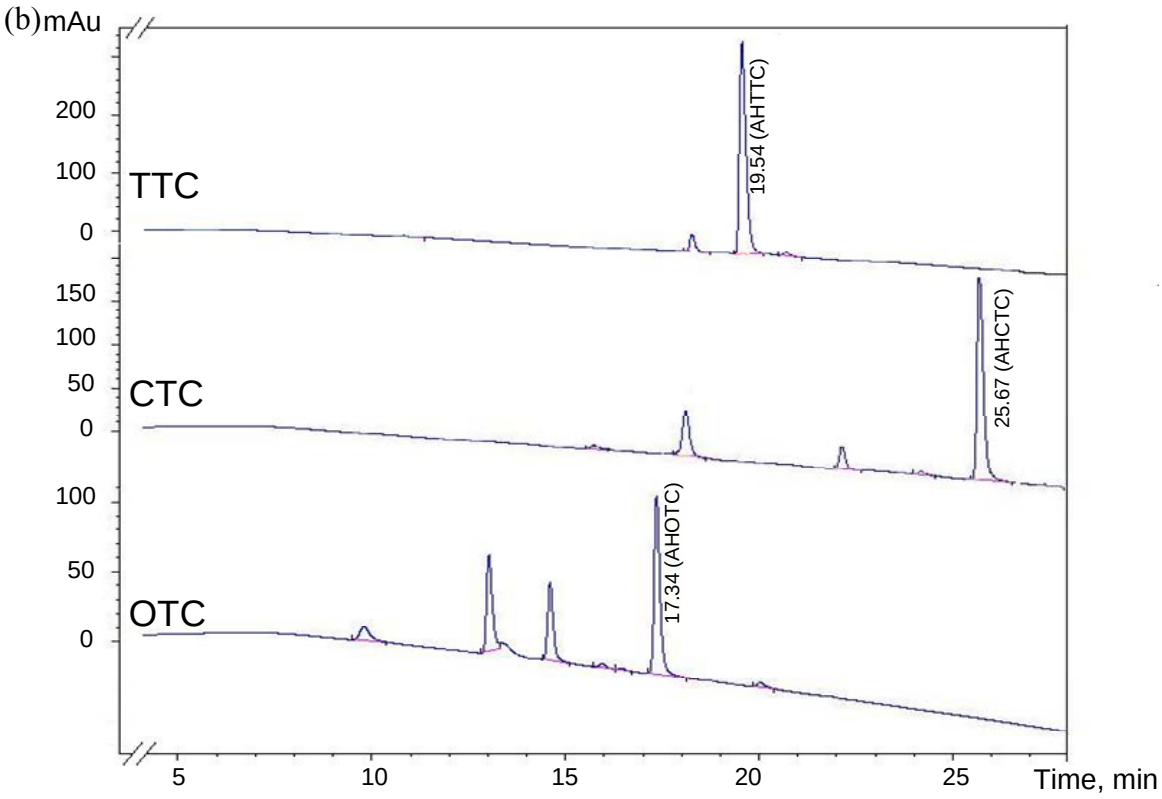

Figure 5.5 (Continued) HPLC-UV chromatograms of (a) TCs and their transformation products at 275 nm with Al_2O_3 after approximately 25% TCs transformed. ($[TCs]_0$=40 μM, $[Al_2O_3]_0$=0.178 g/L, pH 5) (b) synthesized AHTC standards.

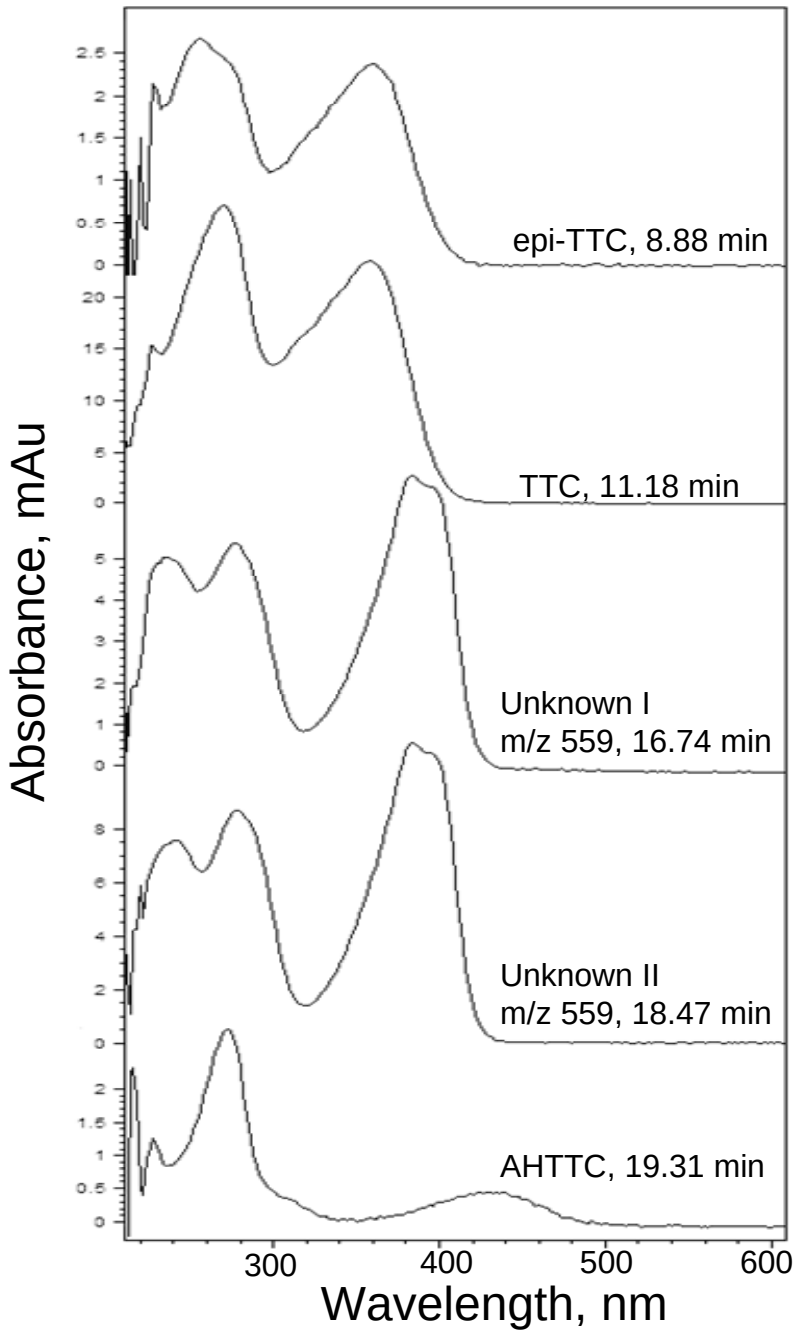

Figure 5.6 UV-vis spectra of TTC and its reaction products with Al_2O_3. ($[TTC]_0$=40 μM, $[Al_2O_3]_0$=0.178 g/L, pH 5)

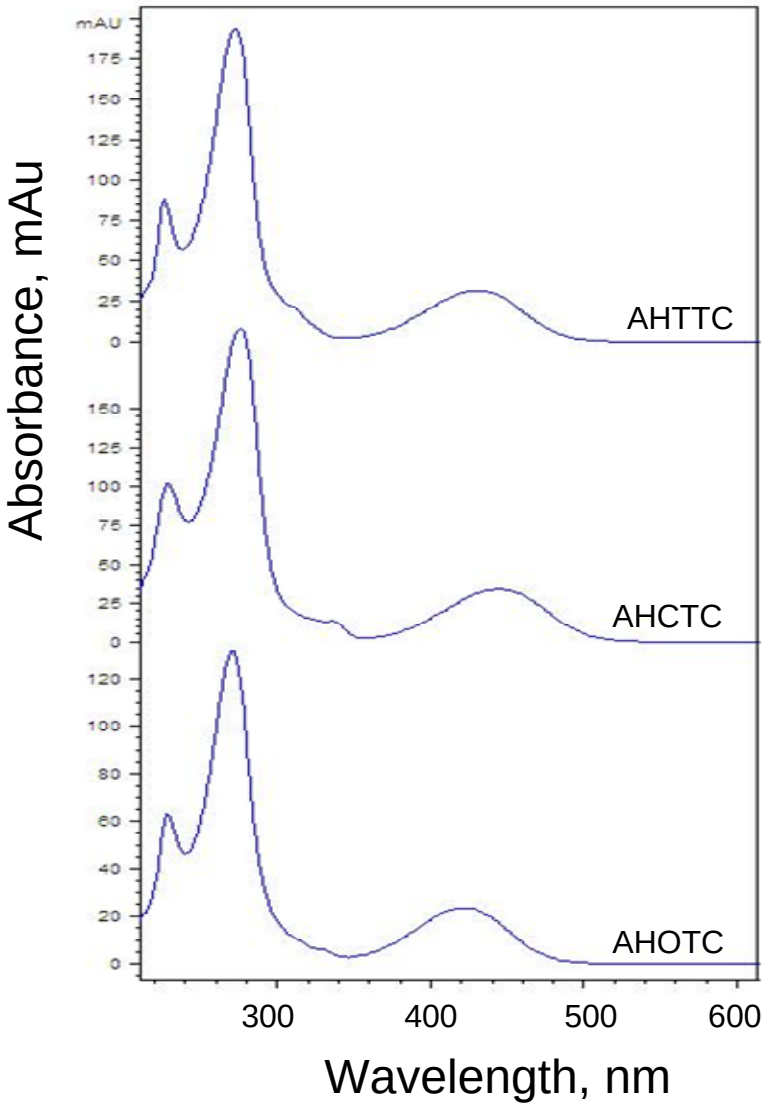

Figure 5.7 UV-vis spectra of AHTC standards.

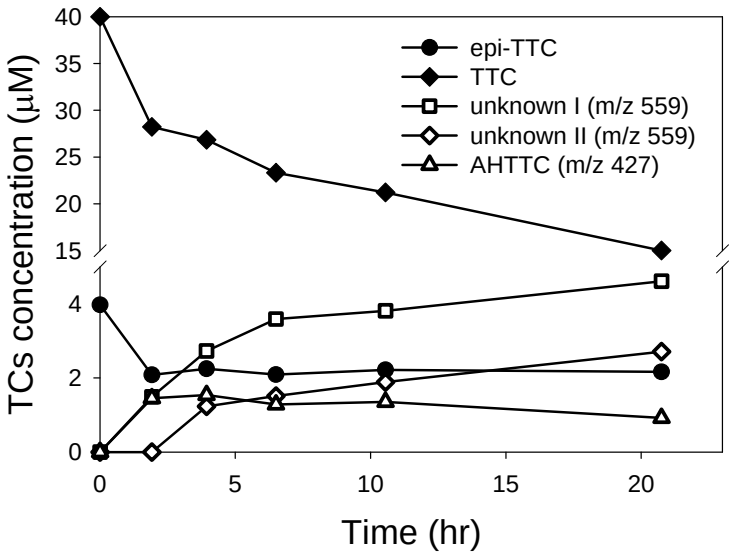

Figure 5.8 Product revolution of TTC reacts with Al_2O_3. Measurement was conducted by HPLC UV-Vis absorbance (275 nm).

CHAPTER 6

CONCLUSION

Antibacterial agents are a notable group among the emerging contaminants because of the concern over their potential to foster the development of resistance in microbes in the environment. As the high usage of tetracycline antibiotic (TCs) remains a common practice, their fate and transformation in the environment needs to be fully addressed. Because TCs form strong complexes with metal species readily, the impact of environmental metal species on the transport and abiotic transformation of TCs needs to be evaluated. This research investigated the transformation of TCs at the mineral-water interfaces and with dissolved metal species, with the aim to elucidate the involved reaction kinetics and mechanisms. This study demonstrated that TCs can be oxidized in the presence of MnO_2, Mn^{II} ions and Cu^{II} ions under environmentally relevant conditions. The presence of oxygen is required for the oxidation of TCs mediated by Mn^{II} ions. This study also discovered that Al_2O_3 surfaces can promote the acid-catalyzed isomeration and decomposition of TCs. Significantly, the reactions with the above metal species involve rather different mechanisms. The results clearly show that the transformation of TCs can occur via different structural moieties when different metal species are involved. These phenomena may lead to significantly different reactivities among different members of TCs in environmental systems where metal speciation and abundance vary. Overall, the study results strongly suggest that the metal species such as MnO_2, Al_2O_3, Mn^{II} ions and Cu^{II} ions commonly existing in the aquatic environment will likely have a signifincant impact on controlling the mobility and stability of TCs in the soil-water system. Further

details of the specific findings regarding the above reactions of TCs with metal species are summarized in the sections of 6.1-6.3.

6.1 Metal Ion-promoted Transformation of TCs

This study found that Mn^{II} and Cu^{II} ions can significantly catalyze the transformation of TCs in the presence of oxygen at pH 8-9.5 and pH 4-6, respectively. The two systems share some characteristics: (1) reactions were homogenous and no mixing was needed, (2) reaction kinetics followed pseudo-first order decay, (3) transformation rate increases with increasing TC or metal ion concentration, (4) both reactions are highly pH dependent (but with different trends), and (5) complexation is the first step for the transformation to take place. For (5), the transformation of TCs was inhibited by the presence of EDTA, validating the crucial role of metal-TC complex formation for the reaction to occur. However, different results were observed for Mn^{II} and Cu^{II} from the oxygen-free experimental set-up. The absence of oxygen completely blocked the Mn^{II}–catalyzed reactions but had only mild effects on the reaction rate of Cu^{II}-catalyzed reaction. This suggests that the two reactions involve different mechanisms.

In the TC-Mn^{II}-O_2 system, oxidation of the TC-complexed Mn^{II} to Mn^{III} by oxygen occurs, followed by oxidation of TC by Mn^{III} to regenerate Mn^{II}. In the TC-Cu^{II}-O_2 system, Cu^{II} oxidizes TC within the complex and the yielded Cu^{I} is re-oxidized by the presence of oxygen. Opposite reactivity trends were observed with the two metals: OTC > TTC >> iso-CTC for the Mn^{II}- and CTC > TTC > OTC > epimers for the Cu^{II}-mediated

reactions. The reactivity results and the examination of TC-metal ion complexation and transformation products strongly suggest that the Mn^{II}-catalyzed reaction occurs at the BCD ring of TCs while Cu^{II} induces TCs' transformation through the A ring. The above results clearly show that the transformation of TCs can occur via different structural moieties when different metal species are involved.

6.2 Surface Promoted Transformation of TCs

This study demonstrated that TCs undergo different transformations in the presence of MnO_2 and Al_2O_3 under environmentally relevant conditions. Consistent with previous studies, TCs adsorbed strongly to manganese and aluminum oxide surfaces followed by rapid transformation. Evaluation of the influence of initial TC concentration, initial oxide concentration and pH indicates that the reaction kinetics for both oxides were strongly related to adsorption. The two systems share some common characteristics: (1) the reaction rate increases when TTC loading decreases or oxide loading increases; (2) the reactivity order of three TCs (*i.e.*, CTC > TTC > OTC) is the same.

For the MnO_2 system, the transformation rate of TCs were limited by surface complex formations (*i.e.*, adsorption of TCs to MnO_2 surfaces). MnO_2 acts as a strong oxidant to oxidize adsorbed TCs at the mineral-water interface, in which the reaction rate is linearly dependent on pH and the transformation involves several oxygenation steps. However, Al_2O_3, a non-redox reactive oxide, also promoted structural transformation of the TCs – a phenomenon not recognized by previouse studies. Experiments conducted under oxygen-free conditions yielded the same results as those in the presence of oxygen, indicating that redox reactions were not involved. The fact that no oxidation products

were observed also suggests that TCs undergo a different transformation pathway with Al_2O_3 than with MnO_2. In the presence of Al_2O_3, the steady decrease of TCs after initial rapid adsorption (usually within the first 3 hours) could be fitted by a first-order decay model to yield a reaction rate constant. The transformation rate constant strongly correlates to adsorption on Al_2O_3 surface - higher adsorption, faster rate. The pH dependency on reaction rate was a bell shaped curve with the highest reaction rate at pH 7 to 8.

Transformation product identification and evolution suggest that MnO_2 promoted isomerization at the C ring to form iso-TTC and oxidized the phenolic diketone and tricarbonylamide groups leading to insertion of up to 2 O most likely at the C9 and C2 positions. In contrast, reaction of OTC with MnO_2 yielded little iso-OTC, but occurred mainly at the A ring's dimethylamine group to yield N-demethylated intermediates and products. CTC had the most complicated product formation, encompassing transformation patterns observed in both TTC and OTC cases and others. In the case of CTC, MnO_2 surface-promoted formation of iso-CTC was the dominant initial step, followed by further oxidation of iso-CTC. Despite rapid transformation, the structural modification of TCs by MnO_2 is modest and antibacterial activity may not decrease in some of the products based on their structures.

On the other hand, product evaluation indicated that Al_2O_3 transformed TTC to its anhydrotetracycline (AHTC) and two other unidentified products, transformed CTC to iso-CTC, and transformed OTC to an unidentified isomer product. Al oxide surfaces, owing to their strong Lewis acidity, likely facilitated the above acid-catalyzed

isomerization and dehydration of TCs. The formation of AHTC is of particular concern because it exhibits considerably higher cytotoxicity than the parent TTC.

6.3 Reaction Kinetics of Surface Promoted Transformation

Rapid degradation of several antibacterial agent groups, including tetracyclines, phenols, fluoroquinolones and aromatic *N*-oxides was observed in the presence of MnO_2. The reaction kinetics of these compounds with MnO_2 were complicated and apparently deviated from pseudo-first-order decay and could not fit any typical rate equation. A new MnO_2 surface kinetic model (the MnOII model) was therefore developed.

In this model, either the precursor complex formation or the electron transfer within the precursor complex is the rate-limiting step for the overall reaction. While the MnOII(i) with electron transfer within the precursor complex as the rate-limiting step fits well with the reactions of phenols, fluoroquinolones and aromatic *N*-oxides with MnO_2, the reactions of TCs with MnO_2 were described by the MnOII(ii) model with the surface complexation formation (*i.e.,* adsorption) as the rate-limiting step. The different rate-limiting step was chosen for TCs because of two reasons: (1) there was no delay in forming Mn^{2+} after the reaction was initiated, and (2) only a negligible amount of absorbed but unreacted TCs accumulated on the MnO_2 surfaces. These observations indicated rapid electron transfer immediately after the molecules of TCs adsorb onto the MnO_2 surfaces.

The MnOII model characterizes the kinetics of parent antibiotic loss in the reaction with MnO_2 by two independent parameters: the reaction rate constant (k'') and the total reactive surface sites (S_{rxn}). Based on the MnOII model, the reaction reaches a plateau as

$t \rightarrow \infty$, *i.e.*, the antibiotic concentration (C) eventually decreases to a constant value $C_e = C_0 - S_{rxn}$, where C_0 is the antibiotic concentration at t = 0. The S_{rxn} value was estimated from the kinetic trend in the later stage of the experimental results (*i.e.*, $S_{rxn} = C_0 - C_e$). By setting a fixed S_{rxn}, the rate constant *k* can be generated by experimental data fitting. The MnOII model and its two associated rate-limiting step assumptions were further verified by examining the impact of reactant concentration and solution pH on the reaction kinetics. This mechanism-based kinetic model successfully described the entire range of kinetic data for a total of 21 compounds of various structural characteristics for their oxidative reactions with MnO_2. This new model provides environmental scientists a very useful tool to quantitatively evaluate the kinetics of oxidative transformation for organic contaminants by manganese oxides.

6.4 Environmental Significance

As the usage of antimicrobials continues to grow, the proliferation of antibiotic-resistant pathogens and the presence of teratogenic antimicrobials in the environment will become increasingly important issues in the future. TCs are among the most frequently detected antibacterial agents in wastewaters and surface waters, posing potential ecological and health risks. The effect of metal species on isomerization and degradation of TCs had not yet been explored before this current study. This research has demonstrated that the metal species, including MnO_2, Al_2O_3, Mn^{II} and Cu^{II}, will play a significant role in the attenuation of TCs in the soil-water environment.

This study has provided new understanding on the transformation mechanisms and product formation of tetracycline antibiotics with several common environmental metal

species. The metal oxide-promoted generation of a more toxic product (anhydro-TTC) under environmentally relevant conditions raised the concern of potential adverse health and ecological effects. The mechanisms and kinetic results of several new reaction pathway elucidated in this study provided the basis for predicting the reactivity and transformation of TCs and their persistence in the soil-water system, and help assess the potential risk of such abiotic transformation. Results of this study also warrant further investigation on the interactions and potential transformation of TCs with environmentally important minerals and metal species, such as iron oxides and silica as well as other transition metal ions.

For many other antibacterial agents and emerging contaminants, it is necessary to continue the study to investigate their occurrence and fate and transport in the aquatic environment. Various metal oxides and dissolved metal species will likely affect the fate and transport of the above contaminants as long as the organic contaminants possess properties that favor metal interactions. The advancement made in this study in the fundamental understanding of the reaction mechanisms involving the complex molecules of tetracycline antibiotics will be helpful in better understanding the environmental transformation of other structurally-related organic contaminants.

6.5 Future Work

6.5.1 Further Product Characterization

TC molecules adopt complicated chemical structure with two major resonance moieties: the BCD ring diketone moiety and the A ring tricarbonylamide moiety. In addition, TCs have multiple functional groups that are highly susceptible to transform. Those special chemical properties proved a significant difficulty when interpreting their transformation products. Only several product structures with moderate structure alteration were identified in this study. The further breakdown products were not able to be identified at this moment. Other techniques such as ^{1}H-NMR, ^{13}C-NMR, two dimensional (2D) NMR spectroscopy, and isotope analytical technique can be applied to gain more information about the product structures,

6.5.2 Toxicity Analysis of TC Transformation Products

Followed by the transformation mechanism determination, the potential threat of TCs' degradation products on human health and ecological systems is necessary to be evaluated. For those product structures that have been identified in this study, only andro-TCs were known for their higher toxicity. For the rest of the products which have not been reported by other studies, their toxicity and impact on humans and the environment are currently unknown. The potential threat to human health can be evaluated by determining the levels of these contaminants in human bodies, which can be conducted by testing human biological fluid samples, such as breast milk, tissue, saliva, urine and blood samples, to determine levels of these contaminants in human bodies. This

information can be used to evaluate the likelihood that adverse human health effects may occur as a result of the occurrence of TC transformation.

6.5.3 Further Development of the MnOII Model

The current MnOII model already offers a significant improvement over the past studies in the ability to fully characterize the reaction kinetics of MnO_2-meidated oxidation in well-defined systems. The possibility of applying the MnOII model to a even wider range of organic and inorganic contamintatns for their reactions with MnO_2 in well-defined reaction systems is likely and should be explored. However, the current MnOII model is a limited predictive tool at this stage because the two key paramters rate constant (k) and total reactive surface sites (S_{rxn}) are dependent on reaction conditions. To predict the reaction kinetics of other organic compounds for their oxidation by MnO_2 at different reaction conditions or flow systems, further development needs to be conducted from the current model. For example, the generation of Mn^{2+} data needs to be collected in conjuction with the organic compound degradation kinetics in order to fully characterize the reaction if multiple electron transfer is the case. The MnOII model has the potential to be further developed by incorporating reaction condition variables into the equations to broaden its ability to predict reaction kinetics under varying conditions and be utilized to characterize other heterogeneous oxidants.

6.5.4 Impact of Other Metal Species

This study focuses on the transformation of TCs by natural metal species including MnO_2, Al_2O_3, Mn^{II} ion and Cu^{II} ion, providing important information about the relationships between metal ion catalysis and enhanced transformation caused by metal oxide surfaces. Many other metal species such as Fe, Si and Ti oxides can be found at an appreciable level in the aquatic environment, and as reactive surfaces to enhance pollutant degradation for waste treatment purposes. The research can be extended to other metal species which have the potential to facilitate abiotic reactions of organic pollutants via hydrolysis, substitution, redox, and polymerization. In addition, metal oxides with strong adsorption capacity can be developed as reactive sorbents to retard and degradate TCs and other related organic pollutants. In studying these reactions, the effects of environmental factors such as pH, temperature, and the presence of competing ions are likely important and should also be investrigated.

6.5.5 Environmental Fate of Other Emerging Contaminants

Modern chemistry has produced numerous compounds that facilitate everyday life and has helped save lives through human and veterinary medicine. One byproduct of these advances is the accumulation of these synthetic chemicals in streams and other water sources all over the world. In recent years, an increasingly growing number of studies have shown that many chemical and microbial constituents that have not historically been considered as contaminants are actually present in the environment on a global scale. There are numerous emerging contaminants found at appreciable levels in the environment with varying chemical structure and properties. Beside the antibiotic

chemicals that this study focuses on, household chemicals, pesticides, endocrine-disruptors (EDCs), and pharmaceuticals and personal-care products (PPCPs) can be included in future studies because their increasing use has led to frequent detection of new and potentially harmful contaminants in our water resources.

The reaction kinetic and mechanism examined by this study provide a fundamental knowledge and may be applied on other structurally-related compounds. Many emerging contaminants recognized thus far possess ketone, carboxyl, amino, and hydroxyl groups to coordinate with metal ions and thus may be susceptible to metal-mediated transformation. The reaction between other emerging contaminants and metal species with the influence of environmental factors needs to be conducted and the transformation product needs to be identified to determine their transformation mechanisms in the environmental media. This can strengthen our knowledge and properly assess the adverse effect they may cause.

6.5.6 Other Oxidation Treatment Processes of TCs

Wastewater is an important source of many surface-water contaminants, including pharmaceuticals, hormones, as well as other emerging contaminants. The main concern regarding emerging contaminants is that they are being introduced continuously into water bodies as pollutants and due to their biological activity, can potentially impact drinking water supplies and lead to adverse human health effects. As society becomes more concerned with the potential adverse biological and human health effects of organic contaminants and their residues in the environment, it is imperative to develop an efficient method to remove those contaminants in drinking water and wastewater.

Results of this research have provided an important foundation to understand the possible transformation of TCs in soil and water. This study showed that TCs are highly susceptible to oxidative transformation by MnO_2, Mn^{II} and Cu^{II} and to isomerization and dehydration by Al_2O_3; all of the reactions occur relatively fast (within 3 hours to 2 days). The relatively high reactivity of TCs suggests that TCs can likely also degrade by other oxidation processes such as photooxidation, chlorination, ozonation and Fenton reaction. Although some of the above reactions were discussed in the literature, however the reaction mechanisms are still not well understood. If developed properly, those processes may be very effective in removing TCs in drinking water and wastewater.

6.5.7 Actual Soil Samples

Actual soil systems are considerably more complicated than model experimental systems in the lab. Due to the non-uniform matrix, it is a challenge to interpret the reaction kinetics and mechanisms with actual soil samples. However, to more accurately predict the fate of TCs in the environment, the interaction between the organic contaminants and actual soil samples need to be investigated. In addition, more reconnaissance efforts need to be made in order to assess the presence of the TCs and related transformation products in the aquatic environemnt. Due to dilution and possible degradation of TCs in soil-water systems, low concentration levels can be expected. New analytical methods need to be developed to sensitive and selective detection at trace levels in environmental matrices. This may be achieved by using solid-phase extraction (SPE) and sensitive detection methods such as gas chromatography-mass spectrometry

(GC-MS), liquid chromatography-mass spectrometry (LC-MS), and tandem mass spectrometry (MS/MS).

REFERENCES

Aga Diana, S., Goldfish, R. and Kulshrestha, P. (2003). Application of ELISA in determining the fate of tetracyclines in land-applied livestock wastes. *Analyst, 128*(6), 658-662.

Aga, D. S., O'Connor, S., Ensley, S., Payero, J. O., Snow, D. and Tarkalson, D. (2005). Determination of the Persistence of Tetracycline Antibiotics and Their Degradates in Manure-Amended Soil Using Enzyme-Linked Immunosorbent Assay and Liquid Chromatography-Mass Spectrometry. *J. Agric. Food Chem., 53*(18), 7165-7171.

Albini, A. P., S. (1991). *Heterocyclic N-oxides*. Boston: CRC Press.

Arikan, O. A., Sikora, L. J., Mulbry, W., Khan, S. U., Rice, C. and Foster, G. D. (2006). The fate and effect of oxytetracycline during the anaerobic digestion of manure from therapeutically treated calves. *Process Biochem. (Amsterdam, Neth.) 41*(7), 1637-1643.

Avena, M. J. and Koopal, L. K. (1999). Kinetics of Humic Acid Adsorption at Solid-Water Interfaces. *Environ. Sci. Technol., 33*(16), 2739-2744.

Baker, W. A., Jr. and Brown, P. M. (1966). Metal binding in tetracyclines. Cobalt(II) and nickel(II) complexes. *J. Am. Chem. Soc., 88*(6), 1314-1317.

Barrett, J. R. (2005). Airborne Bacteria in CAFOs: Transfer of Resistance from Animals to Humans. *Environ. Health. Perspect., 113*(2), A116-A117.

Bartlett, R. J. (1988). Manganese redox reactions and organic interactions in soils. *Dev. Plant Soil Sci., 33*(Manganese Soils Plants), 59-73.

Beckett, M. A. and Hua, I. (2003). Enhanced sonochemical decomposition of 1,4-dioxane by ferrous iron. *Water Res., 37*(10), 2372-2376.

Bielski, B. H. J. and Allen, A. O. (1977). Mechanism of the disproportionation of superoxide radicals. *J. Phys. Chem., 81*(11), 1048-1050.

Blanchflower, J. W., McCracken, R. J., Haggan, A. S. and Kennedy, G. D. (1997). Confirmatory assay for the determination of tetracycline, oxytetracycline,

chlortetracycline and its isomers in muscle and kidney using liquid chromatography-mass spectrometry. *J. Chromatogr., B: Biomed. Sci. Appl., 692*(2), 351-360.

Canle L, M., Santaballa, J. A. and Vulliet, E. (2005). On the mechanism of TiO2-photocatalyzed degradation of aniline derivatives. *J. Photochem. Photobiol., A, 175*(2-3), 192-200.

Caswell, A. H. and Hutchison, J. D. (1971). Selectivity of cation chelation to tetracyclines: evidence for special conformation of calcium chelate. *Biochem. Biophys. Res. Commun., 43*(3), 625-630.

Chapin, A., Rule, A., Gibson, K., Buckley, T. and Schwab, K. (2005). Airborne multidrug-resistant bacteria isolated from a concentrated swine feeding operation. *Environ. Health. Perspect., 113*(2), 137-142.

Chee-Sanford, J. C., Aminov, R. I., Krapac, I. J., Garrigues-Jeanjean, N. and Mackie, R. I. (2001). Occurrence and diversity of tetracycline resistance genes in lagoons and groundwater underlying two swine production facilities. *Appl. Environ. Microbiol., 67*(4), 1494-1502.

Clive, D. L. J. (1968). Chemistry of tetracyclines. *Quart. Rev. (London), 22*(4), 435-456.

Colaizzi, J. L., Knevel, A. M. and Martin, A. N. (1965). Biophysical study of the mode of action of the tetracycline antibiotics. Inhibition of metalloflavoenzyme NADH cytochrome oxidoreductase. *J. Pharm. Sci., 54*(10), 1425-1436.

Cooper, A. D., Stubbings, G. W. F., Kelly, M., Tarbin, J. A., Farrington, W. H. H. and Shearer, G. (1998). Improved method for the online metal chelate affinity chromatography-high-performance liquid chromatographic determination of tetracycline antibiotics in animal products. *J. Chromatogr., A, 812*(1 + 2), 321-326.

Croubels, S. M., Vanoosthuyze, K. E. I. and Van Peteghem, C. H. (1997). Use of metal chelate affinity chromatography and membrane-based ion-exchange as clean-up procedure for trace residue analysis of tetracyclines in animal tissues and egg. *J. Chromatogr., B: Biomed. Appl., 690*(1 + 2), 173-179.

Dalmazio, I., Almeida, M. O., Augusti, R. and Alves, T. M. A. (2007). Monitoring the Degradation of Tetracycline by Ozone in Aqueous Medium Via Atmospheric Pressure Ionization Mass Spectrometry. *J. Am. Soc. Mass Spectrom., 18*(4), 679-687.

Davis, J. A. and Gloor, R. (1981). Adsorption of dissolved organics in lake water by aluminum oxide. Effect of molecular weight. *Environ. Sci. Technol., 15*(10), 1223-1229.

De Ruyck, H., De Ridder, H., Van Renterghem, R. and Van Wambeke, F. (1999). Validation of HPLC method of analysis of tetracycline residues in eggs and broiler meat and its application to a feeding trial. *Food Addit. Contam., 16*(2), 47-56.

Ferguson, M. A., Hoffmann, M. R. and Hering, J. G. (2005). TiO2-Photocatalyzed As(III) Oxidation in Aqueous Suspensions: Reaction Kinetics and Effects of Adsorption. *Environ. Sci. Technol., 39*(6), 1880-1886.

Fierro, e. b. J. L. G. (2006). *Metal oxides : chemistry and applications*. Boca Raton, FL: CRC Taylor & Francis.

Figueroa, R. A., Leonard, A. and MacKay, A. A. (2004). Modeling Tetracycline Antibiotic Sorption to Clays. *Environ. Sci. Technol., 38*(2), 476-483.

Figueroa, R. A. and MacKay, A. A. (2005). Sorption of Oxytetracycline to Iron Oxides and Iron Oxide-Rich Soils. *Environ. Sci. Technol., 39*(17), 6664-6671.

Furrer, G. and Stumm, W. (1986). The coordination chemistry of weathering: I. Dissolution kinetics of alumina and beryllium oxide. *Geochim. Cosmochim. Acta, 50*(9), 1847-1860.

Gartiser, S., Urich, E., Alexy, R. and Kuemmerer, K. (2007). Ultimate biodegradation and elimination of antibiotics in inherent tests. *Chemosphere, 67*(3), 604-613.

Graslund, S. and Bengtsson, B.-E. (2001). Chemicals and biological products used in south-east Asian shrimp farming, and their potential impact on the environment - a review. *Sci. Total Environ., 280*(1-3), 93-131.

Gratacos-Cubarsi, M., Fernandez-Garcia, A., Picouet, P., Valero-Pamplona, A., Garcia-Regueiro, J.-A. and Castellari, M. (2007). Formation of Tetracycline Degradation

Products in Chicken and Pig Meat under Different Thermal Processing Conditions. *J. Agric. Food Chem., 55*(11), 4610-4616.

Gu, C. and Karthikeyan, K. G. (2005). Interaction of Tetracycline with Aluminum and Iron Hydrous Oxides. *Environ. Sci. Technol., 39*(8), 2660-2667.

Guest, C. A., Schulze, D. G., Thompson, I. A. and Huber, D. M. (2002). Correlating manganese X-ray absorption near-edge structure spectra with extractable soil manganese. *Soil Sci. Soc. Am. J., 66*(4), 1172-1181.

Halling-Sorensen, B., Lykkeberg, A., Ingerslev, F., Blackwell, P. and Tjornelund, J. (2003). Characterization of the abiotic degradation pathways of oxytetracyclines in soil interstitial water using LC-MS-MS. *Chemosphere, 50*(10), 1331-1342.

Halling-Sorensen, B., Nors Nielsen, S., Lanzky, P. F., Ingerslev, F., Holten Lutzhoft, H. C. and Jorgensen, S. E. (1998). Occurrence, fate and effects of pharmaceutical substances in the environment--a review. *Chemosphere, 36*(2), 357-393.

Hamscher, G., Sczesny, S., Hoeper, H. and Nau, H. (2002). Determination of Persistent Tetracycline Residues in Soil Fertilized with Liquid Manure by High-Performance Liquid Chromatography with Electrospray Ionization Tandem Mass Spectrometry. *Anal. Chem., 74*(7), 1509-1518.

Hirsch, R., Ternes, T., Haberer, K. and Kratz, K.-L. (1999). Occurrence of antibiotics in the aquatic environment. *Sci. Total Environ., 225*(1,2), 109-118.

Housecroft, C. E. and Sharpe, A. G. (2001). *Inorganic Chemistry* (First ed.). Madrid, Spain: Pearson Education Limited.

Huang, C.-H. and Stone Alan, T. (2003). Transformation of the plant growth regulator daminozide (Alar) and structurally related compounds with CuII ions: oxidation versus hydrolysis. *Environ. Sci. Technol., 37*(9), 1829-1837.

Hughes, L. J., Stezowski, J. J. and Hughes, R. E. (1979). Chemical-structural properties of tetracycline derivatives. 7. Evidence for the coexistence of the zwitterionic and nonionized forms of the free base in solution. *J. Am. Chem. Soc., 101*(26), 7655-7656.

Hussar, D. A., Nieberga.Pj, Sugita, E. T. and Doluisio, J. T. (1968). Aspects of Epimerization of Certain Tetracycline Derivatives. *J. Pharm. Pharmacol., 20*(7), 539-546.

Jacobsen, P. and Berglind, L. (1988). Persistence of oxytetracycline in sediments from fish farms. *Aquaculture 70*(4), 365-370.

Jezowska-Bojczuk, M., Lambs, L., Kozlowski, H. and Berthon, G. (1993). Metal ion-tetracycline interactions in biological fluids. 10. Structural investigations on copper(II) complexes of tetracycline, oxytetracycline, chlortetracycline, 4-(dedimethylamino)tetracycline, and 6-desoxy-6-demethyltetracycline and discussion of their binding modes. *Inorg. Chem., 32*(4), 428-437.

Jogun, K. H. and Stezowski, J. J. (1976). Chemical-structural properties of tetracycline derivatives. 2. Coordination and conformational aspects of oxytetracycline metal ion complexation. *J. Am. Chem. Soc., 98*(19), 6018-6026.

Karthikeyan, K. G., Chorover, J., Bortiatynski, J. M. and Hatcher, P. G. (1999). Interaction of 1-naphthol and its oxidation products with aluminum hydroxide. *Environ. Sci. Technol., 33*(22), 4009-4015.

Katritzky, A., R.; Lagowski, J. M. (1971). *Chemistry of the Heterocyclic N-oxides* (Vol. 19). New York: Academic Press.

Khachatourians, G. G. (1998). Agricultural use of antibiotics and the evolution and transfer of antibiotic-resistant bacteria. *CMAJ, 159*(9), 1129-1136.

Kim, S., Eichhorn, P., Jensen, J. N., Weber, A. S. and Aga, D. S. (2005). Removal of Antibiotics in Wastewater: Effect of Hydraulic and Solid Retention Times on the Fate of Tetracycline in the Activated Sludge Process. *Environ. Sci. Technol., 39*(15), 5816-5823.

Klausen, J., Haderlein, S. B. and Schwarzenbach, R. P. (1997). Oxidation of Substituted Anilines by Aqueous MnO2: Effect of Co-Solutes on Initial and Quasi-Steady-State Kinetics. *Environ. Sci. Technol., 31*(9), 2642-2649.

Klewicki, J. K. and Morgan, J. J. (1998). Kinetic Behavior of Mn(III) Complexes of Pyrophosphate, EDTA, and Citrate. *Environ. Sci. Technol., 32*(19), 2916-2922.

Klewicki, J. K. and Morgan, J. J. (1999). Dissolution of b-MnOOH particles by ligands: pyrophosphate, ethylenediaminetetraacetate, and citrate. *Geochim. Cosmochim. Acta, 63*(19/20), 3017-3024.

Klimova, N. E. and Ermolova, O. B. (1976). Embryotoxicity and the immunodepressive action of tetracycline and its epi- and anhydro- derivatives. *Antibiotiki, 21*(11), 1018-1022.

Kolpin, D. W., Furlong, E. T., Meyer, M. T., Thurman, E. M., Zaugg, S. D., Barber, L. B., et al. (2002). Pharmaceuticals, Hormones, and Other Organic Wastewater Contaminants in U..S. Streams, 1999-2000: A National Reconnaissance. *Environ. Sci. Technol., 36*(6), 1202-1211.

Kosaka, K., Yamada, H., Matsui, S., Echigo, S. and Shishida, K. (1998). Comparison among the Methods for Hydrogen Peroxide Measurements to Evaluate Advanced Oxidation Processes: Application of a Spectrophotometric Method Using Copper(II) Ion and 2,9-Dimethyl-1,10-phenanthroline. *Environ. Sci. Technol., 32*(23), 3821-3824.

Kosmulski, M. (1997). Standard enthalpies of adsorption of di- and trivalent cations on alumina. *J. Colloid Interface Sci., 192*(1), 215-227.

Kostka, J. E., Luther, G. W., III, & Nealson, K. H. (1995). Chemical and biological reduction of Mn(III)-pyrophosphate complexes: potential importance of dissolved Mn(III) as an environmental oxidant. *Geochim. Cosmochim. Acta 59*(5), 885-894.

Kraemer, S. M., Chiu, V. Q. and Hering, J. G. (1998). Influence of pH and Competitive Adsorption on the Kinetics of Ligand-Promoted Dissolution of Aluminum Oxide. *Environ. Sci. Technol., 32*(19), 2876-2882.

Kulshrestha, P., Giese, R. F., Jr. and Aga, D. S. (2004). Investigating the Molecular Interactions of Oxytetracycline in Clay and Organic Matter: Insights on Factors Affecting Its Mobility in Soil. *Environ. Sci. Technol., 38*(15), 4097-4105.

Kummert, R. and Stumm, W. (1980). The surface complexation of organic acids on hydrous gamma -alumina. *J. Colloid Interface Sci., 75*(2), 373-385.

Laha, S. and Luthy, R. G. (1990). Oxidation of aniline and other primary aromatic amines by manganese dioxide. *Environ. Sci. Technol., 24*(3), 363-373.

Lambs, L., Brion, M. and Berthon, G. (1984). Metal ion-tetracycline interactions in biological fluids. Part 3. Formation of mixed-metal ternary complexes of tetracycline, oxytetracycline, doxycycline and minocycline with calcium and magnesium, and their involvement in the bioavailability of these antibiotics in blood plasma. *Agents Actions, 14*(5-6), 743-750.

Lambs, L., Decock-Le Reverend, B., Kozlowski, H. and Berthon, G. (1988). Metal ion-tetracycline interactions in biological fluids. 9. Circular dichroism spectra of calcium and magnesium complexes with tetracycline, oxytetracycline, doxycycline, and chlortetracycline and discussion of their binding modes. *Inorg. Chem., 27*(17), 3001-3012.

Lee, J. Y. and Everett, G. W., Jr. (1981). Binding of manganese(II) by tetracycline. Carbon-13 NMR spin-lattice relaxation study. *J. Am. Chem. Soc., 103*(17), 5221-5225.

Levy, S. B. and Marshall, B. (2004). Antibacterial resistance worldwide: causes, challenges and responses *Nature Medicine (N.Y.), 10*, S122-S129.

Li, H., Lee, L. S., Schulze, D. G. and Guest, C. A. (2003). Role of Soil Manganese in the Oxidation of Aromatic Amines. *Environ. Sci. Technol., 37*(12), 2686-2693.

Liang, Y., Denton, M. B. and Bates, R. B. (1998). Stability studies of tetracycline in methanol solution. *J. Chromatogr., A 827*(1), 45-55.

Lindberg, R. H., Wennberg, P., Johansson, M. I., Tysklind, M. and Andersson, B. A. V. (2005). Screening of human antibiotic substances and determination of weekly mass flows in five sewage treatment plants in Sweden. *Environ. Sci. Technol., 39*, 3421-3429.

Lindsey, M. E., Meyer, M. and Thurman, E. M. (2001). Analysis of trace levels of sulfonamide and tetracycline antimicrobials in groundwater and surface water using solid-phase extraction and liquid chromatography/mass spectrometry. *Anal. Chem., 73*(19), 4640-4646.

Loke Marie, L., Jespersen, S., Vreeken, R., Halling-Sorensen, B. and Tjornelund, J. (2003). Determination of oxytetracycline and its degradation products by high-performance liquid chromatography-tandem mass spectrometry in manure-

containing anaerobic test systems. *J.Chromatogr. B, Analyt.Technol.Biomed.Life Sci., 783*(1), 11-23.

Lovley, D. R., Coates, J. D., Blunt-Harris, E. L., Phillips, E. J. P. and Woodward, J. C. (1996). Humic substances as electron acceptors for microbial respiration. *Nature, 382*(1), 445-448.

Lykkeberg Anne, K., Halling-Sorensen, B., Cornett, C., Tjornelund, J. and Honore Hansen, S. (2004). Quantitative analysis of oxytetracycline and its impurities by LC-MS-MS. *J. Pharm. Biomed. Anal., 34*(2), 325-332.

MacKay, A. A. and Canterbury, B. (2005). Oxytetracycline sorption to organic matter by metal-bridging. *J. Environ. Qual., 34*(6), 1964-1971.

McArdell, C. S., Stone, A. T. and Tian, J. (1998). Reaction of EDTA and Related Aminocarboxylate Chelating Agents with CoIIIOOH (Heterogenite) and MnIIIOOH (Manganite). *Environ. Sci. Technol., 32*(19), 2923-2930.

McBride, M. B. (1994). *Environmental Chemistry of Soils*.

McBride, M. B. and Sikora, F. J. (1990). Catalyzed oxidation reactions of 1,2-dihydroxybenzene (catechol) in aerated aqueous solutions of aluminum(3+). *J. Inorg. Biochem., 39*(3), 247-262.

McCormick, J. R. D., Fox, S. M., Smith, L. L., Bitler, B. A., Reichenthal, J., Origoni, V. E., et al. (1957). The reversible epimerization occurring in the tetracycline family. The preparation, properties and proof of structure of some 4-epitetracyclines. *J. Am. Chem. Soc., 79*, 2849-2858.

Miao, X.-S., Bishay, F., Chen, M. and Metcalfe, C. D. (2004). Occurrence of antimicrobials in the final effluents of wastewater treatment plants in Canada. *Environ. Sci. Technol., 38*, 3542-3550.

Mikulski, C. M., Fleming, J., Fleming, D. and Karayannis, N. M. (1988). Chelates of tetracycline with first row transition metal perchlorates. *Inorg. Chim. Acta, 144*(1), 9-16.

Miskoski, S., Sanchez, E., Garavano, M., Lopez, M., Soltermann, A. T. and Garcia, N. A. (1998). Singlet molecular oxygen-mediated photo-oxidation of tetracyclines:

kinetics, mechanism and microbiological implications. *J. Photochem. Photobiol., B, 43*(2), 164-171.

Mitscher, L. A., Slater-Eng, B. and Sokoloski, T. D. (1972). Circular dichroism measurements of the tetracyclines. IV. 5-Hydroxylated derivatives. *Antimicrob. Agents Chemother., 2*(2), 66-72.

Moffett, J. W., Zika, R. G. and Petasne, R. G. (1985). Evaluation of Bathocuproine for the Spectrophotometric Determination of Copper(I) in Copper Redox Studies with Applications in Studies of Natural-Waters. *Anal. Chim. Acta 175*(SEP), 171-179.

Moore, D. E., Fallon, M. P. and Burt, C. D. (1983). Photooxidation of tetracycline - a differential pulse polarographic study. *Int. J. Pharm., 14*(2-3), 133-142.

Morel, F. M. M. and Hering, J. G. (1993). *Principles and Applications of Aquatic Chemistry*. New York: John Wiley & Sons, Inc.

Morgan, J. J. (2004). Kinetics of reaction between O2 and Mn(II) species in aqueous solutions. *Geochim. Cosmochim. Acta 69*(1), 35-48.

Murray, J. W. (1974). Surface chemistry of hydrous manganese dioxide. *J. Colloid Interface Sci., 46*(3), 357-371.

Murray, J. W., Balistrieri, L. S. and Paul, B. (1984). The oxidation state of manganese in marine sediments and ferromanganese nodules. *Geochim. Cosmochim. Acta 48*(6), 1237-1247.

Nico, P. S. and Zasoski, R. J. (2001). Mn(III) Center Availability as a Rate Controlling Factor in the Oxidation of Phenol and Sulfide on d-MnO2. *Environ. Sci. Technol., 35*(16), 3338-3343.

Nowack, B. and Stone, A. T. (2000). Degradation of nitrilotris(methylenephosphonic acid) and related (amino)phosphonate chelating agents in the presence of manganese and molecular oxygen. *Environ. Sci. Technol., 34*(22), 4759-4765.

Nowack, B. and Stone, A. T. (2003). Manganese-catalyzed degradation of phosphonic acids. *Environ. Chem. Lett., 1*(1), 24-31.

Ohyama, T. and Cowan, J. A. (1995). Calorimetric Studies of Metal Binding to Tetracycline. Role of Solvent Structure in Defining the Selectivity of Metal Ion-Drug Interactions. *Inorg. Chem., 34*(11), 3083-3086.

Oka, H., Ikai, Y., Kawamura, N., Yamada, M., Harada, K., Ito, S., et al. (1989). Photodecomposition products of tetracycline in aqueous solution. *J. Agric. Food Chem., 37*(1), 226-231.

Olack, G. and Morrison, H. (1991). Organic photochemistry. 92. Formation and characterization of lumitetracycline-type photoproducts from members of the tetracycline family. *J. Org. Chem., 56*(16), 4969-4971.

Pecher, K., Haderlein, S. B. and Schwarzenbach, R. P. (2002). Reduction of Polyhalogenated Methanes by Surface-Bound Fe(II) in Aqueous Suspensions of Iron Oxides. *Environ. Sci. Technol., 36*(8), 1734-1741.

Pena, A., Carmona, A., Barbosa, A., Lino, C., Silveira, I. and Castillo, B. (1998). Determination of tetracycline and its major degradation products by liquid chromatography with fluorescence detection. *J. Pharm. Biomed. Anal., 18*(4,5), 839-845.

Pick-Kaplan, M. and Rabani, J. (1976). Pulse radiolytic studies of aqueous manganese(II) perchlorate solutions. *J. Phys. Chem., 80*(17), 1840-1843.

Pils, J. R. V. and Laird, D. A. (2007). Sorption of Tetracycline and Chlortetracycline on K- and Ca-Saturated Soil Clays, Humic Substances, and Clay-Humic Complexes. *Environ. Sci. Technol., 41*(6), 1928-1933.

Pines, H. and Haag, W. O. (1960). Alumina: Catalyst and support. I. Alumina, its intrinsic acidity and catalytic activity. *J. Am. Chem. Soc., 82*, 2471-2483.

Pizzigallo, M. D. R., Ruggiero, P., Crecchio, C. and Mascolo, G. (1998). Oxidation of chloroanilines at metal oxide surfaces. *J. Agric. Food Chem., 46*(5), 2049-2054.

Pizzigallo, M. D. R., Ruggiero, P., Crecchio, C. and Mininni, R. (1995). Manganese and iron oxides as reactants for oxidation of chlorophenols. *Soil Sci. Soc. Am. J. , 59*(2), 444-452.

Prewo, R. and Stezowski, J. J. (1977). Chemical-structural properties of tetracycline derivatives. 3. The integrity of the conformation of the nonionized free base. *J. Am. Chem. Soc., 99*(4), 1117-1121.

Qiang, Z. and Adams, C. (2004). Potentiometric determination of acid dissociation constants (pKa) for human and veterinary antibiotics. *Water Res., 38*(12), 2874-2890.

Quinlan, G. J. and Gutteridge, J. M. (1988). Hydroxyl radical generation by the tetracycline antibiotics with free radical damage to DNA, lipids and carbohydrate in the presence of iron and copper salts. *Free Radical Biol. Med., 5*(5-6), 341-348.

Quinlan, G. J. and Gutteridge, J. M. C. (1991). DNA base damage by beta -lactam, tetracycline, bacitracin and rifamycin antibacterial antibiotics. *Biochem. Pharmacol., 42*(8), 1595-1599.

Rubert, K. F. and Pedersen, J. A. (2006). Kinetics of oxytetracycline reaction with a hydrous manganese oxide. *Environ. Sci. Technol., 40*(23), 7216-7221.

Sahai, N. and Sverjensky, D. A. (1997). Evaluation of internally consistent parameters for the triple-layer model by the systematic analysis of oxide surface titration data. *Geochim. Cosmochim. Acta, 61*(14), 2801-2826.

Sanniez, W. H. K. and Pilpel, N. (1980). Photodecomposition of sulfonamides and tetracyclines at oil-water interfaces. *J. Pharm. Sci., 69*(1), 5-8.

Sassman, S. A. and Lee, L. S. (2005). Sorption of Three Tetracyclines by Several Soils: Assessing the Role of pH and Cation Exchange. *Environ. Sci. Technol., 39*(19), 7452-7459.

Schecher, W. D. and McAvoy, D. C. (2001). MINEQL+: A Chemical equilibrium modeling system, version 4.5 for windows. Hallowell, ME, USA: Environmental Research Software.

Schnappinger, D. and Hillen, W. (1996). Tetracyclines. Antibiotic action, uptake, and resistance mechanisms. *Arch. Microbiol., 165*(6), 359-369.

Schneider, S., Schmitt, M. O., Brehm, G., Reiher, M., Matousek, P. and Towrie, M. (2003). Fluorescence kinetics of aqueous solutions of tetracycline and its complexes with Mg2+ and Ca2+. *Photochem. Photobiol. Sci., 2*(11), 1107-1117.

Shin, J. Y. and Cheney, M. A. (2004). Abiotic transformation of atrazine in aqueous suspension of four synthetic manganese oxides. *Colloids Surf., A 242*(1-3), 85-92.

Shindo, H., Oshita, T., Matsudomi, N., Usui, K. and Goh, T. B. (1996). Catalytic role of Mn(IV) oxide in the formation of humic-enzyme complexes in the soil ecosystem. *Soil Sci. Plant Nutr. (Tokyo), 42*(1), 141-146.

Skotak, M., Karpinski, Z., Juszczyk, W., Pielaszek, J., Kepinski, L., Kazachkin, D. V., et al. (2004). Characterization and catalytic activity of differently pretreated Pd/Al2O3 catalysts: the role of acid sites and of palladium-alumina interactions. *J. Catal., 227*(1), 11-25.

Smith, P. (1996). Is sediment deposition the dominant fate of oxytetracycline used in marine salmonid farms: a review of available evidence. *Aquaculture 146*(3,4), 157-169.

Sohn, J. R., Park, W. C. and Shin, D. C. (2006). Characterization of nickel sulfate supported on SiO2 for ethylene dimerization and promoting effect of Al2O3 on catalytic activity. *J. Mol. Catal. A: Chem., 256*(1-2), 156-163.

Sokoloski, T. D., Mitscher, L. A., Yuen, P. H., Juvarkar, J. V. and Hoener, B. (1977). Rate and proposed mechanism of anhydrotetracycline epimerization in acid solution. *J. Pharm. Sci., 66*(8), 1159-1165.

Stephens, C. R., Conover, L. H., Pasternack, R., Hochstein, F. A., Moreland, W. T., Regna, P. P., et al. (1954). Terramycin .12. the Structure of Aureomycin. *J. Am. Chem. Soc., 76*(13), 3568-3575.

Stephens, C. R., Murai, K., Brunings, K. J. and Woodward, R. B. (1956). Acidity constants of the tetracycline antibiotics. *J. Am. Chem. Soc., 78*, 4155-4158.

Stezowski, J. J. (1976). Chemical-structural properties of tetracycline derivatives. 1. Molecular structure and conformation of the free base derivatives. *J. Am. Chem. Soc., 98*(19), 6012-6018.

Stone, A. T. (1987). Microbial metabolites and the reductive dissolution of manganese oxides: Oxalate and pyruvate. *Geochim. Cosmochim. Acta 51*(4), 919-925.

Stone, A. T. (1987). Reductive Dissolution of Manganese(III/IV) Oxides by Substituted Phenols. *Environ. Sci. Technol., 21*(10), 979-988.

Stone, A. T. and Morgan, J. J. (1984a). Reduction and Dissolution of Manganese(III) and Manganese(IV) Oxides by Organics .1. Reaction with Hydroquinone. *Environ. Sci. Technol., 18*(6), 450-456.

Stone, A. T. and Morgan, J. J. (1984b). Reduction and Dissolution of Manganese(III) and Manganese(IV) Oxides by Organics .2. Survey of the Reactivity of Organics. *Environ. Sci. Technol., 18*(8), 617-624.

Stone, A. T. and Torrents, A. (1995). The role of dissolved metals and metal-containing surfaces in catalyzing the hydrolysis of organic pollutants. *Environ. Impact Soil Compon. Interact., 1*, 275-298.

Stone, A. T., Torrents, A., Smolen, J., Vasudevan, D. and Hadley, J. (1993). Adsorption of organic compounds possessing ligand donor groups at the oxide/water interface. *Environ. Sci. Technol., 27*(5), 895-909.

Strathmann, T. J. and Stone, A. T. (2001). Reduction of the carbamate pesticides oxamyl and methomyl by dissolved FeII and CuI. *Environ. Sci. Technol., 35*(12), 2461-2469.

Stumm, W. (1992). *Chemistry of the Solid-Water Interface: Processes at the Mineral-Water and Particle-Water Interface in Natural Systems*.

Stumm, W. and Morgan, J. J. (1996). *Aquatic Chemistry; Third Edition*: Wiley: New York.

Sulzberger, B., Suter, D., Siffert, C., Banwart, S. and Stumm, W. (1989). Dissolution of iron(III) (hydr)oxides in natural waters; laboratory assessment on the kinetics controlled by surface coordination. *Mar. Chem., 28*(1-3), 127-144.

Suzuki, Y., Ishihara, M., Segami, T. and Ito, M. (1998). Anti-ulcer effects of antioxidants, quercetin, alpha -tocopherol, nifedipine and tetracycline in rats. *Jpn. J. Pharmacol., 78*(4), 435-441.

Tamura, H., Goto, K. and Nagayama, M. (1976). The effect of ferric hydroxide on the oxygenation of ferrous ions in neutral solutions. *Corrosion Science, 16*(4), 197-207.

Thiele-Bruhn, S. (2003). Pharmaceutical antibiotic compounds in soils - a review. *J. Plant Nutr. Soil Sci., 166*(2), 145-167.

Tolls, J. (2001). Sorption of Veterinary Pharmaceuticals in Soils: A Review. *Environ. Sci. Technol., 35*(17), 3397-3406.

Tongaree, S., Flanagan, D. R. and Poust, R. I. (1999). The effects of pH and mixed solvent systems on the solubility of oxytetracycline. *Pharm. Dev. Technol., 4*(4), 571-580.

Ukrainczyk, L. and McBride, M. B. (1992). Oxidation of phenol in acidic aqueous suspensions of manganese oxides. *Clays Clay Miner., 40*(2), 157-166.

Ukrainczyk, L. and McBride, M. B. (1993). Oxidation and dechlorination of chlorophenols in dilute aqueous suspensions of manganese oxides: Reaction products. *Environ. Toxicol. Chem., 12*(11), 2015-2022.

Ulrich, H. J. and Stone, A. T. (1989). Oxidation of Chlorophenols Adsorbed to Manganese Oxide Surfaces. *Environ. Sci. Technol., 23*(4), 421-428.

Ungemach Fritz, R., Muller-Bahrdt, D. and Abraham, G. (2006). Guidelines for prudent use of antimicrobials and their implications on antibiotic usage in veterinary medicine. *Int. J. Med. Microbiol., 296 Suppl 41*, 33-38.

Waller, C. W., Hutchings, B. L., Wolf, C. F., Goldman, A. A., Broschard, R. W. and Williams, J. H. (1952). Degradation of Aureomycin. VI. Isoaureomycin and Aureomycin. *J. Am. Chem. Soc., 74*, 4981.

Walling, C. (1975). Fenton's reagent revisited. *Acc. Chem. Res., 8*(4), 125-131.

Walling, C. and Kato, S. (1971). Oxidation of alcohols by Fenton's reagent. Effect of copper ion. *J. Amer. Chem. Soc., 93*(17), 4275-4281.

Walsh, C. (2003). *Antibiotics: Actions, Origins, Resistance*. Washington, D.C.: ASM Press.

Walton, V. C., Howlett, M. R. and Selzer, G. B. (1970). Anhydrotetracycline and 4-epianhydrotetracycline in market tetracyclines and aged tetracycline products. *J. Pharm. Sci., 59*(8), 1160-1164.

Wang, D., Shin, J. Y., Cheney, M. A., Sposito, G. and Spiro, T. G. (1999). Manganese Dioxide as a Catalyst for Oxygen-Independent Atrazine Dealkylation. *Environ. Sci. Technol., 33*(18), 3160-3165.

Wang, Y. and Stone, A. T. (2006). The citric acid-MnIII,IVO2(birnessite) reaction. Electron transfer, complex formation, and autocatalytic feedback. *Geochim. Cosmochim. Acta 70*(17), 4463-4476.

Wehrli, B., Ibric, S. and Stumm, W. (1990). Adsorption kinetics of vanadyl(IV) and chromium(III) to aluminum oxide: Evidence for a two-step mechanism. *Colloids Surf., 51*, 77-88.

Wehrli, B. and Stumm, W. (1989). Vanadyl in natural waters: Adsorption and hydrolysis promote oxygenation. *Geochim. Cosmochim. Acta, 53*(1), 69-77.

Werner, J. J., Arnold, W. A. and McNeill, K. (2006). Water Hardness as a Photochemical Parameter: Tetracycline Photolysis as a Function of Calcium Concentration, Magnesium Concentration, and pH. *Environ. Sci. Technol., 40*(23), 7236-7241.

Wessels, J. M., Ford, W. E., Szymczak, W. and Schneider, S. (1998). The Complexation of Tetracycline and Anhydrotetracycline with Mg2+ and Ca2+: A Spectroscopic Study. *J. Phys. Chem., B 102*(46), 9323-9331.

Wootton, P. D., Kramer, T. A., Cheek, D. M. and Lange, C. R. (1998). Treatment of heavy metal contaminated wastewater using powdered and granular alumina. *Hazard. Ind. Wastes 30th*, 726-734.

Yamamoto, T., Tanaka, T., Matsuyama, T., Funabiki, T. and Yoshida, S. (2001). Alumina-Supported Rare-Earth Oxides Characterized by Acid-Catalyzed Reactions and Spectroscopic Methods. *J. Phys. Chem. B 105*(9), 1908-1916.

Yuen, P. H. and Sokoloski, T. D. (1977). Kinetics of concomitant degradation of tetracycline to epitetracycline, anhydrotetracycline, and epianhydrotetracycline in acid phosphate solution. *J. Pharm. Sci., 66*(11), 1648-1650.

Zhang, H. and Huang, C.-H. (2003). Oxidative Transformation of Triclosan and Chlorophene by Manganese Oxides. *Environ. Sci. Technol., 37*(11), 2421-2430.

Zhang, H. and Huang, C.-H. (2005a). Oxidative Transformation of Fluoroquinolone Antibacterial Agents and Structurally Related Amines by Manganese Oxide. *Environ. Sci. Technol., 39*(12), 4474-4483.

Zhang, H. and Huang, C.-H. (2005b). Reactivity and transformation of antibacterial N-oxides in the presence of manganese oxide. *Environ. Sci. Technol., 39*(2), 593-601.

Zhu, J., Snow, D. D., Cassada, D. A., Monson, S. J. and Spalding, R. F. (2001). Analysis of oxytetracycline, tetracycline, and chlortetracycline in water using solid-phase extraction and liquid chromatography-tandem mass spectrometry. *J. Chromatogr., A, 928*(2), 177-186.

Zou, W., Han, R., Chen, Z., Zhang, J. and Shi, J. (2006). Kinetic study of adsorption of Cu(II) and Pb(II) from aqueous solutions using manganese oxide coated zeolite in batch mode. *Colloids Surf., A, 279*(1-3), 238-246.

Zurhelle, G., Muller-Seitz, E. and Petz, M. (2000). Automated residue analysis of tetracyclines and their metabolites in whole egg, egg white, egg yolk and hen's plasma utilizing a modified ASTED system. *J. Chromatogr., B: Biomed. Sci. Appl., 739*(1), 191-203.

VITA

WAN-RU CHEN

Wan-Ru Chen was born in Taipei, Taiwan on March 11, 1977. She graduated from National Taiwan University in July 1999 with a Bachelor of Engineering degree in Civil Engineering. Wan-Ru began her graduate studies at the Graduate Institute of Environmental Engineering at National Taiwan University in September 1999. She continued her research as a research assistant while completing her Master of Engineering degree in July 2001. While at National Taiwan University, Wan-Ru conducted an independent research on heavy metal leaching from the regenerated building materials by fly ash.

In August 2003, Wan-Ru came to Georgia Institute of Technology to pursue a doctorate in Environmental Engineering. She completed her Ph.D. dissertation in May 2008. Her research examined the effect of metal oxides and metal ions on the abiotic transformation of tetracycline antibiotics. After completing her degree, Wan-Ru will join the Department of Crop and Soil Sciences at Michigan State University as a postdoctoral research scientist.